

PROCESS-BASED METHODS TO DETERMINE LAKE EVAPORATION
ON DIFFERENT TIME SCALES

By

RALEIGH GRYSKO

A thesis submitted in partial fulfillment of
the requirements for the degree of

MASTER OF SCIENCE IN ENVIRONMENTAL ENGINEERING

WASHINGTON STATE UNIVERSITY
Department of Civil and Environmental Engineering

DECEMBER 2017

© Copyright by RALEIGH GRYSKO, 2017
All Rights Reserved

© Copyright by RALEIGH GRYSKO, 2017
All Rights Reserved

To the Faculty of Washington State University:

The members of the Committee appointed to examine the thesis of RALEIGH GRYSKO
find it satisfactory and recommend that it be accepted.

Heping Liu, Ph.D., Chair

Brian Lamb, Ph.D.

Shelley Pressley, Ph.D.

ACKNOWLEDGMENT

I would first and foremost like to thank my advisor, Dr. Heping Liu, for his continued support and research advice. With Dr. Liu's help, my quality as a researcher improved significantly and I was able to become much more well versed in the micrometeorological field. I look forward to seeing what we can accomplish together in the future.

I would also like to thank my committee members, Dr. Brian Lamb and Dr. Shelley Pressley, for the feedback and advice they were able to provide during my time at WSU. Also, deserving of thanks are the LAR faculty and students that worked or assisted me with my studies and/or research. The experience and knowledge gained from working with my committee members, peers, and the faculty in LAR was invaluable.

Lastly, I would like to thank my friends and family for their continued support. With their help and encouragement, I was able to find the motivation and drive necessary to complete my Master's degree.

PROCESS-BASED METHODS TO DETERMINE LAKE EVAPORATION
ON DIFFERENT TIME SCALES

Abstract

by Raleigh Grysko, M.S.
Washington State University
December 2017

Chair: Heping Liu

Process-based methods for estimating open-water evaporation are needed by many scientific communities because methods of direct evaporation measurement are generally not widely available. The performance of the Priestley-Taylor (PT), deBruin-Keijman (DBK), Bowen ratio energy budget (BREB), Penman (PM), Brutsaert-Stricker (BS), and deBruin (DB) evaporation models were validated using eddy covariance-derived direct measurements of evaporation on monthly, daily, and 30-minute timescales. Eddy covariance and meteorological measurements used in this study were gathered from the Ross Barnett Reservoir in Mississippi, U.S.A., throughout the year of 2008.

Performance of the evaporation models was determined using three metrics: ability for the evaporation models to explain variance in measured evaporation, magnitude of evaporation difference, and consistency in bias. It was concluded that the models fell into three performance tiers for the monthly (daily) timescale, with BREB, PT, and DBK (DBK, and PT) being in the top tier, PM and BS model falling in the middle performance tier, and the DB model being in the

lowest performance tier; relative performance within each tier is indicated by the order in which the models are listed. The models did not naturally fall into three performance tiers for a 30-minute timescale, but were in the same order of performance as the monthly and daily timescales; PT and DBK performance were considered equal for this timescale. Performance of evaporation models were generally consistent throughout all timescales and could be ranked as follows: BREB, DBK/PT, PM, BS, and DB.

30-minute model performance was determined for both varying wind speed and stability conditions. A clear negative feedback trend in model performance was observed for wind speed, meaning that as wind speed increased in magnitude, model performance decreased. It was also determined that when atmospheric stability was unstable, model performance was better relative to when the atmosphere was stable.

Near neutral stability points with evaporation under/overestimation exceeding ± 3 standard deviations were isolated and displayed a discernible correlation with wind speed. This correlation revealed that the isolated points primarily occurred when wind speeds were high. It was therefore concluded that all models performed poorest when atmospheric stability was near-neutral and wind speeds were high.

TABLE OF CONTENTS

	Page
ACKNOWLEDGMENTS	iii
ABSTRACT	iv
LIST OF TABLES.....	viii
LIST OF FIGURES	ix
1. Introduction.....	1
2. Methods.....	8
2.1. Site description.....	8
2.2. Instruments.....	10
2.3. Evaporation models	11
3. Results and discussion	21
3.1. General climate	21
3.1.1. Annual variability in local meteorology	21
3.1.2. Annual variability in local surface energy budget	26
3.2. Performance of evaporation models under multiple temporal scales	28
3.2.1. Validating modeled evaporation performance with $H + LE$ in place of $Rn - Q_x$	28
3.2.2. Performance of evaporation models on a monthly temporal scale	30
3.2.3. Performance of evaporation models on a daily temporal scale	38
3.2.4. Performance of evaporation models on a 30-minute temporal scale	43
3.3. Impact of physical characteristics on modeled evaporation estimates	47
3.3.1. Impact of wind speed on modeled evaporation estimates	48
3.3.1.1. Impact of wind speed on PT-modeled evaporation estimates	50

3.3.1.2. Impact of wind speed on DBK-modeled evaporation estimates.....	53
3.3.1.3. Impact of wind speed on BREB-modeled evaporation estimates.....	56
3.3.1.4. Impact of wind speed on PM-modeled evaporation estimates	60
3.3.1.5. Impact of wind speed on BS-modeled evaporation estimates	62
3.3.1.6. Impact of wind speed on DB-modeled evaporation estimates.....	63
3.3.1.7. Summary of wind speed impact on modeled evaporation estimates	67
3.3.2. Impact of stability on modeled evaporation estimates.....	70
3.3.2.1. Impact of stability on PT-modeled evaporation estimates.....	71
3.3.2.2. Impact of stability on DBK-modeled evaporation estimates.....	74
3.3.2.3. Impact of stability on BREB-modeled evaporation estimates.....	74
3.3.2.4. Impact of stability on PM-modeled evaporation estimates.....	80
3.3.2.5. Impact of stability on BS-modeled evaporation estimates	83
3.3.2.6. Impact of stability on DB-modeled evaporation estimates.....	84
3.3.2.7. Summary of stability impact on modeled evaporation estimates	88
3.4. Physical causes of poor evaporation estimates during near-neutral stability	90
4. Summary and conclusions	96
REFERENCES	101

LIST OF TABLES

	Page
Table 1: List of instruments used in this study	12
Table 2: Empirical coefficients used in Lowe's saturation vapor pressure polynomial	17

LIST OF FIGURES

	Page
Figure 1: Location of the reservoir, platform location, and picture of platform and tower.....	9
Figure 2: Weekly averages of meteorological parameters.....	22
Figure 3: Monthly averages of 2-meter air temperature and all-layer water temperature	23
Figure 4: Monthly averages of atmospheric pressure and precipitation	25
Figure 5: Weekly averages of surface energy budget parameters	27
Figure 6: Weekly averages of Bowen ratio.....	27
Figure 7: Linear regression of PT-modeled and measured evaporation for $R_n - Q_x$ and $H + LE$.	29
Figure 8: Monthly mean modeled and measured evaporation time series.....	32
Figure 9: Monthly mean measured and modeled (PT, DBK, BREB) time series and differences	33
Figure 10: Monthly mean measured and modeled (PM, BS, DB) time series and differences	35
Figure 11: Linear regressions of modeled versus measured monthly evaporation.....	37
Figure 12: Daily mean measured and modeled (PT, DBK, BREB) time series and differences...39	39
Figure 13: Daily mean measured and modeled (PM, BS, DB) time series and differences.....	41
Figure 14: Linear regressions of modeled versus measured daily evaporation	44
Figure 15: Linear regressions of modeled versus measured 30-minute evaporation.....	46
Figure 16: Wind direction windrose indicating wind speed	49
Figure 17: Linear regressions of 30-minute PT-modeled versus measured evaporation for wind speed regimes.....	51
Figure 18: PT-modeled and measured evaporation difference boxplots for wind speed regimes.53	53
Figure 19: Linear regressions of 30-minute DBK-modeled versus measured evaporation for wind speed regimes.....	55

Figure 20: DBK-modeled and measured evaporation difference boxplots for wind speed regimes.....	56
Figure 21: Linear regressions of 30-minute BREB-modeled versus measured evaporation for wind speed regimes.....	58
Figure 22: BREB-modeled and measured evaporation difference boxplots for wind speed regime	59
Figure 23: Linear regressions of 30-minute PM-modeled versus measured evaporation for wind speed regimes.....	61
Figure 24: PM-modeled and measured evaporation difference boxplots for wind speed regimes	64
Figure 25: Linear regressions of 30-minute BS-modeled versus measured evaporation for wind speed regimes.....	65
Figure 26: BS-modeled and measured evaporation difference boxplots for wind speed regimes	66
Figure 27: Linear regressions of 30-minute DB-modeled versus measured evaporation for wind speed regimes.....	68
Figure 28: DB-modeled and measured evaporation difference boxplots for wind speed regimes	69
Figure 29: Wind direction windrose indicating atmospheric stability.....	71
Figure 30: Linear regressions of 30-minute PT-modeled versus measured evaporation for stability regimes.....	73
Figure 31: PT-modeled and measured evaporation difference boxplots for stability regimes ..	74
Figure 32: Linear regressions of 30-minute DBK-modeled versus measured evaporation for stability regimes.....	77
Figure 33: DBK-modeled and measured evaporation difference boxplots for stability regimes ..	78

Figure 34: Linear regressions of 30-minute BREB-modeled versus measured evaporation for stability regimes	79
Figure 35: BREB-modeled and measured evaporation difference boxplots for stability regimes	81
Figure 36: Linear regressions of 30-minute PM-modeled versus measured evaporation for stability regimes	82
Figure 37: PM-modeled and measured evaporation difference boxplots for stability regimes	84
Figure 38: Linear regressions of 30-minute BS-modeled versus measured evaporation for stability regimes	85
Figure 39: BS-modeled and measured evaporation difference boxplots for stability regimes	86
Figure 40: Linear regressions of 30-minute DB-modeled versus measured evaporation for stability regimes	87
Figure 41: DB-modeled and measured evaporation difference boxplots for stability regimes	89
Figure 42: Modeled and measured evaporation different versus stability	91,92
Figure 43: Regression of measured and modeled evaporation difference of isolated near-neutral points versus wind speed	95

1. Introduction

Roughly 304 million lakes of varying sizes and volumes exist on Earth's surface, covering an area of 4.2 million km² (~3% of Earth's continental surface) (*Downing et al.*, 2006). Worldwide evaporation and evapotranspiration account for returning roughly 64% of land-based precipitation back to the atmosphere (*Baumgartner and Reichel*, 1975). Inland water bodies can have a large impact on the climate in local, regional, and global climatic scales, primarily because of large differences in roughness, energy exchange, albedo, heat capacity, and surface-atmospheric trace gas exchange between inland water and their surrounding land surfaces (*Bates et al.*, 1993; 1995; *Bonan*, 1995; *Cole et al.*, 2007; *Eaton et al.*, 2001; *Eugster et al.*, 2003; *Jonsson et al.*, 2008; *Long et al.*, 2007; *Rouse et al.*, 2005). However, the impact of lakes on the atmospheric processes is still being parameterized crudely in climate and weather models due to over-water surface energy components, such as sensible heat flux (H) and latent heat flux (LE), having not been studied as extensively as surface energy budget components over land (*Bonan*, 1995; *Nordbo et al.*, 2011). As a result, surface energy budget components over water bodies are not as well understood (*Liu et al.*, 2009). All lakes have unique characteristics, such as geographic location, depth, surface area, fetch, albedo, heat capacity of water, etc., which impact the surface energy budget components differently, making the lake's effect on atmospheric processes difficult, but necessary, to quantify for use in hydrologic and meteorological models (*Sumner and Jacobs*, 2005). Given the large number of inland water storages and importance of evaporative fluxes, it is imperative to improve means of estimating evaporation (*Sumner and Jacobs*, 2005; *Rosenberry et al.*, 2007).

LE is the dominant surface energy budget component over inland water bodies and high-moisture areas. LE, which reflects evaporation, is driven primarily by mechanically-induced turbulence and the vapor pressure gradient between the water-air interface and overlying air under the influence of atmospheric stability conditions (*Liu et al.*, 2011). Quantifying evaporation from fresh-water lakes and reservoirs is critically important for water resource management services due to its important role in the water budget and local weather (*Sumner and Jacobs*, 2005). Having a complete understanding of the magnitude of evaporation of a region will allow for an increase in understanding of that area's hydrologic cycle, surface energy budget, and biosphere-atmosphere interactions (*Kaufman and Gao*, 1992).

Processes for estimating evaporation have changed and improved with recent technological advances (*McJannet et al.*, 2013). Despite the improvements, evaporation quantification can be a difficult, error-prone task, depending on the method and available measurement instruments. One of the most basic methods for estimating evaporation is the pan evaporation method. Despite the many studies that have identified the problems and limitations of this approach (e.g., *Kohler et al.*, 1955; *Shuttleworth*, 1992; *Lowe et al.*, 2009), this method is still widely used due to its simplicity and relatively low instrument cost and data requirements. Measuring evaporation from a Class A evaporation pan is as easy as measuring the change in water level every 24 hours. If the desire is to relate pan evaporation measurements to open-water evaporation, a site-specific, monthly pan evaporation coefficient is required. Evaporation estimates using pan evaporation can also be sparse, depending on location, and can be incomplete due to heavy precipitation or seasonal changes in temperature (*Kohler et al.*, 1955). When compared to evaporation measured using the

eddy covariance technique from a reservoir, pan evaporation estimates were shown to significantly exceed eddy covariance measurements (*Shuttleworth et al.*, 1992; *Lowe et al.*, 2009; *McJannet et al.*, 2011; 2013; . Overestimation of pan evaporation estimates were largely due to the significant difference in thermal conductance between the water being evaporated in the pan and the reservoir water. Differences in capacity for energy storage and conduits for energy transfer, such as inflow and outflow, between the pan water and the reservoir water also contribute to the large evaporation difference. Enhanced advective heat fluxes through the base and sides of the pan may also contribute to poor evaporation pan estimates (e.g., *Tanny et al.*, 2008). In addition to differences in heat storage capacity and heat transfer through the walls and base of the pan, the aerodynamic differences, different climatic conditions, and water body size between the pan and water body resulted in poor evaporation estimation from the pan evaporation method (e.g., *Brutsaert and Yeh*, 1970; *Jensen et al.*, 1990; *Kohler et al.*, 1955; *Morton*, 1983).

Another method used for estimating open-water evaporation is the water budget method, which estimates evaporation by the rearrangement of the water budget equation (e.g., *Abtew*, 2001; *Cheng*, 1978; *Gibson*, 2002; *McJannet et al.*, 2013). The water budget equation is described as

$$Q_{in} + P_g - \Delta S = Q_{out} + E + L, \quad (1)$$

where Q_{in} is inflow, P_g is input from direct rainfall, ΔS is change in stored water, Q_{out} is outflow, E is evaporative loss, and L is loss due to leakage into the water body bed. Equation 1 can be

rearranged and solved for evaporative loss if all inputs and outputs to the water body are known or can be accurately estimated. The largest form of uncertainty with this method is due to the quantification of the leakage loss term. As leakage loss rates for water bodies are rarely directly measured due to the associated difficulty, this term is typically estimated and, in some cases, assumed to be constant. Leakage loss rates are not likely to be constant in time due to responses to cycles of wet and dry periods. In some instances, such as large lakes formed on hard, semi-impermeable surfaces, it is acceptable to assume the leakage loss term to be negligible (*Abtew, 2001; Cheng, 1978; Sadek et al., 1997; Shepherd, 1971*). When compared to evaporation measured using eddy covariance measurements, the water budget method can estimate evaporation poorly if the leakage loss term is not measured or estimated accurately. Even if the leakage loss term is accurately represented or neglected, evaporation estimate errors can still occur if the inflow and outflow terms of Equation 1 are not accurately measured (*McJannet et al., 2013*).

The ability for evaporation models to accurately estimate evaporation over open water bodies has been the topic of multiple studies (e.g., *Dalton et al., 2004; Rasmussen et al., 1995; Rosenberry et al., 2004; 2007; Singh and Xu, 1997; Xu and Singh, 2001; Winter et al., 1995*). When working with open water, it can be assumed that models developed to estimate evapotranspiration can be used to estimate evaporation (*Rosenberry et al., 2007*). Difficulties in applying evaporation models can be due to the requirement of site-based measurements and the associated cost and availability (*McJannet et al., 2013*). Evaporation estimate accuracy is generally sacrificed as the number of required on-site measurements necessary for calculation decreases. For example, evaporation models that fall within a category known as “combination methods” are

commonly recognized as the most accurate methods, but are the most difficult to calculate due to the amount of required measurements. Additional difficulties and potential errors associated with evaporative models could occur due to the models being developed for specific geographic and climatic settings or timescales (*Rosenberry et al.*, 2007). Models for estimating evaporation and their intricacies will be discussed in much greater detail in Chapter 2.3.

More modern means for directly measuring evaporation have relatively recently been developed and applied to the science. H and LE, and subsequently evaporation, can be directly measured using scintillometry (*McJannet et al.*, 2011; 2013). Scintillometry is used to measure spatially-averaged fluctuations in temperature and humidity over a horizontal distance ranging from 100 m to 4.5 km. A scintillometer uses a transmitter and receiver to measure intensity fluctuations, known as scintillations, to characterize atmospheric turbulent intensity averaged over the distance between the transmitter and receiver (*Campbell Scientific*, 2016). Scintillometers primarily exist in two model types that specialize in measuring different variables and operate using different wavelengths. Radio wave scintillometers operate in the radio wave portion of the electromagnetic spectrum and are used to measure fluctuations in humidity. The more common type of scintillometer is the large-aperture scintillometer (LAS), which operates in the visible and near-infrared wavelengths and measures fluctuations in temperature (*McJannet et al.*, 2011). Radio wave scintillometers are seldom used due to the higher amount of maintenance and setup required to operate relative to their LAS counterpart (*Meijninger et al.*, 2002). H, once calculated using LAS measurements, can be used to estimate open-water evaporation using the “linearized-Bowen ratio” method (*McJannet et al.*, 2011; 2013; *Vercauteren et al.*, 2009).

A more common method for directly measuring open-water evaporation is through the use of the previously-mentioned eddy covariance technique (e.g., *Blanken et al.*, 2000; *Liu et al.*, 2009; *McGowan et al.*, 2010; *McJannet et al.*, 2013; *Nordbo et al.*, 2011; *Tanny et al.*, 2008). Eddy covariance systems consist of a three-dimensional sonic anemometer (3D-sonic) and an infrared gas analyzer (IRGA) that measure turbulent fluctuations in temperature, atmospheric carbon dioxide, atmospheric water vapor, and three-dimensional wind speed (*Liu et al.*, 2012). The eddy covariance-measured turbulent fluctuations can be used to calculate H and LE. The eddy covariance technique was the method used in this study for direct evaporative measurements. Determining evaporation using direct eddy covariance or scintillometer measurements has the significant drawbacks of advanced technical requirements and high instrument cost.

Environmental and atmospheric influences have varying impacts on the magnitude of open-water evaporation intensity. Atmospheric and environmental variables that have the largest impact on LE include wind speed (U), vapor pressure gradient (Δe) (*Blanken et al.*, 2003; 2011; *Zhang and Liu*, 2014), atmospheric stability (z/L) (*Bouin et al.*, 2012, *Lenters et al.*, 2005; *Verburg and Antenucci*, 2010), and water body size and subsequently wind direction (WD) (*Gibblett*, 1921; *McJannet et al.*, 2013; *Sartori*, 2000; *Weisman and Brutsaert*, 1974); relative importance of these variables is dependent on the timescale of the study (*Bouin et al.*, 2012; *Granger and Hedstrom*, 2011; *Lenters et al.*, 2005; *Nordbo et al.*, 2011). Δe , defined as the difference in vapor pressure between the water surface and atmosphere, U, and their product ($U\Delta e$) all display a positive feedback relationship – as U, Δe , and $U\Delta e$ increase, LE increases. Unstable atmospheric conditions promote H and LE, while stable atmospheric conditions suppress the turbulent fluxes. LE is a

function of water body size because the longer an air parcel travels over water, the lower the Δe between the water surface and air parcel and subsequently the lower the LE. Related to the previous point, wind direction impacts LE as it is an indicator of the fetch and the air's origin. For example, in this study, wind direction can be the difference between a 2 km or 14 km fetch or a continental or maritime airmass.

Directly measuring open-water evaporation with either eddy covariance or scintillometer measurements might not be possible for a multitude of reasons, meaning the community is still in need of process-based models for when direct measurements cannot be obtained. In this study, open-water eddy covariance measurements from the Ross Barnett Reservoir over the entire year of 2008 were used to evaluate the performance of evaporation models. Findings from this study will be applicable to other inland water bodies of similar geographic, physical, and climatic characteristics. The objectives of this study are to evaluate the performance of seven process-based evaporation models over varying timescales and to determine the physical processes that are or are not well parameterized in the models.

2. Methods and Data

2.1. Site Description

Data used in this study were gathered from a tower located near the center of the Ross Barnett Reservoir (hereafter referred to as ‘the Reservoir’). The Reservoir is located just outside Ridgeland, Mississippi ($32^{\circ}26'N$, $90^{\circ}02'W$) and is fed by the Pearl River from the northeast. Discharge from the Reservoir back into the Pearl River is through a 5.6 km man-made spillway along the southwestern shore. The Reservoir ranges in depth from 4 m to 8 m with an approximate area of 134 km^2 . Average water elevation ranges from 90.7 m to 90.2 m above sea level from summer to winter (*Liu et al.*, 2011, *Liu et al.*, 2012, *Zhang and Liu*, 2013).

Measurements were made by instruments on a 5-m aluminum tower (Climatronics Corp.) atop a stationary 9 m^2 wooden platform anchored to the reservoir bed located roughly 1 m above the water surface. The platform is located in the center of the Reservoir with sufficient fetch in all directions, ranging from 2 km to 14 km. The sufficient fetch in all directions allows for minimal impact on turbulent fluxes from the surrounding land. Average water depth around the platform was roughly 5 m throughout the measurement period. (*Liu et al.*, 2011) (Figure 1).

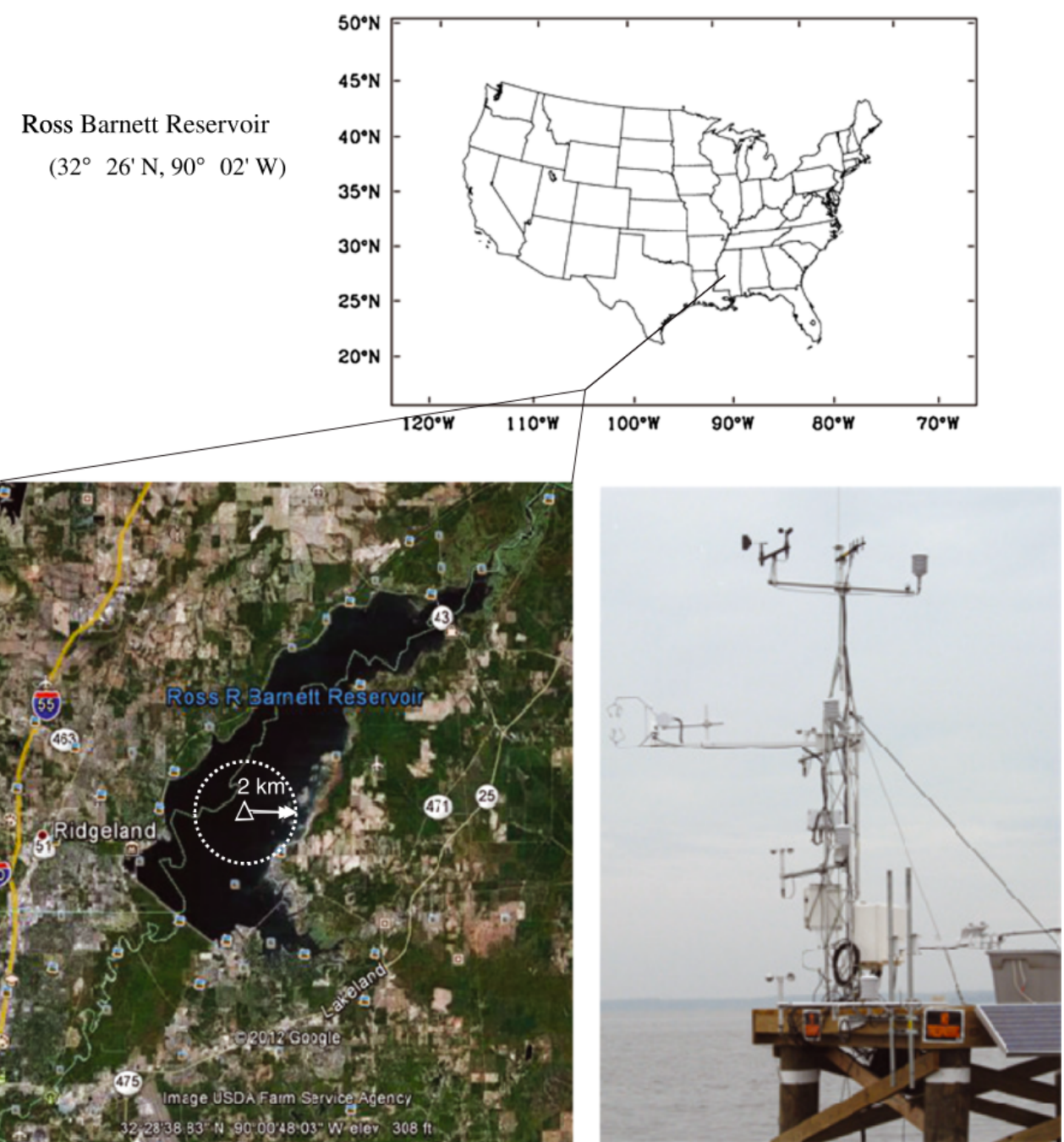


Figure 1: Location of the reservoir in the United States (top panel; Google, 2012), location of platform in the reservoir (bottom left panel), and picture of platform and tower (bottom right panel) (from Zhang and Liu, 2013).

2.2. Instruments

High frequency (10 Hz) data were measured from an eddy covariance system mounted on the 5-m aluminum tower, 4 m above the surface of the water. The eddy covariance system was comprised of an open-path CO₂ and H₂O IRGA (LI 7500, LI-COR Inc.) and a 3D-sonic (CSAT3, Campbell Scientific Inc.). The IRGA measured fluctuations in atmospheric carbon dioxide (ρ_c) and water vapor density (ρ_v), while the 3D-sonic measured fluctuations of sonic temperature (T_{sonic}) and wind velocity components (u, v, and w). 10 Hz signals from the eddy covariance system were recorded with a datalogger (model CR5000, Campbell Scientific Inc.) (*Liu et al.*, 2011).

A variety of microclimate variables were also measured in this study. Net radiation (Rn) was measured with a net radiometer (model Q-7.1, Radiation and Energy Balance Systems Inc.). Incoming shortwave radiation (Q_s) was measured using a silicon pyranometer (model LI-200, LI-COR Inc.). Air temperature (T_a) and relative humidity (RH) profiles were measured using four heights (approximately 1.90, 3.00, 4.00, and 5.46 m above the water surface) of T_a and RH probes (model HMP45C, Vaisala Inc.). The T_a and RH probes were mounted on the south side of the tower with 10-plate radiation shields. Coupled with the T_a and RH probes, wind speed (U) and wind direction (WD) were measured at the four heights. Three 3-cup anemometers (model 03101, RM Young Inc.) were mounted at 1.90, 3.00, and 4.00 m above the water surface to measure U, while wind measurements at 5.46 m were made with a wind sentry unit to measure both U and WD (model 03001, RM Young Inc.). Water surface temperature (T_s) was measured using an infrared thermometer (model IRR-P, Apogee Inc.). The infrared thermometer was mounted on a

1.5 m horizontally-oriented boom approximately 1 m above the surface of the water. A vertical water temperature profile was measured using seven water temperature probes attached to a buoy under the wooden platform anchored into the Reservoir's sediment. The water temperature probes were placed at depths of 0.25, 0.5, 1.0, 1.5, 2.5, 3.5, and 4.5 m below the water's surface (model 107-L, Campbell Scientific Inc.). Measurements from the shallowest water temperature probe (0.25 m) were used for T_s in this study due to a sensor malfunction in the infrared skin temperature sensor. Measurements of rainfall totals were recorded at half-hour intervals using an automated tipping-bucket rain gauge (model TE525, Texas Instruments Inc.). Like the high frequency data, all slow-response data were recorded by the CR5000 datalogger. All instruments mounted on the wooden platform were powered by two 65 W solar panels (model SP65, Campbell Scientific Inc.) and six deep-cycle marine batteries (*Liu et al.*, 2011) (Table 1).

2.3. Evaporation Models

Many methods for quantifying evaporation exist and can be placed in the following five categories of varying measurement requirements: combination methods, solar radiation and temperature group, Dalton group, temperature and day length group, and temperature group. Evaporation equations that fall within the combination methods group are the most measurement-intensive methods, all requiring an available-energy and aerodynamic term in some form (*Rosenberry et al.*, 2007). Combination methods account for both the mechanism by which energy is diffused out from the system and the energy required for evaporation to be sustained

Table 1: List of fast (10 Hz) and slow (1 s) response instruments used in this study (from Zhang, 2012).

Instruments	Variables	Model and Maker	Heights/Depths (m)
<i>Fast response variables measured at 10 Hz</i>			
Three-Dimensional Sonic Anemometer	U, v, w, T _{sonic}	Model CSAT3, Campbell Scientific, Inc.	4.0
Open Path CO₂/H₂O Infrared Gas Analyzer	ρ_v , ρ_c	Model LI-7500, LI-COR, Inc.	4.0
<i>Slow response variables measured at 1 s</i>			
Net Radiometer	R _n	Model Q-7.1, Campbell Scientific, Inc.	1.2
Silicon Pyranometer	Q _s	Model LI-200, LI-COR, Inc.	1.2
Air Temperature and Relative Humidity Probe	T _a , RH	Model HMP45C, Vaisala, Inc.	1.9, 3.0, 4.0, and 5.46
Wind Sentry Unit	U, WD	Model 03001, RM Young, Inc.	5.46
Wind Speed Sensor	U	Model 03101, RM Young, Inc.	1.9, 3.0, and 4.0
Infrared Temperature Sensor	T _s	Model IRR-P, Apogee, Inc.	-
Water Temperature Sensor	T _w	Model 107-L, Model Q-7.1, Campbell Scientific, Inc.	0.10, 0.25, 0.5, 1.0, 1.5, 2.5, 3.5, and 4.5
Tipping Bucket Rain Gauge	Precipitation	Model TE525, Texas Instruments, Inc.	-

(Shuttleworth, 1992). This is frequently done by requiring measurements of Rn, change in heat stored in the water body (Q_x), T_a , U, and atmospheric vapor pressure (e_a); not all combination methods require all the listed measurements. Solar radiation and temperature group evaporation methods require measurement of only shortwave solar radiation (Q_s) and T_a . The Dalton group requires measurements of U, T_s , T_a , e_a , and, if applicable, a site-dependent empirical constant. The final two evaporation groups, temperature and day length group and temperature group, only require measurement of T_a (Rosenberry *et al.*, 2007).

An additional method for determining evaporation is through means of direct measurement or estimation of LE. Measurements or estimates of LE can be used to calculate evaporation as

$$E = \frac{LE}{\rho_w \times l_v} \times UCM, \quad (2)$$

where E is evaporation (mm day^{-1}), LE is latent heat flux (W m^{-2}), ρ_w is density of water (kg m^{-3}), l_v is latent heat of vaporization (J kg^{-1}), and UCM is a unit conversion multiplier used to convert evaporation units from m s^{-1} to mm day^{-1} that is equal to 86,400,000 (Equation 3). For this study, ρ_w was assumed to be a constant equal to 998 kg m^{-3} . Evaporation calculated with LE will hereafter be referred to as “LE evaporation.” LE evaporation with the eddy covariance measurements is assumed to be “true” and all other evaporation models will be compared to it in this study. The evaporation estimation methods that will be compared to LE evaporation all fall within the combination methods group. l_v can be defined as (Dalton *et al.*, 2004)

$$l_v = \left((2.501 - (0.002361 \times T_s)) \times 1,000,000 \right) \approx 2,260,000, \quad (3)$$

where T_s is water surface temperature ($^{\circ}\text{C}$). The multiplier of 1,000,000 is to convert MJ to J. l_v is assumed to be a constant equal to 2,260,000 (J kg^{-1}) in this study.

Six combination methods were used for comparison in this study. The first evaporation model is the Priestley-Taylor (PT) method (*Stewart and Rouse*, 1976) and can be described as

$$E = \left(\alpha \times \left(\frac{s}{s + \gamma} \right) \times \left(\frac{R_n - Q_x}{l_v \times \rho_w} \right) \right) \times UCM, \quad (4)$$

where α is the Priestley-Taylor empirically-derived coefficient (unitless; Equation 5) (*Holtslag and Van Ulden*, 1983), s is the slope of the saturation vapor pressure-temperature curve at mean air temperature ($\text{Pa } ^{\circ}\text{C}$; Equation 6) (*Zotarelli et al.*, 2015), γ is the temperature- and atmospheric pressure-dependent psychrometric “constant” ($\text{Pa } ^{\circ}\text{C}$; Equation 7), R_n is net radiation (W m^{-2}), Q_x is the change in heat stored in the water body (W m^{-2} ; Equation 8) (*Blanken et al.*, 2003; *Lenters et al.*, 2005; *Liu et al.*, 2009; *Nordbo et al.*, 2011).

$$\alpha = \frac{1 + \frac{\gamma}{s}}{1 + BR} \approx 1.26, \quad (5)$$

where BR is the Bowen ratio, defined as the ratio of sensible heat flux and latent heat flux (unitless, Equations 9 and 10). α is, on average, equal to 1.26 and was assumed to be so for this study. An average α value of 1.26 has been frequently validated using experimental data (e.g., *Baldocchi*, 1994; *Davies and Allen*, 1973; *deBruin and Keijman*, 1979; *Eichinger et al.*, 1996; *Stewart and Rouse*, 1977). It is assumed that α will remain relatively constant when there are no moisture constraints (*Stewart and Rouse*, 1976), meaning that a constant α of 1.26 is a good assumption for this study.

$$s = \frac{4098 \times \left(0.6108 \times e^{\frac{17.27 \times T_a}{T_a + 237.3}}\right)}{(T_a + 237.3)^2} \times 1000, \quad (6)$$

where T_a is the mean air temperature. All multipliers of 1,000 are to convert kPa to Pa.

$$\gamma = \frac{C_{p,a} \times P}{l_v \times MW_{ratio}} \times 1000, \quad (7)$$

where $C_{p,a}$ is the specific heat of air at constant pressure ($\text{J kg}^{-1} \text{ }^\circ\text{C}^{-1}$) equal to $1,013 \text{ J kg}^{-1} \text{ }^\circ\text{C}^{-1}$, P is atmospheric pressure (Pa), and MW_{ratio} is the ratio of molecular weight of water vapor and molecular weight of dry air (unitless) equal to 0.622.

$$Q_x = \rho_w \times C_{p,w} \times z \times \frac{\Delta\bar{T}_w}{\Delta t} \times \frac{1}{86,400}, \quad (8)$$

where $C_{p,w}$ is the specific heat of water ($\text{J kg}^{-1} \text{ }^{\circ}\text{C}^{-1}$) equal to $4,182 \text{ J kg}^{-1} \text{ }^{\circ}\text{C}^{-1}$, z is the total water depth of the profile measurement (m) equal to 4.5 m , $\frac{\Delta\bar{T}_w}{\Delta t}$ is the change in water temperature over the period Δt ($^{\circ}\text{C time}^{-1}$), $\Delta\bar{T}_w$ is the water temperature averaged from all layers ($^{\circ}\text{C}$). Daily averaging periods were used for Δt ($^{\circ}\text{C day}^{-1}$). The multiplier of $\frac{1}{86,400}$ is to convert $\text{J day}^{-1} \text{ m}^{-2}$ to W m^{-2} .

$$BR = \frac{H}{LE}, \quad (9)$$

where H is sensible heat flux (W m^{-2}) and LE is latent heat flux (W m^{-2}). BR can also be expressed as

$$BR = c_B \times P_{std} \times \frac{T_s - T_a}{e_s - e_a}, \quad (10)$$

where c_B is an empirical constant (unitless) determined by Bowen (1926) equal to 0.61 , P_{std} is standard pressure at the Reservoir's altitude (Pa) (Allen *et al.*, 2008; Equation 11), and e_s is saturation vapor pressure at the water's surface (Pa) (Lowe, 1977; Equation 12).

$$P_{std} = 101.3 \times \frac{293 - 0.0065 \times alt}{293} \times 1,000, \quad (11)$$

where alt is altitude above sea level (m).

$$e_s = a_0 + T \left(a_1 + T \left(a_2 + T \left(a_3 + T \left(a_4 + T \left(a_5 + (a_6 \times T) \right) \right) \right) \right) \right) \times 100, \quad (12)$$

where T is the temperature of the air above the water-atmosphere interface ($^{\circ}\text{C}$ or K), assumed to be equal to T_s for this study, and a_{0-6} are empirical constants (Table 2). The multiplier of 100 is

Table 2: Empirical coefficients used in Lowe's saturation vapor pressure sixth-order polynomial for temperature in $^{\circ}\text{C}$ and K (Lowe, 1977).

Empirical Coefficient	Temperature ($^{\circ}\text{C}$)	Temperature (K)
a₀	6.107799961	6984.505294
a₁	$4.436518521 \times 10^{-1}$	-188.9039310
a₂	$1.428945805 \times 10^{-2}$	2.133357675
a₃	$2.650648471 \times 10^{-4}$	$-1.288580973 \times 10^{-2}$
a₄	$3.031240396 \times 10^{-6}$	$4.393587233 \times 10^{-5}$
a₅	$2.034080948 \times 10^{-8}$	$-8.023923082 \times 10^{-8}$
a₆	$6.136820929 \times 10^{-11}$	$6.136820929 \times 10^{-11}$

to convert from hPa to Pa.

The second combination method used in this study is the deBruin-Keijman (DBK) method (*deBruin and Keijman*, 1979) can be described as

$$E = \left(\frac{s}{(0.85 \times s) + (0.63 \times \gamma)} \times \left(\frac{R_n - Q_x}{l_v \times \rho_w} \right) \right) \times UCM. \quad (13)$$

The method for quantifying DBK evaporation is similar to the PT evaporation method, and the only difference between the two is the lack of α and the coefficients in the denominator of the first term of the DBK evaporation method.

The Bowen Ratio Energy Budget (BREB) method for estimating evaporation (*Ficke*, 1972; *Sturrock*, 1978) is considered one of the most robust methods of estimating evaporation (*Brutsaert*, 1982; *Gunaji*, 1968; *Harbeck et al.*, 1958; *Lenters et al.*, 2005; *Sturrock et al.*, 1992). BREB evaporation can be expressed as

$$E = \left(\frac{Q_s - Q_r + Q_a - Q_{ar} - Q_{bs} - Q_x + Q_v - Q_b}{\rho_w \times (l_v \times (1 + BR) + c_{p,w} \times T_s)} \right) \times UCM, \quad (14)$$

where Q_r is reflected solar shortwave radiation (W m^{-2}), Q_a is incoming atmospheric longwave radiation (W m^{-2}), Q_{ar} is reflected atmospheric longwave radiation (W m^{-2}), Q_{bs} is longwave

atmospheric radiation emitted from the water surface (W m^{-2}), Q_v is net energy from precipitation, surface water, and ground water (W m^{-2}), and Q_b is net energy conducted from the lake to the sediments (W m^{-2}). The sum of the first five terms of Equation 13, $Q_s - Q_r + Q_a - Q_{ar} - Q_{bs}$, are equal to Rn . Q_v and Q_b are frequently neglected and were subsequently neglected for this study. Equation 14 can therefore be represented as

$$E = \left(\frac{Rn - Q_x}{\rho_w \times (l_v \times (1 + BR) + c_{p,w} \times T_s)} \right) \times UCM. \quad (15)$$

BR used in the BREB method is typically calculated using Equation 10 rather than Equation 9 because direct measurements of H and LE are likely not available. It is important to note that the BREB method has been assumed to be “true” in multiple studies where direct evaporation measurements were not available (e.g., *Dalton et al.*, 2004; *Rosenberry et al.*, 2004; 2007; *Winter et al.*, 1995).

The final three combination methods that were used to estimate evaporation in this study are the Penman (PM) method (*Brutsaert*, 1982; Equation 16), the Brutsaert-Stricker (BS) method (*Brutsaert and Stricket*, 1979; Equation 17), and the deBruin (DB) method (*deBruin*, 1978; Equation 18) and can be described as

$$E = \left(\frac{s}{s + \gamma} \right) \left(\frac{Rn - Q_x}{l_v \times \rho_w} \right) \times UCM + \left(\frac{s}{s + \gamma} \right) (0.26 \times (0.5 + 0.54 \times U) \times (e_s - e_a)), \quad (16)$$

$$E = (2\alpha - 1) \left(\frac{s}{s + \gamma} \right) \left(\frac{Rn - Q_x}{l_v \times \rho_w} \right) \times UCM + \left(\frac{s}{s + \gamma} \right) (0.26 \times (0.5 + 0.54 \times U) \times (e_s - e_a)), \quad (17)$$

$$E = 1.192 \times \left(\frac{\alpha}{\alpha - 1} \right) \left(\frac{s}{s + \gamma} \right) \left(\frac{(2.9 + 2.1 \times U)(e_s - e_a)}{l_v \times \rho_w} \right) \times UCM, \quad (18)$$

where e_s and e_a are in hPa.

3. Results and Discussion

3.1. General climate

Data used in this study were measured over the entire year of 2008. All data, both fast- and slow-response readings, were averaged into 30-minute averages. 30-minute averages were used to smooth out naturally-occurring fluctuations in the data, while still maintaining a discernible diurnal variation. The quality and availability of the data were overall good throughout the year of 2008. Thirty-minute data availability for Rn, H, LE, U, T_a, RH, and all-layer water temperature were 97.2%, 92.3%, 92.2%, 91.9%, 93.1%, 93.1%, and 94.7%, respectively.

3.1.1. Annual variability in local meteorology

Weekly averages of 2-meter air temperature, all-layer water temperature, 2-meter relative humidity (RH), 2-meter wind speed, and atmospheric pressure were calculated to display the meteorological variability of this location; weekly sums of precipitation were also calculated for the same purpose (Figure 2). Mean air and water temperature ranged from roughly 5°C during the end of January to roughly 30°C during the end of July and remained relatively close in magnitude throughout the year. Interestingly, weekly averages of all-layer water temperature were generally

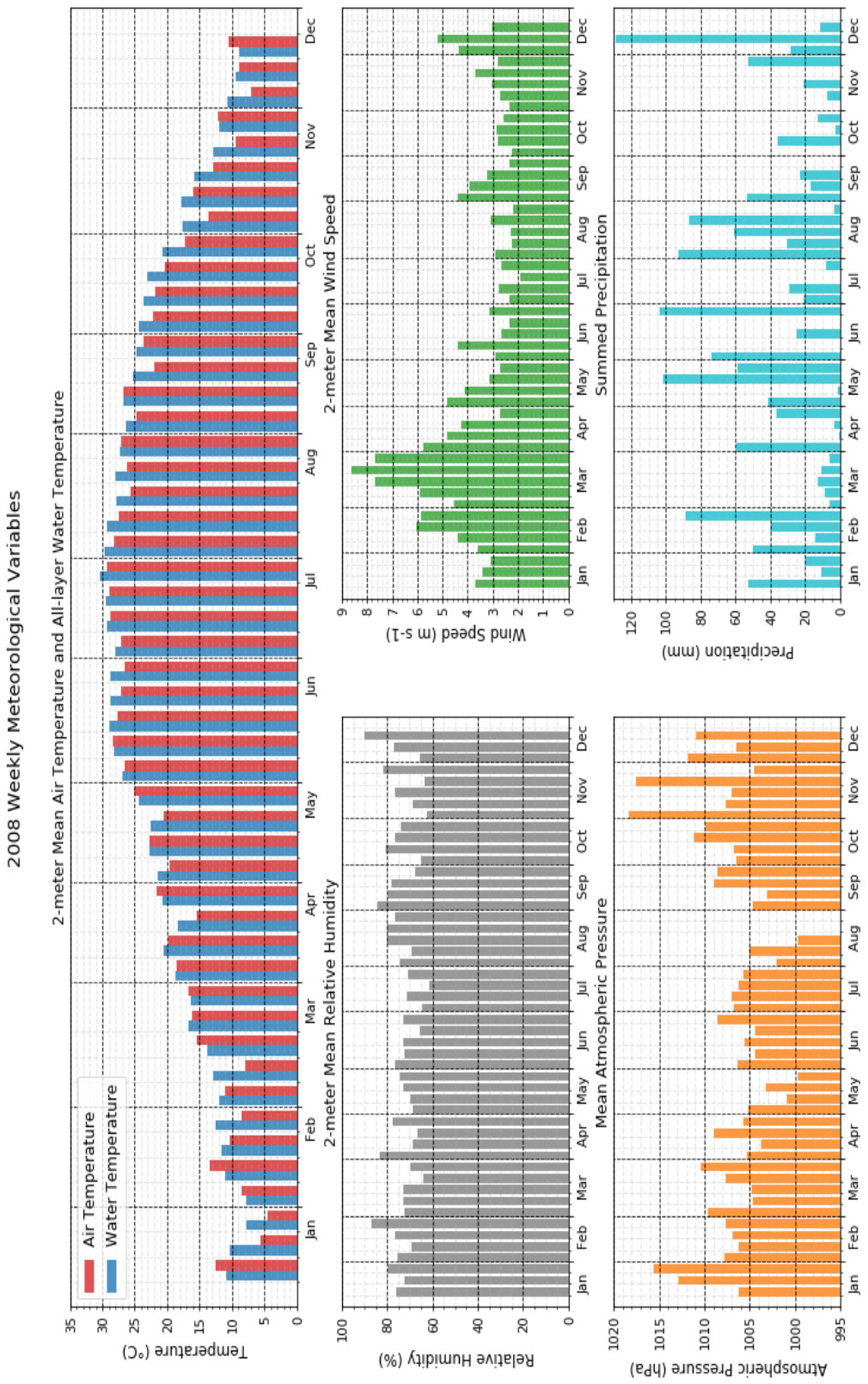


Figure 2: Weekly averages of 2-meter air temperature ($^{\circ}\text{C}$) and all-layer water temperature ($^{\circ}\text{C}$), 2-meter relative humidity (%), 2-meter wind speed (m s^{-1}), and atmospheric pressure (hPa) and weekly sums of precipitation (mm) for 2008.

larger in magnitude, even reaching a greater maximum, than 2-meter air temperature weekly averages. This trend could have been a result of mean 2-meter air temperature having larger diurnal variability than all-layer water temperature (due to a higher specific heat for water) and subsequently lower weekly averages due to the lower nocturnal 2-meter air temperatures. All-layer water temperature became increasingly greater in magnitude than 2-meter air temperature as the year transitioned from the warm season to the end-of-the-year cool season, which can be more easily seen in monthly averages (Figure 3). This trend could also likely be explained by the greater thermal inertia of water, meaning there was a temporal lag between the seasonal change in air temperature and water temperature.

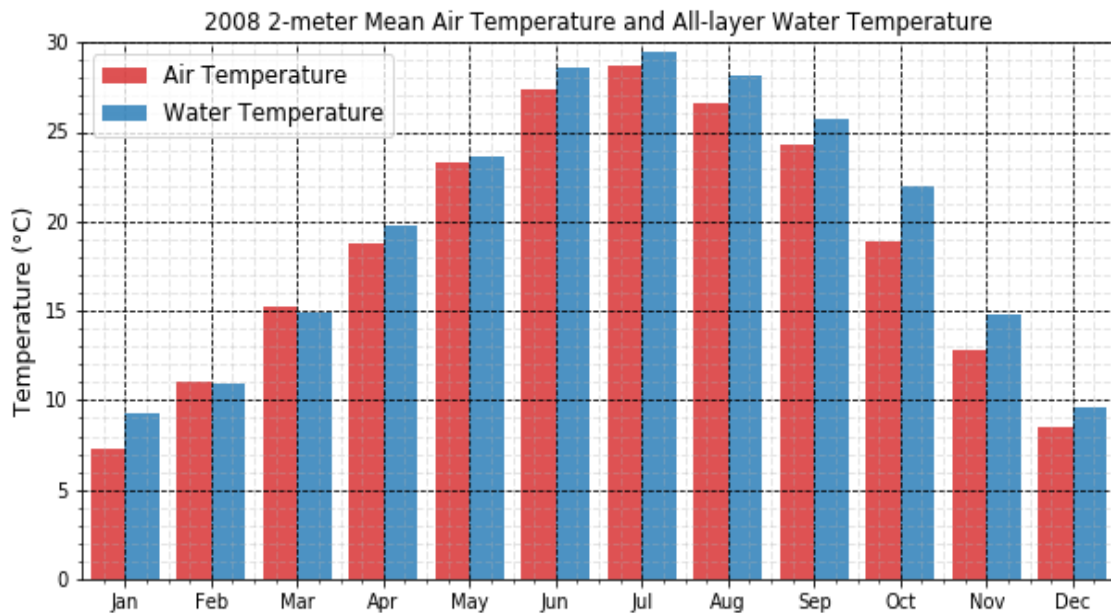


Figure 3: Monthly averages of 2-meter mean air temperature (°C) and all-layer water temperature (°C) for 2008.

Weekly averages of 2-meter RH remained relatively consistent throughout the year, ranging from roughly 65% to up to 90% (Figure 2). The consistently moist atmospheric conditions and relatively warm temperatures were indicative of the subtropical climate associated with the latitude of the reservoir. It should be noted that the RH weekly averages might not have been indicative of the surrounding land due to the instrument being in the middle of the reservoir.

2-meter wind speed weekly averages ranged from roughly 2 m s^{-1} to 8.5 m s^{-1} throughout 2008, but also displayed a large seasonal dependence (Figure 2). Weekly mean wind speeds throughout February and March were consistently high, ranging from roughly 3.5 m s^{-1} to 8.5 m s^{-1} , while wind speed weekly averages ranged from roughly 2 m s^{-1} to 5 m s^{-1} throughout the rest of the year. The cause of the relatively high wind speeds during the beginning of the spring transitional season was likely to be the strong temperature- and subsequent pressure-gradients that tend to exist during this time of year. It is interesting to note that the months with relatively high wind speeds were the only months where 2-meter air temperature monthly averages exceeded monthly averages of all-layer water temperature.

Weekly-averaged atmospheric pressure throughout 2008 displayed slight seasonal variation, with relatively high (low) pressure occurring during the cool (warm) months (Figure 2). Mean atmospheric pressure ranged from roughly 1000 (1005) hPa to 1010 (1018) hPa during the warm (cool) season. Excluding August, which was plagued with data gaps, lowest monthly pressure occurred in May, while highest pressures were recorded during November.

Little to no discernible trend was displayed by weekly sums of precipitation throughout 2008. The lowest weekly precipitation sums occurred during the month of March, while the highest precipitation weeks occurred during May and August. It is interesting to note that the highest sums of precipitation occurred during the months in which atmospheric pressure was the lowest, which can more easily be seen in monthly averages (sums) of atmospheric pressure (precipitation) (Figure 4). The two months with lowest atmospheric pressure and highest precipitation, May and August, had precipitation on nearly every day with roughly 11 and 13 days impacted by frontal passages, respectively. It is also interesting to note that two tropical systems made landfall near Mississippi during August that resulted in precipitation at the study location.

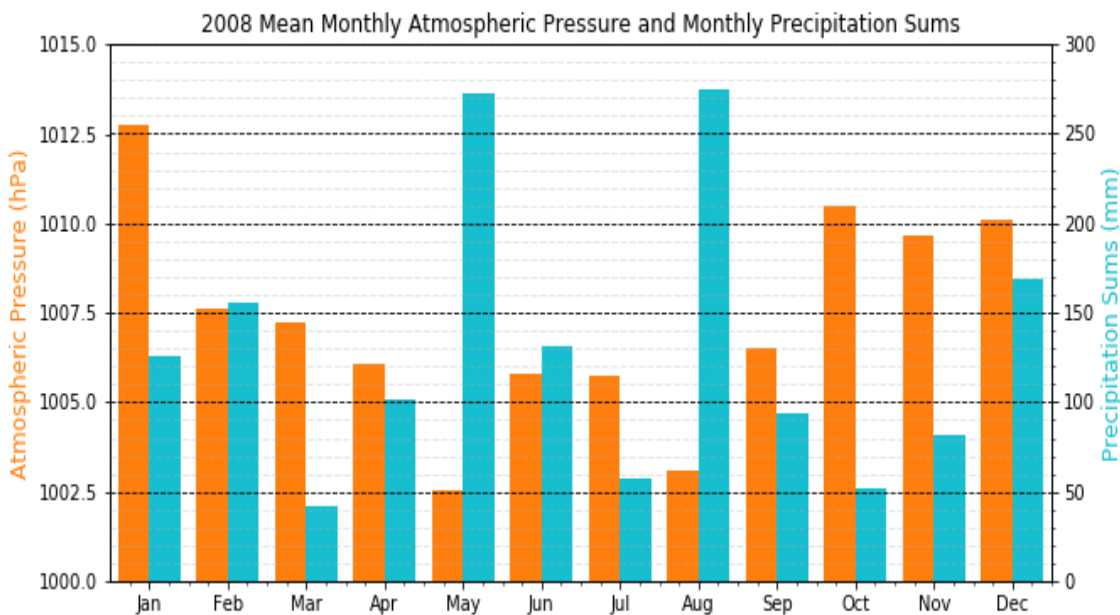


Figure 4: Monthly averages of atmospheric pressure (hPa) and sums of precipitation (mm) for 2008.

3.1.2. Annual variability in local surface energy budget

Weekly averages of local surface energy budget (SEB) components, such as Rn, H, LE, and Q_x, were calculated to characterize the annual variability in SEB components for the reservoir (Figure 5). Note that the scale for the Q_x term was made different than other SEB terms because of the relative magnitude between terms. Seasonal variation could be seen Rn, LE, and Q_x. These three SEB components all tended to increase in magnitude from the beginning of the year through July, before steadily decreasing throughout the remainder of the year. This was an expected result, because as Rn increased from the beginning of the year through the summer, more energy was available to drive evaporation and to be stored in the water, causing LE and Q_x to increase. On the other hand, as Rn decreased in magnitude from the summer to the winter, LE and Q_x decrease in magnitude because of the lessening amount of available energy.

The lack of a discernible seasonal variation in H was likely a result of how dominant a turbulent flux LE was relative to H due to the availability of moisture at this site. Relative magnitude between H and LE could more easily be seen in weekly averages of BR (Figure 6). BR averages ranged in magnitude from near-zero to 0.7 and always remained below 1, meaning LE was always greater than H.

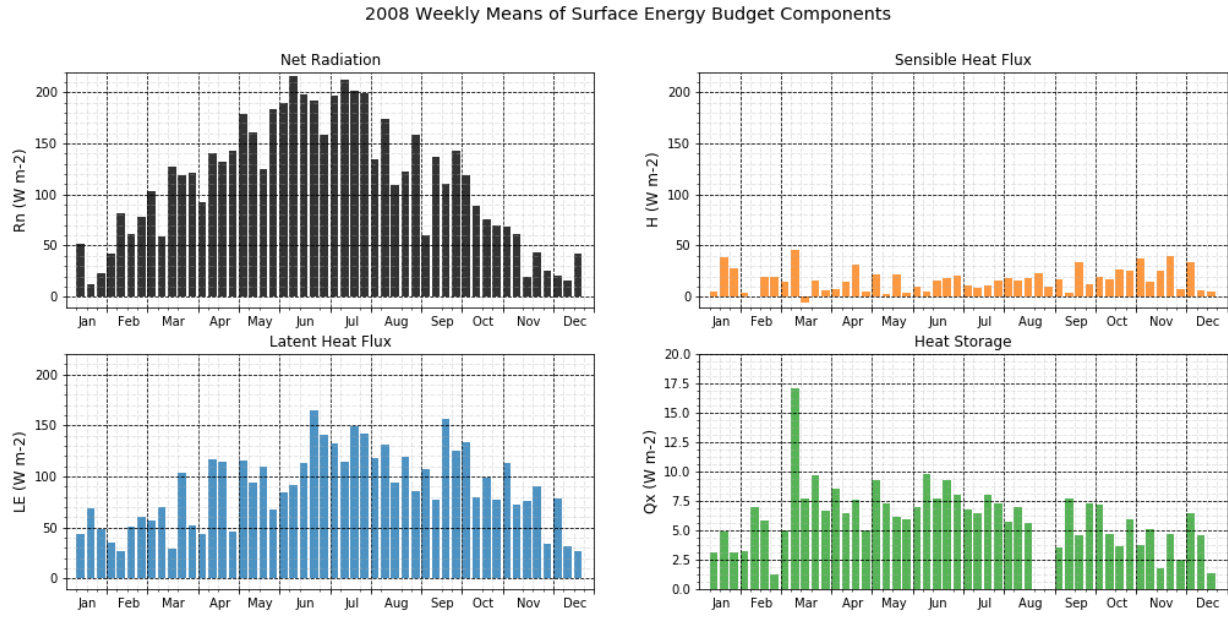


Figure 5: Weekly averages of net radiation (R_n ; W m^{-2}), sensible heat flux (H ; W m^{-2}), latent heat flux (LE ; W m^{-2}), and energy storage (Q_x ; W m^{-2}) for 2008.

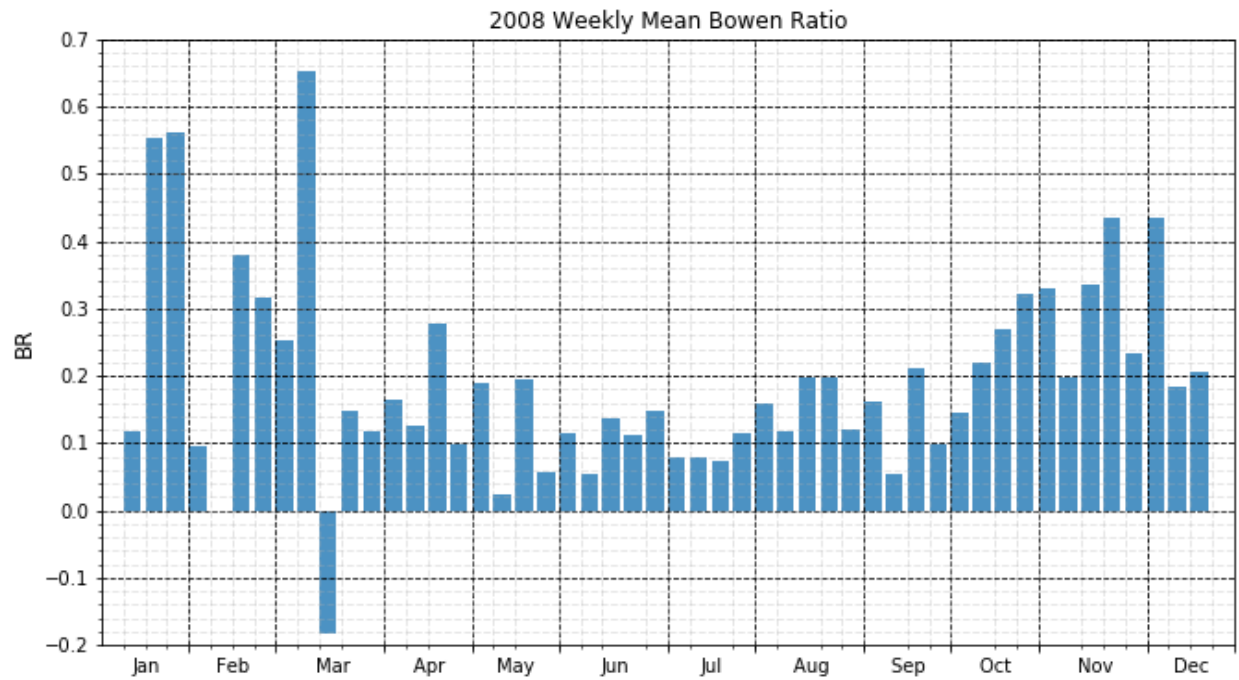


Figure 6: Weekly mean Bowen ratio (BR; unitless) for 2008.

3.2. Performance of evaporation models under multiple temporal scales

3.2.1. Validating modeled evaporation performance with $H + LE$ in place of $Rn - Q_x$

When evaluating the performance of a model, it is important to remove all possible error from model inputs. Doing so will ensure that results for the performance of the model are true and not being altered by factors outside the model's control. Previous studies have encountered complications in evaporation estimation related to the in situ determination of $Rn - Q_x$ (Vercauteren et al., 2009; Guo et al., 2015). Studies in which the errors associated with using $Rn - Q_x$ were avoided, $H + LE$, if available, were substituted in to take their place. This substitution can be made by making the assumption of energy balance, which states that $Rn - Q_x$ is equal to $H + LE$.

In this study, evaporation estimations using the PT model were made using both $Rn - Q_x$ and $H + LE$ for a preliminary test to determine if it would be necessary or beneficial to use $H + LE$ to associate any errors in evaporation estimation to any particular model rather than using $Rn - Q_x$. PT was chosen for this test because it was one of the best-performing models evaluated in this study. However, among the other top-performing models, PT was arbitrarily chosen. Performance of the PT model in differing timescales relative to other modeled methods will be explained in much greater detail in subsequent sections. PT evaporation was calculated using $Rn - Q_x$ (Figure 7a, c, e) and $H + LE$ (Figure 7b, d, f) for monthly (Figure 7a, b), daily (Figure 7c,

PT vs. Measured Evaporation using $Rn - Q_x$ and $H + LE$ for Monthly, Daily, and 30-minute Timescales

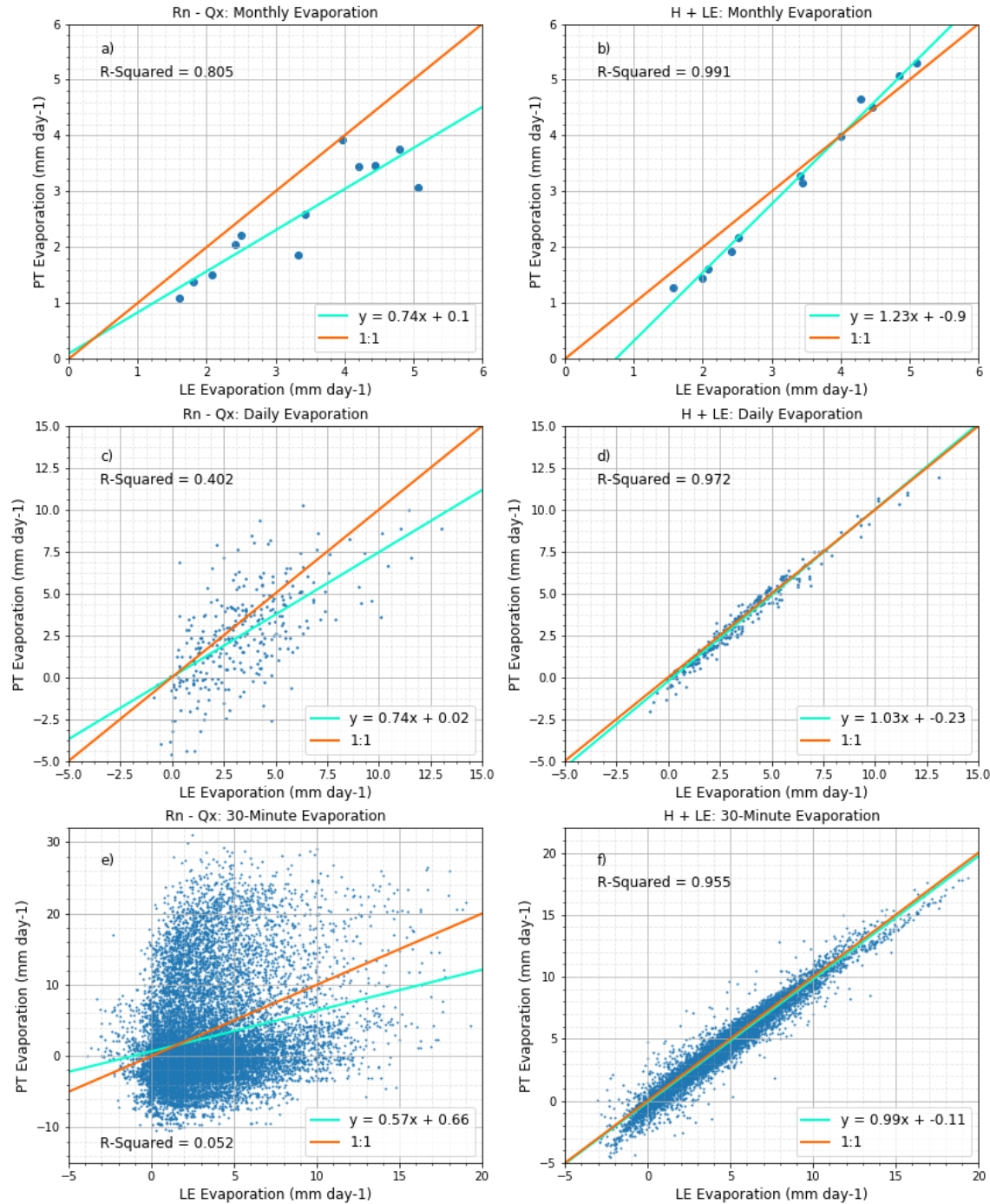


Figure 7: Linear regressions of PT modeled evaporation (mm day^{-1}) versus measured evaporation (mm day^{-1}) using $Rn - Q_x$ (a, c, e) and $H + LE$ (b, d, f) for monthly (a, b), daily (c, d), and 30-minute (e, f) for 2008.

d), and 30-minute (Figure 7e, f) timescales. Throughout all timescales, PT evaporation was able to explain more of the variance in measured evaporation as the timescale decreased for both $Rn - Q_x$ and $H + LE$. Although both $Rn - Q_x$ and $H + LE$ caused PT evaporation to decrease in ability to explain the variance in measured evaporation, the magnitude of which the R^2 decreased as timescale shortened was much larger when using $Rn - Q_x$. For example, the R^2 for $Rn - Q_x$ ($H + LE$) decreased from 0.805 (0.991) to 0.402 (0.972) when the timescale shortened from monthly to daily and from 0.402 (0.972) to 0.052 (0.955) when the timescale shortened from daily to 30-minute; R^2 values decreased by 0.753 between monthly to 30-minute timescales or $Rn - Q_x$, while $H + LE$ only decreased by 0.036. The cause of the decrease in PT evaporation's ability to explain the variance of measured evaporation as timescales shortened for both $Rn - Q_x$ and $H + LE$ is likely due to measurement errors or anomalous occurrences being less "averaged-out" as timescales decrease. $Rn - Q_x$ causing a larger decrease in R^2 value magnitude as timescales shortened relative to the decrease in R^2 values associated with $H + LE$ can be attributed to the difficulty of measuring and calculating Rn and Q_x – particularly Q_x . It was therefore determined that using $Rn - Q_x$ for analysis of model performance would introduce external errors outside of the control of the models. *As a result, $Rn - Q_x$ were replaced with $H + LE$ wherever applicable.*

3.2.2. Performance of evaporation models on a monthly temporal scale

Monthly averages of measured, LE, and all modeled evaporation methods, PT, DBK, BREB, PM, BS, and DB, were calculated for the year of 2008, with typical measured values ranging from roughly 2 to 5 mm day⁻¹. A time series of these evaporation calculations, with

standard error used for the error bars, was used to show the monthly estimation of evaporation for all the methods (Figure 8). All methods show a similar general trend throughout the year, increasing from the beginning of the year until July, before steadily decreasing throughout the remainder of the year; this was an expected result as this was the seasonal trend LE measurements followed. Modeled methods PT, DBK, and BREB followed the seasonal trend of LE evaporation the closest of all models, with overlapping error bars for nearly every month. PM and BS models followed the seasonal trend of LE evaporation well from June through the rest of the year, but deviated from LE evaporation by a relatively large amount during the spring months. DB evaporation typically performed the worst of all modeled methods throughout the year, particularly from the beginning of the year until June. The poor performance of the PM, BS, and DB models during the beginning of the year, particularly during March, was likely due to the inclusion or method of inclusion of wind speed in these models; March was the month with the highest wind speed and was consistently the month with the highest magnitude of under/overestimation of evaporation for these models. The method in which wind speed was included in the models did not work well for such high average wind speeds. The method in which wind speed was implemented in the model also seemed to determine whether the wind speed-dependent models, PM, BS, and DB, underestimated or overestimated evaporation. For example, PM and DB positively implemented wind speed into the model by addition and multiplication, respectively, and had general biases toward the overestimation of evaporation during the high wind speed months. On the other hand, BS negatively implemented wind speed into the model via subtraction and had a general bias toward the underestimation of evaporation for the same months.

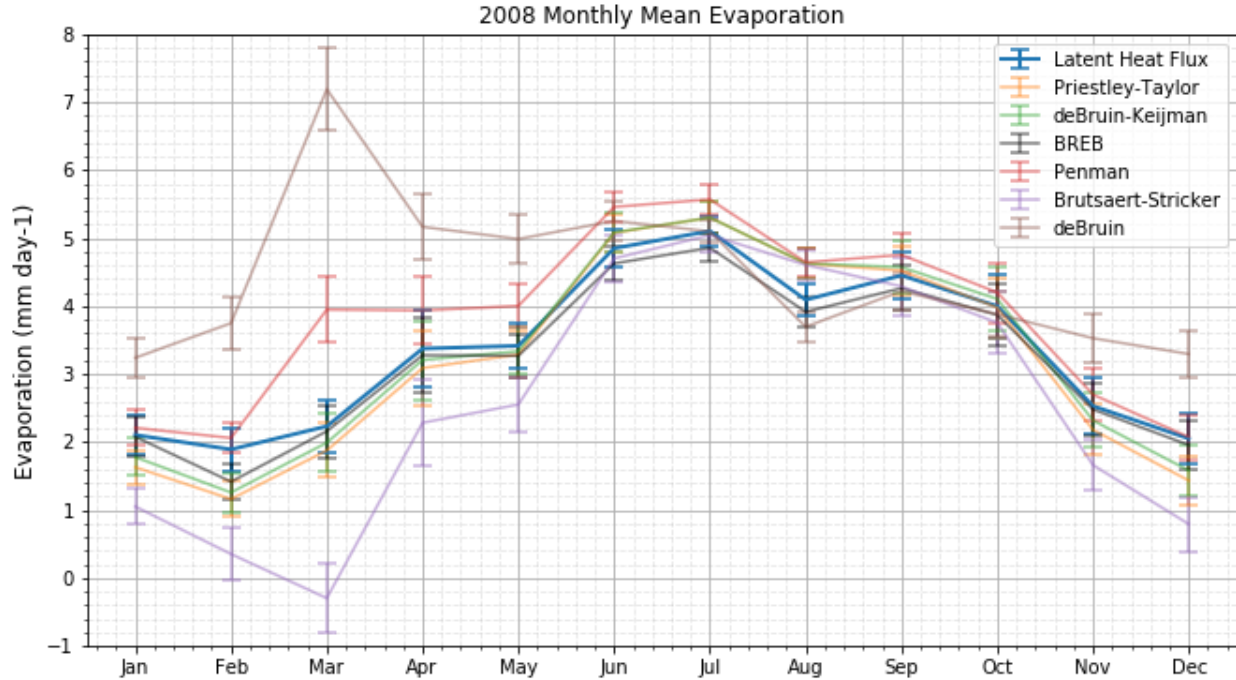


Figure 8: Monthly mean evaporation for measured (LE) evaporation and modeled (PT, DBK, BREB, PM, BS, and DB) evaporation (mm day^{-1}) for 2008. Standard error was used as the error bars.

Monthly evaporation difference and percent error ranged from roughly -0.9 to 0.6 mm day^{-1} and -60 to 40%, respectively, for both PT and DBK models (Figure 9). The seasonal variation in modeled and measured evaporation difference for PT and DBK models also displayed a similar trend; generally underestimating during the cool months and overestimating during the warm months. The only months in which PT and DBK had inconsistencies in sign of under/overestimation were September and October, although slight in magnitude. BREB-modeled evaporation consistently underestimated evaporation throughout the year, with evaporation differences and percent error ranging from roughly -0.7 to 0 mm day^{-1} and -45 to 0%, respectively. Excluding the month of February, a slight seasonal trend in BREB underestimation could be seen,

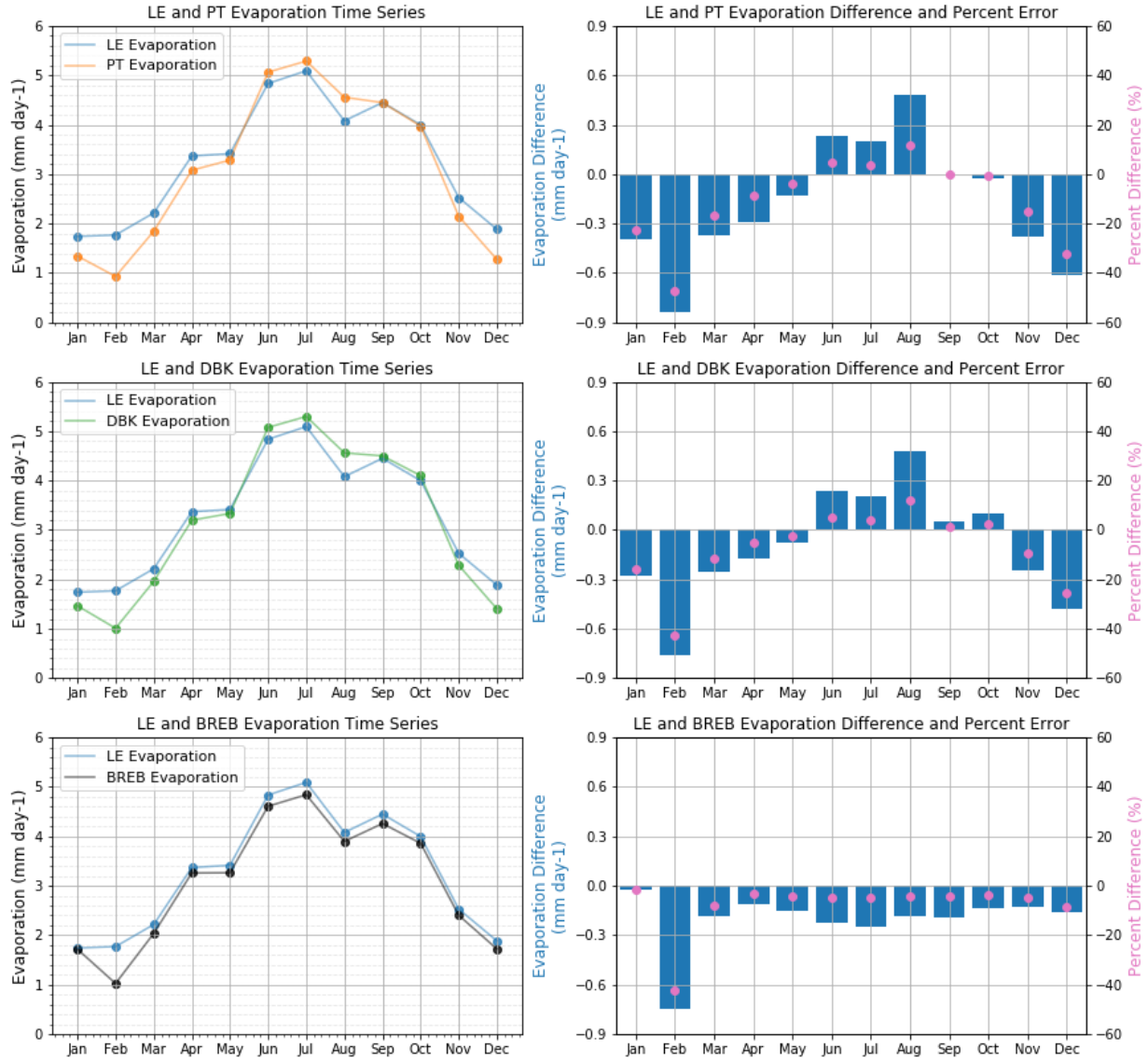


Figure 9: Monthly measured (LE) and modeled (PT, DBK, and BREB) evaporation (mm day^{-1}) time series (left column) and monthly measured (LE) and modeled (PT, DBK, and BREB) evaporation difference (mm day^{-1} ; in blue) and percent error (%) (in pink) (right column) for 2008.

in which the magnitude of BREB evaporation underestimation increased from the beginning of the year to July, before decreasing in magnitude through the remainder of the year. Consistent throughout the PT, DBK, and BREB evaporation models, under/overestimation magnitude were largest during the month of February; all models underestimated evaporation during February. The cause of the largest magnitude of evaporation difference between modeled and measured evaporation occurring in February for all three methods was likely due to the relative difference in number of missing points between measured and modeled calculations. For example, the three months with the most 30-minute data gaps were January, February, and December. Missing points for measured (modeled) during the months of January, February, and December were 526 (526, 526, and 532), 347 (760, 760, and 780), and 457 (550, 550, and 586), respectively, for LE (PT, DBK, and BREB modeled) evaporation. Data gaps associated with a malfunction in the pressure sensor during the latter half of August were likely to be the cause of the relatively high overestimation of evaporation in monthly modeled PT and DBK evaporation in August. The August data gaps caused the overestimation for the same reason data gaps caused underestimation during February.

Monthly evaporation differences and percent error ranged from 0 to roughly 2 mm day^{-1} and 0 to roughly 90%, respectively, for the PM model (Figure 10). Evaporation was consistently overestimated between measured and PM-modeled evaporation and tended to decrease in magnitude as the year progressed past March. Monthly evaporation differences and percent error for the BS model ranged from roughly -2.5 to 0.5 mm day^{-1} and -125 to 25%, respectively. Slight seasonal variation could be observed in under/overestimation of evaporation difference and

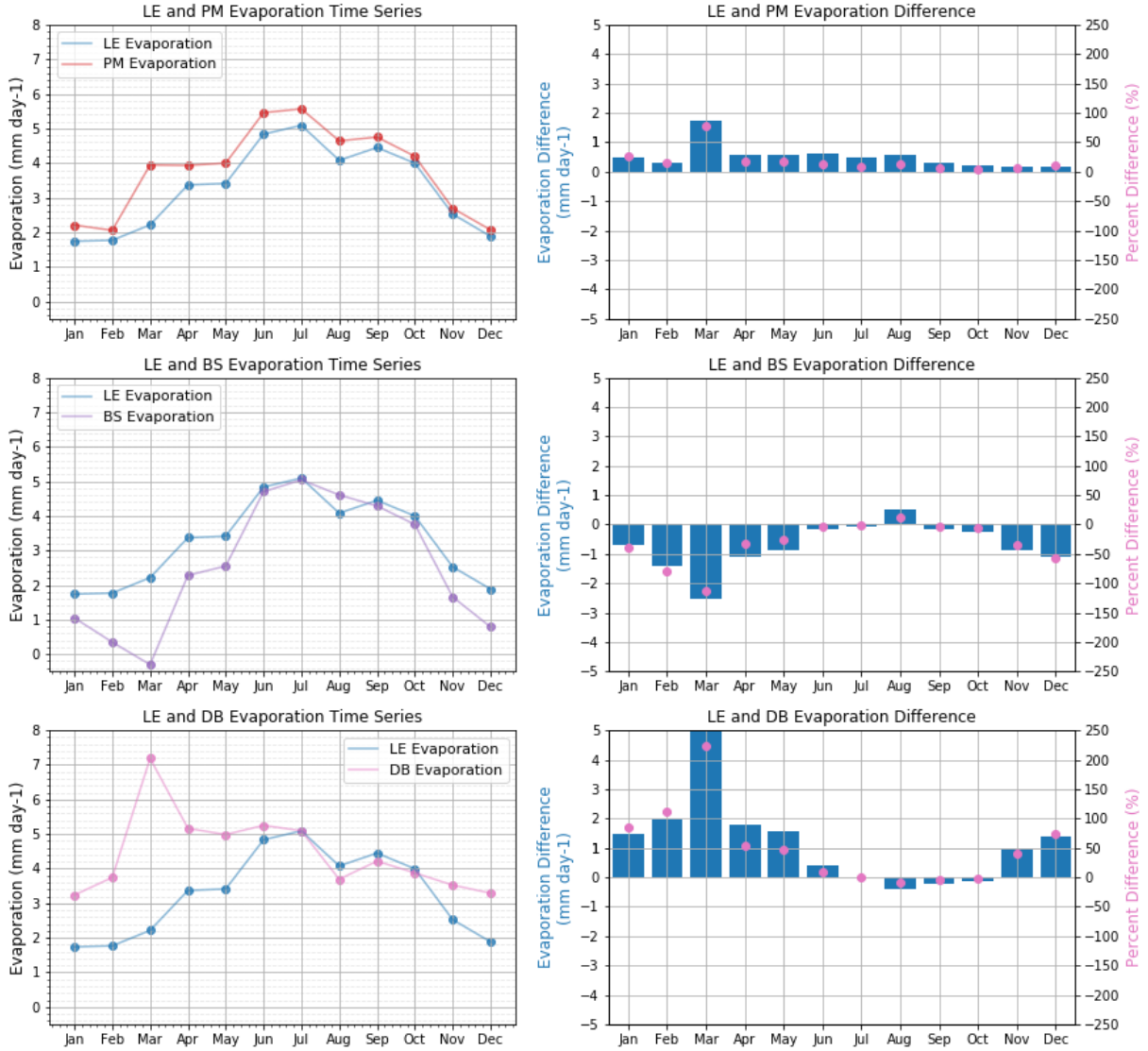


Figure 10: Monthly measured (LE) and modeled (PM, BS, and DB) evaporation (mm day^{-1}) time series (left column) and monthly measured (LE) and modeled (PM, BS, and DB) evaporation difference (mm day^{-1} ; in blue) and percent error (%) (in pink) (right column) for 2008.

percent error for the DB model, which ranged in magnitude from roughly -0.5 to 5 mm day⁻¹ and -10 to 225%, respectively. Poor performance in the PM, BS, and DB models in March, the month with the largest magnitude of evaporation difference, could also easily be found in this figure due to the previously-mentioned errors associated with high wind speeds during this month.

The ability for the variance in monthly measured evaporation to be explained by modeled evaporation estimation methods differed between methods. PT, DBK, and BREB all perform well with R^2 values of 0.987, 0.987, and 0.980, respectively (Figure 11a, b, c). Of the three top-performing models, it should be noted that the BREB method followed the 1:1 line most closely with a slope and intercept of 1.02 and -0.28, respectively. The PM and BS models both performed relatively well on a monthly timescale with R^2 values of 0.891 and 0.912, respectively (Figure 11d, e). Although the BS model could explain more of the variance in measured evaporation, the PM model followed the 1:1 line more closely with a slope of 0.97 and an intercept of 0.61, meaning little seasonal variation and a consistent bias toward overestimating evaporation. The DB model had the most difficulty estimating monthly evaporation of all models with an R^2 of only 0.054 (Figure 11f). It is likely that DB performed the worst of all methods due to the lack of inclusion of an $Rn - Q_x$, or in this case $H + LE$, term. Without an $Rn - Q_x$ or $H + LE$ term, seasonal variations in evaporation were not captured well, particularly when wind speeds were high.

Evaporative models on a monthly temporal scale fell into three tiers of performance based on their ability to explain the variance of measured evaporation, consistency in monthly bias, and

Monthly Modeled vs. Measured Evaporation

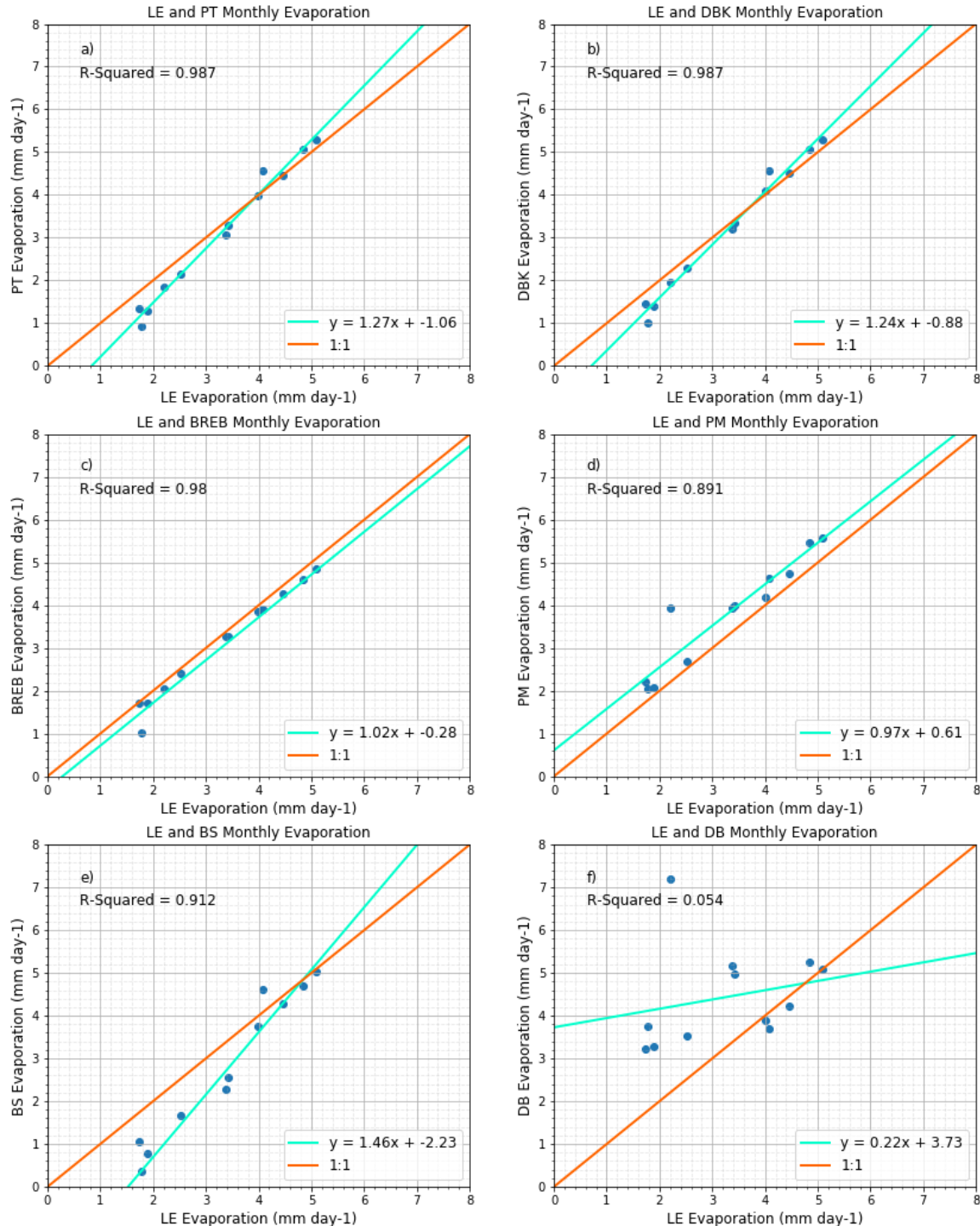


Figure 11: Linear regressions of monthly modeled PT (a), DBK (b), BREB (c), PM (d), BS (e), and DB (f) evaporation (mm day^{-1}) versus measured LE evaporation (mm day^{-1}) for 2008.

magnitude of evaporation difference. PT, DBK, and BREB models fell into the top tier due to their high R^2 values and relatively low magnitude of evaporation difference. Although PT and DBK could explain the variance of measured evaporation slightly better, BREB overall performed better than PT and DBK due to the easily-correctable, consistent bias throughout the year. PM and BS models fell into the middle performance tier due to their lower R^2 values and higher evaporation differences relative, particularly in the beginning of the year, to the top tier models. Among the middle performance tier, the PM model ranked higher than the BS model because of the consistent bias throughout the year, despite BS having been able to explain slightly more of the variance of measured evaporation. The DB model fell into the lowest performance tier because of its relatively poor estimation of evaporation, particularly in the first five months of 2008, relative to the other models. The DB model also explained the variance in measured evaporation very poorly relative to the other models.

3.2.3. Performance of evaporation models on a daily temporal scale

Average daily values of measured and modeled evaporation were calculated for 2008, with typical measured values ranging from roughly -1 to 13 mm day $^{-1}$. Daily time series of LE evaporation with modeled PT, DBK, and BREB evaporation revealed that modeled daily averages followed measured averages well (Figure 12). PT and DBK daily averages of evaporation were similar in magnitude throughout the year, ranging from roughly -2 to 13 mm day $^{-1}$. BREB daily averages of modeled evaporation ranged from roughly -1 to 13 mm day $^{-1}$. Daily-averaged modeled

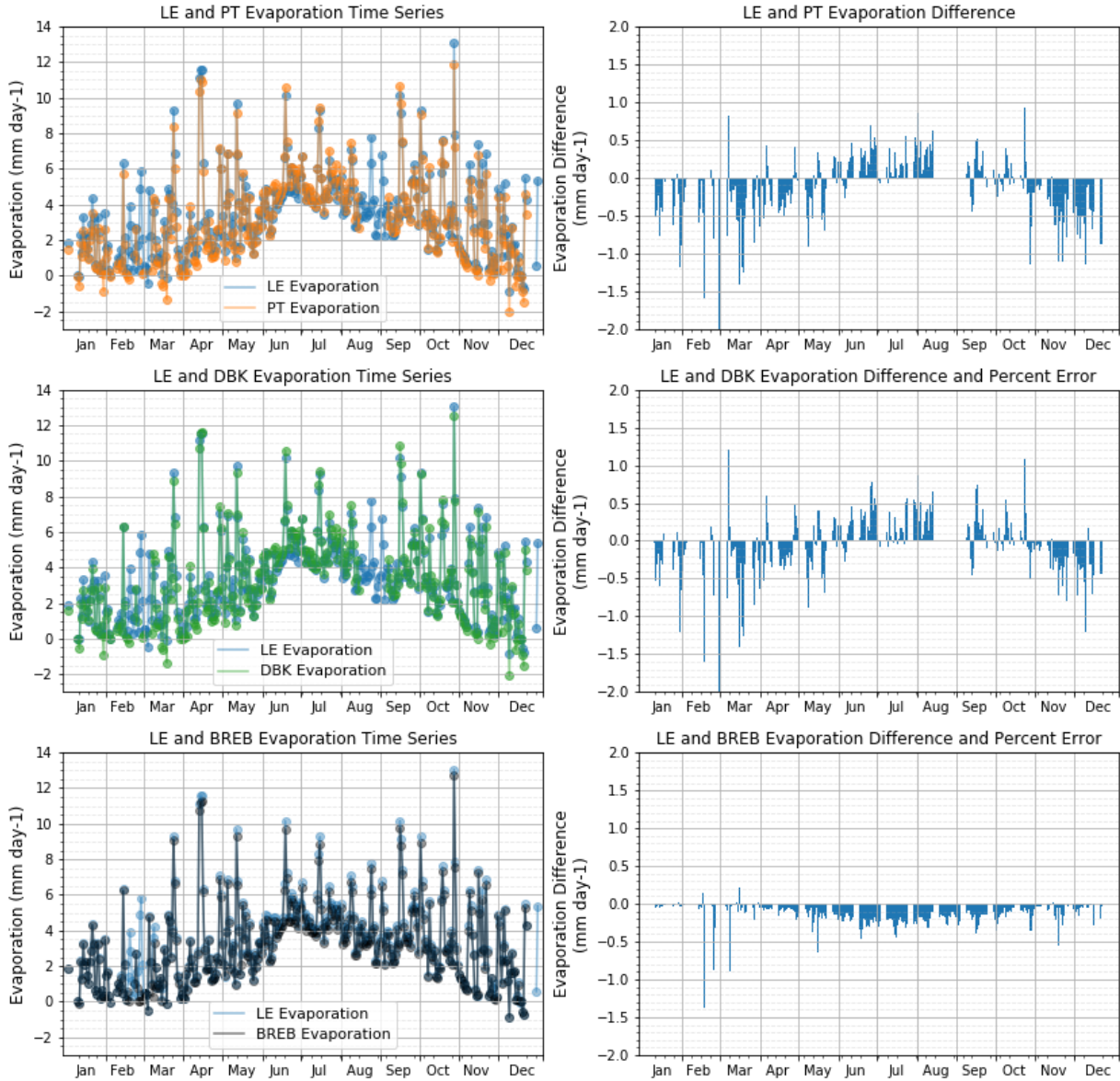


Figure 12: Daily measured (LE) and modeled (PT, DBK, and BREB) evaporation (mm day^{-1}) time series (left column) and monthly measured (LE) and modeled (PT, DBK, and BREB) evaporation difference (mm day^{-1} ; in blue) and percent error (%) (in pink) (right column) for 2008.

PT, DBK, and BREB evaporation accurately displayed the strong seasonal trend of evaporation evident in measured evaporation, in which evaporation generally increased from the beginning of the year until July, before decreasing throughout the remainder of the year. Evaporation difference between LE evaporation and modeled PT and DBK (BREB) evaporation ranged from roughly -2 to 1 (-1.5 to 0.25) mm day⁻¹. A negative pseudo-sinusoidal seasonal trend in evaporation difference could be seen in PT and DBK, in which evaporation underestimation increased in magnitude from the beginning of the year to the end of February, before increasing in value until the middle of September, and consistently decreasing in value throughout the remainder of the year after September. A different seasonal trend was observed for BREB evaporation difference relative to PT and DBK; modeled DBK evaporation generally became increasingly negative from the beginning of the year until July, before decreasing in underestimation magnitude throughout the remainder of the year. The seasonal trends in daily evaporation difference for PT, DBK, and BREB modeled evaporation were relatively consistent with the seasonal trends observed in monthly evaporation difference.

Daily averages of PM, BS, and DB modeled evaporation ranged from roughly -1 to 13 mm day⁻¹, -7 to 11 mm day⁻¹, and -1 to 15 mm day⁻¹, respectively (Figure 13). PM and BS evaporative models both followed the seasonal trend of daily-averaged measured evaporation relatively well, excluding the high wind speed month of March. PM modeled evaporation consistently overestimated evaporation throughout the year of 2008, reaching peak overestimation in March, before decreasing steadily in magnitude throughout the rest of the year. Modeled BS evaporation

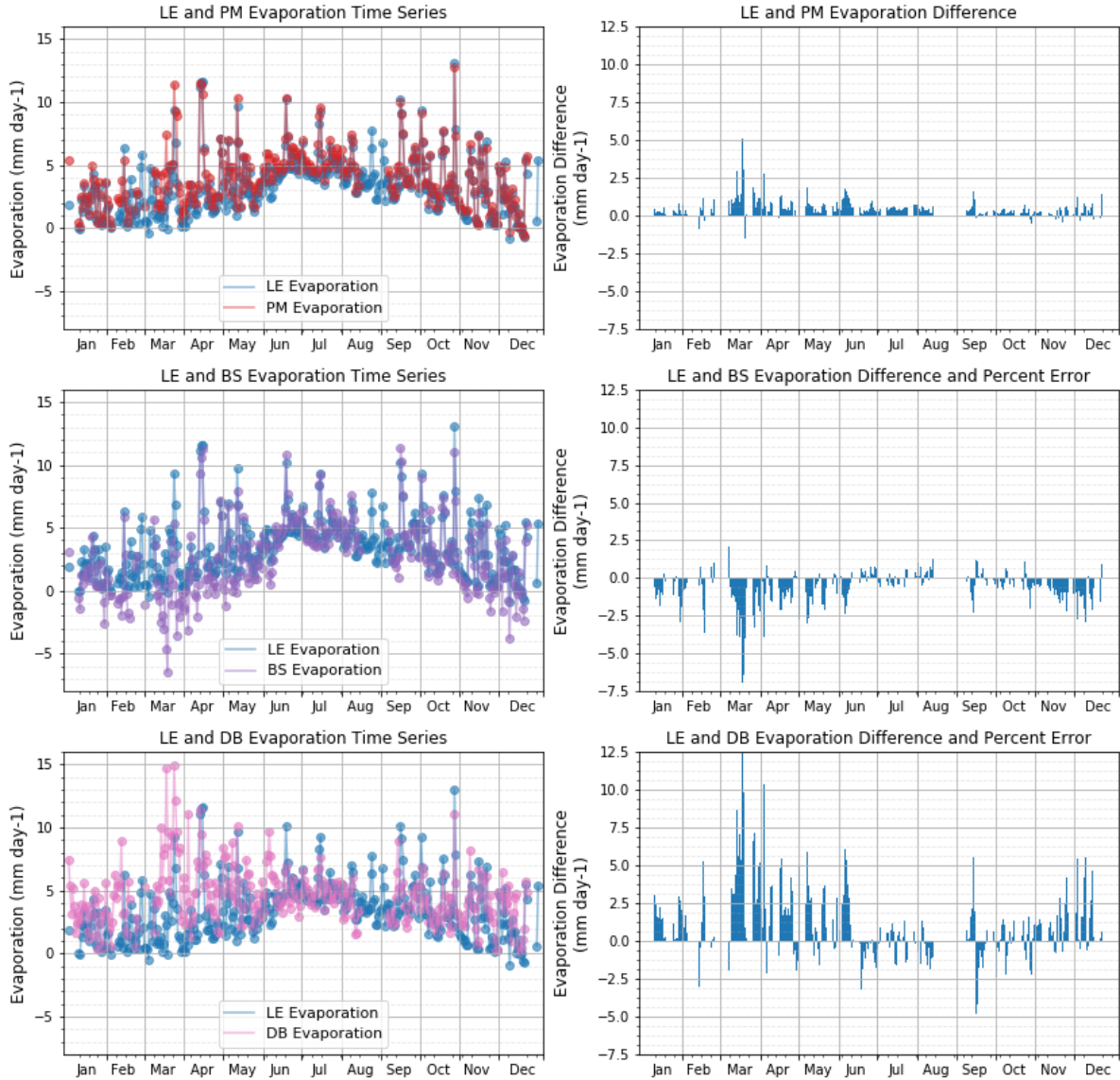


Figure 13: Daily measured (LE) and modeled (PM, BS, and DB) evaporation (mm day^{-1}) time series (left column) and monthly measured (LE) and modeled (PM, BS, and DB) evaporation difference (mm day^{-1} ; in blue) and percent error (%; in pink) (right column) for 2008.

and measured evaporation difference displayed a seasonal variation slightly resembling the negative pseudo-sinusoidal seasonal trend of the PT and DBK models, but of lesser relative magnitude when overestimating evaporation during the warm months. Excluding January through

May, DB modeled evaporation followed the seasonal trend in daily-averaged LE evaporation relatively well. The seasonal trend in the difference in LE evaporation and DB modeled evaporation displayed a similar pseudo-sinusoidal pattern to BS modeled evaporation difference, but inverted.

Linear regressions of measured evaporation and PT, DBK, and BREB evaporation displayed that PT, DBK, and BREB evaporation could explain 97.2, 98.0, and 99.9% of the variance of LE evaporation, respectively (Figure 14a, b, c). All three models followed the 1:1 line closely, with slopes of 1.03, 1.05, and 0.96 as well as intercepts of -0.23, -0.24, and 0.00 for PT, DBK, and BREB, respectively. PM and BS models could explain the variance in daily-averaged measured evaporation 91.9 and 84.4% of the time, respectively (Figure 14d, e). In addition to the higher R^2 , PM followed the 1:1 line more closely with a slope and intercept of 0.93 and 0.71, respectively, relative to BS, which had a slope and intercept of 1.12 and -1.16, respectively. DB modeled evaporation was not able to explain the variance of measured evaporation well, having an R^2 of only 0.193 (Figure 14f).

The modeled evaporation methods fell into the same performance tiers as they did with a monthly temporal scale; PT, DBK, and BREB models fell into the highest performance tier, PM and BS models fell into the middle performance tier, and the DB model fell into the lowest performance tier. Among the highest performance tier, BREB modeled evaporation the best of the three methods, being able to explain the highest percentage of the variance in measured evaporation, having a consistent bias throughout the year, and following the 1:1 line the closest.

BREB evaporation was able to explain more variance in measured evaporation when using a daily temporal scale relative to when using a monthly temporal scale. Although very similar, the DBK model could explain more variance in measured evaporation than the PT model on a daily timescale, but explained the same percentage of variance in measured evaporation as the PT model when evaluated at a monthly scale. Within the middle performance tier, the PM model performed better than the BS model on a daily timescale, due to the PM model's ability to explain more of the variance in measured evaporation and closer adherence to the 1:1 line relative to the BS model. The PM model being able to more closely follow the 1:1 line relative to the BS model is consistent with the conclusion for the monthly timescale. However, the BS model was able to explain more of the variance of measured evaporation than the PM model on a monthly timescale, which cannot be applicable for a daily timescale. Although the worst-performing model, the DB model, was still not able to explain much of the variance of measured evaporation, the DB model explained more measured evaporation variance when calculated for a daily timescale relative to a monthly timescale; daily timescale R^2 of 0.193 compared to a monthly timescale R^2 of 0.054.

3.2.4. Performance of evaporation models on a 30-minute temporal scale

Linear regressions of PT, DBK, BREB, PM, BS, and DB modeled evaporation versus measured evaporation were calculated on a temporal scale of 30 minutes (Figure 15). Typical values of measured evaporation ranged from roughly -4 to 20 mm day⁻¹ for a 30-minute timescale. PT and DBK modeled evaporation explained 95.5 and 95.8% of the variance of 30-minute

Daily Modeled vs. Measured Evaporation

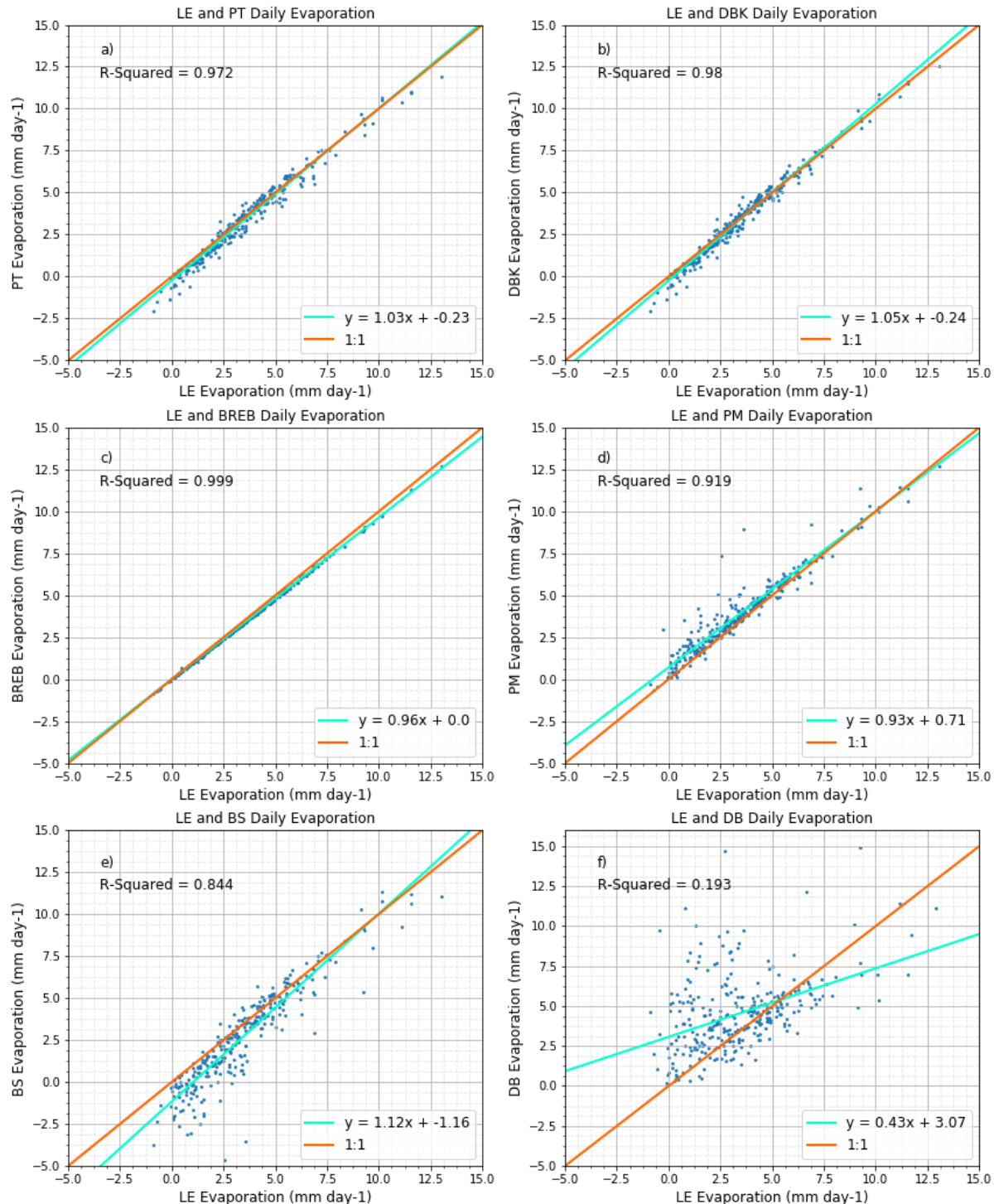


Figure 14: Linear regressions of daily modeled PT (a), DBK (b), BREB (c), PM (d), BS (e), and DB (f) evaporation (mm day^{-1}) versus measured LE evaporation (mm day^{-1}) for 2008.

measured evaporation and, on average, followed the 1:1 line closely with slopes and intercepts of 0.99 and -0.11 and 1.02 and -0.11, respectively (Figure 15a, b). Both modeled PT and DBK evaporation generally deviated farthest from measured evaporation when measured evaporation was both greater than roughly 14 mm day⁻¹ and less than zero. The physical mechanisms driving the largest modeled deviations from measured evaporation will be elaborated on in subsequent sections. BREB evaporation explained 99.8% of the variance in measured evaporation and remained close to the 1:1 line and displayed a relatively consistent underestimating bias in evaporation throughout the year (Figure 15c). Nearly all 30-minute deviations from the regression line for modeled BREB evaporation occurred between measured evaporation values of -5 to 5 mm day⁻¹; this finding is unique to the BREB method for estimating evaporation. Modeled PM evaporation was able to explain 91.1% of the variance in measured 30-minute evaporation (Figure 15d). PM-modeled 30-minute evaporation generally overestimated evaporation, with the largest overestimate magnitudes occurring when measured evaporation was between 0 and 10 mm day⁻¹. 30-minute evaporation predicted by the BS model was able to explain 80.5% of the variance in measured evaporation (Figure 15e). The BS model showed a relatively large bias toward underestimating 30-minute evaporation, with largest underestimation occurring between measured evaporation values of -5 and 10 mm day⁻¹. 30-minute DB-modeled evaporation was only able to explain 20.0% of the variance of measured evaporation, which is at least 60% lower than all other methods (Figure 15f). It is also interesting to note that the DB model never estimated negative values of evaporation. This is due to the model containing only one possibly-negative term ($e_0 - e_a$), meaning the DB model will rarely be able to accurately predict evaporation when measured evaporation drops below zero.

30-minute Modeled vs. Measured Evaporation

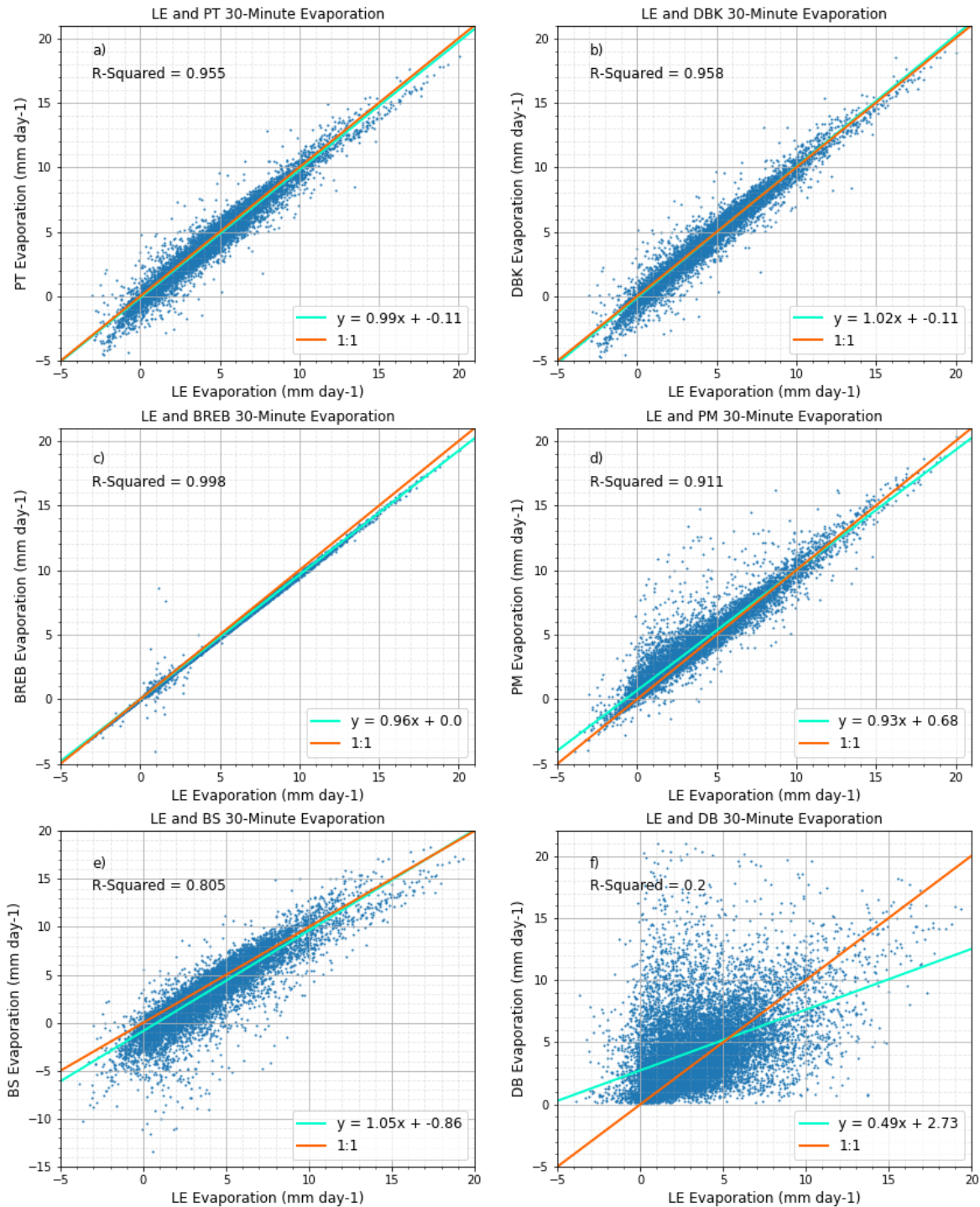


Figure 15: Linear regressions of 30-minute modeled PT (a), DBK (b), BREB (c), PM (d), BS (e), and DB (f) evaporation (mm day^{-1}) versus measured LE evaporation (mm day^{-1}) for 2008.

Contrary to monthly and daily timescales, the six evaporation models did not fall into three general performance categories as easily when using a temporal scale of 30 minutes. The overall top-performing evaporative model for a 30-minute timescale was the BREB model, once again due to the generally consistent bias of underestimating evaporation and its ability to accurately explain the variance of measured evaporation. PT and DBK models both rank second best as they performed very similarly well when using a 30-minute timescale due to their ability to explain the variance in measured evaporation. Of the two models, DBK performed equally as well, if not very slightly better, than PT throughout all tested timescales. The PM model performed better than the BS model when using a 30-minute timescale due to the higher accuracy in explaining measured variance and a generally lower magnitude difference in modeled to measured evaporation. Although the PM model performed better than the BS model through all tested timescales, the difference in performance between these two models is highest for the 30-minute timescale. Among the tested models, the worst-performing evaporative model when evaluating at a 30-minute timescale was the DB model. Although the performance of the DB model's ability to explain the variance in measured evaporation was low for a 30-minute timescale, the 30-minute R^2 value was the highest out of all tested timescales; DB daily timescale R^2 of 0.193 and monthly timescale R^2 of 0.054.

3.3. Impact of physical characteristics on modeled evaporation estimates

To determine the impact of physical parameters on evaporative models, specific variables were isolated for closer analysis. Wind speed and atmospheric stability, two of the main parameters

that dictate and drive evaporation, were chosen to see how well evaporative models could accurately predict evaporation when these parameters changed. This was done by dividing evaporation into multiple wind speed and stability regimes and will be discussed in greater detail in the subsequent sections. It should be noted that, although the vapor pressure gradient ($e_s - e_a$; Δe) between the water and overlying air interface is one of the main factors controlling LE and subsequently evaporation, no discernible relationship was observed between Δe and the performance of the evaporative models. For this reason, no further analysis was conducted on Δe and modeled evaporation performance.

3.3.1. Impact of wind speed on modeled evaporation estimates

Wind speed can have a large impact on the magnitude of evaporation from an open-water source by both advecting relatively dry air from the surrounding area to over the water body and by advecting saturated air from over the water body away from the water body. Wind speed is primarily driven by meso- or synoptic-scale horizontal temperature- and pressure-gradients caused by synoptic-scale pressure centers and associated frontal structures or by local-scale processes. For over-water areas, the fetch, or over-water distance in which air travels, plays a large role in the wind speed recorded at a location. For example, assuming constant atmospheric conditions, wind speed will be faster at a point given a fetch of 5 km relative to a fetch of 2 km; generally, the longer the fetch, the faster the wind speed. The dependence of wind speed on fetch is due to the higher friction between a land-atmosphere interface relative to a water-atmosphere interface. The importance of fetch and subsequently wind direction was seen in this study (Figure 16). The

reservoir, which is northeast-southwest oriented, experienced the highest percentage of high wind speeds (greater than 6 m s^{-1}) when winds were from the north or south; northerly and southerly wind directions lead to greatest fetches for the site location used in this study. Northerly and southerly wind directions can generally be associated to the wind direction during and following the passage of a cold and warm front, respectively.

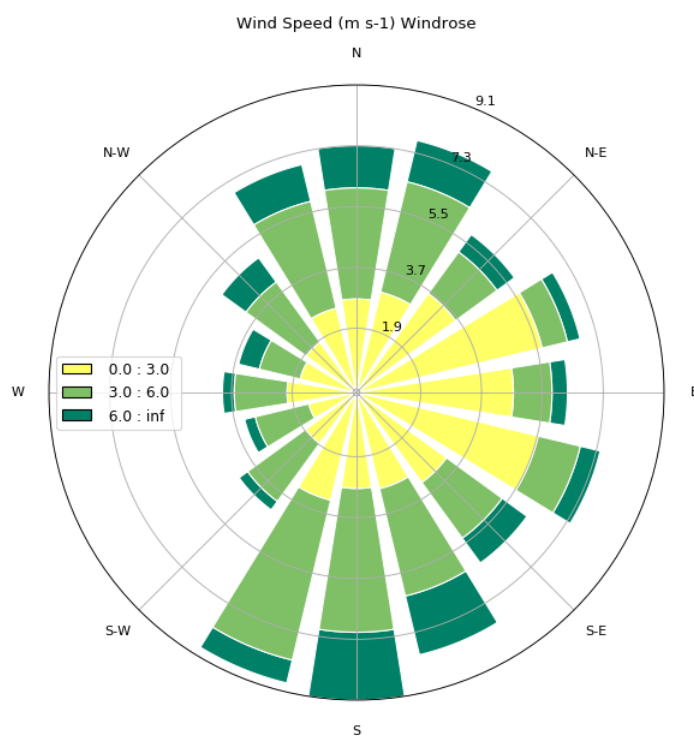


Figure 16: Wind direction windrose with low (less than 3 m s^{-1}), moderate ($3-6 \text{ m s}^{-1}$), and high (greater than 6 m s^{-1}) wind speed regime percentage increments in yellow, light green, and dark green, respectively.

Wind speed was divided into three regimes based on magnitude; the three regimes being low, moderate, and high wind speed. The low wind speed regime was defined as when wind speed

was less than 3 m s^{-1} ; the moderate wind speed regime was defined as when wind speed was greater than or equal to 3 m s^{-1} and less than 6 m s^{-1} ; the high wind speed regime was defined as when wind speed was greater than or equal to 6 m s^{-1} . As one would expect, the quantity of points in each wind speed regime decreased as wind speed regime increased in magnitude. This portion of the study was done only for a 30-minute timescale in an attempt to “average-out” as little detail as possible.

3.3.1.1. Impact of wind speed on PT-modeled evaporation estimates

Linear regressions of modeled PT evaporation versus measured LE evaporation were made for low, moderate, and high wind speed regimes to evaluate the performance of the model for multiple wind speeds (Figure 17). Of the three wind speed regimes, PT evaporation was able to explain the most variance in LE evaporation for the low wind speed regime with an R^2 of 0.969. More variance in measured evaporation could be explained by modeled PT evaporation when wind speeds were high relative to when they were moderate, with R^2 values of 0.959 and 0.951, respectively. Although the R^2 was greater in magnitude when wind speeds were high relative to moderate, the high wind speed regression line deviated farther from the 1:1 line with a slope of 0.981 and intercept of -0.537 relative to the moderate wind speed slope and intercept of 1.000 and -0.150, respectively. It was therefore concluded that modeled PT evaporation estimates slightly decreased in accuracy as wind speed increased.

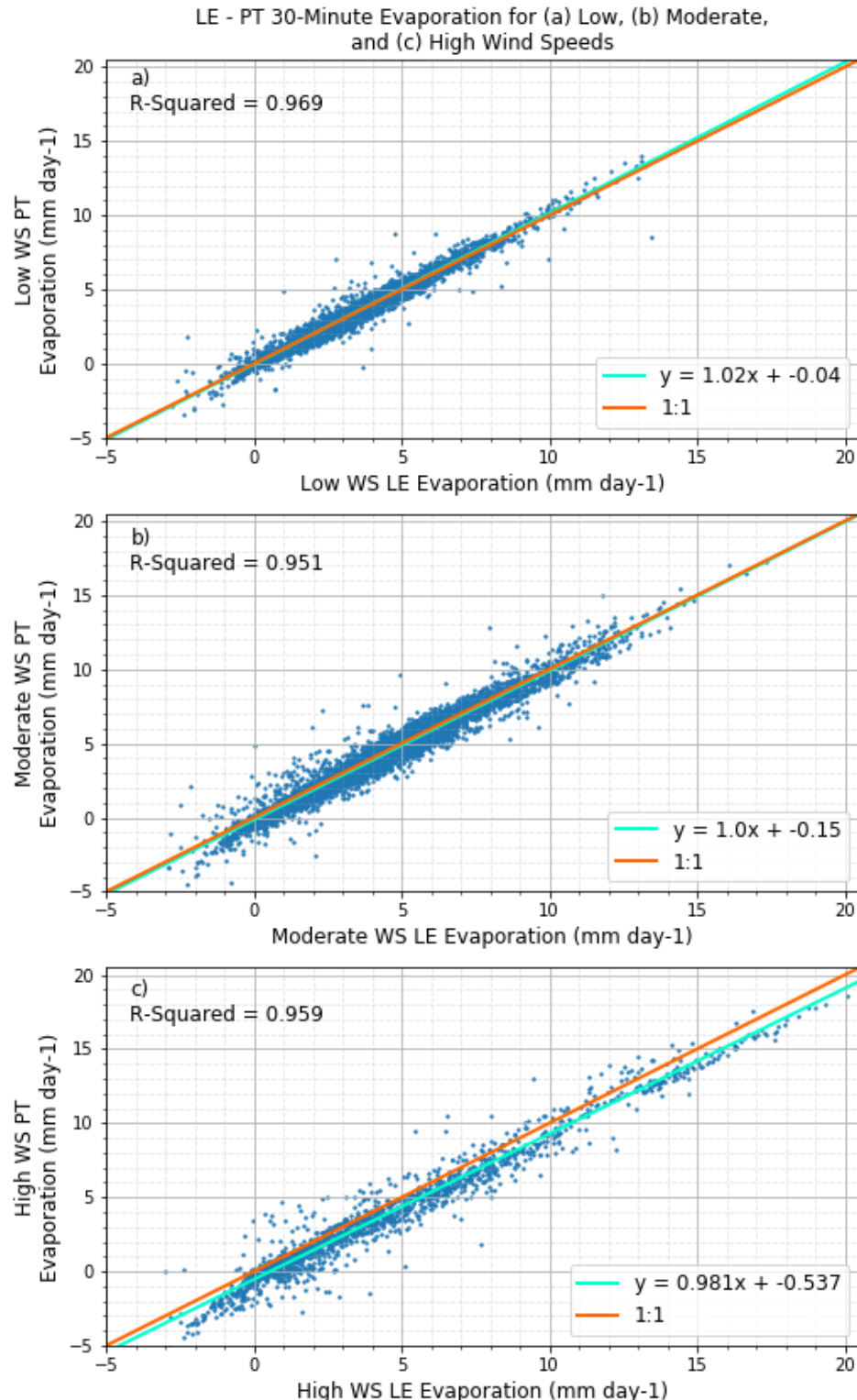


Figure 17: Linear regression of 30-minute modeled PT evaporation (mm day^{-1}) versus measured evaporation (mm day^{-1}) for low (a), moderate (b), and high (c) wind speed regimes for 2008.

Boxplots of the difference in modeled PT and measured LE evaporation were made for low, moderate, and high WS regimes to investigate how the performance of the PT model differed between regimes (Figure 18). Modeled PT and measured evaporation differences, rather than modeled PT and measured evaporation values, were used to show how the performance, rather than values, of the PT model differed between the regimes. In other words, the dependent variable used in the boxplots was evaporation difference rather than evaporation values to show the performance change between regimes, rather than showing how the values change between regimes. The interquartile range for the low wind speed evaporation difference was smallest of the three wind speed regimes, with a total magnitude of 0.5 mm day^{-1} and a near-zero median. Moderate and high wind speed regime interquartile ranges were similar in total magnitude and have medians of roughly -0.2 and -0.6 mm day^{-1} , respectively. The differences in evaporation between modeled PT and measured evaporation were statistically significantly different between all regimes to the 95th percentile. 95th percentile statistical significance could be tested in the boxplots by the overlap of the notches in the low, moderate, and high wind speed boxes. For example, since the notches between low and moderate wind speed evaporation difference did not overlap, the difference between the two groups of data were statistically significant to the 95th percentile; if the notches did overlap, the difference between the two groups of data would not have been statistically significant to the 95th percentile.

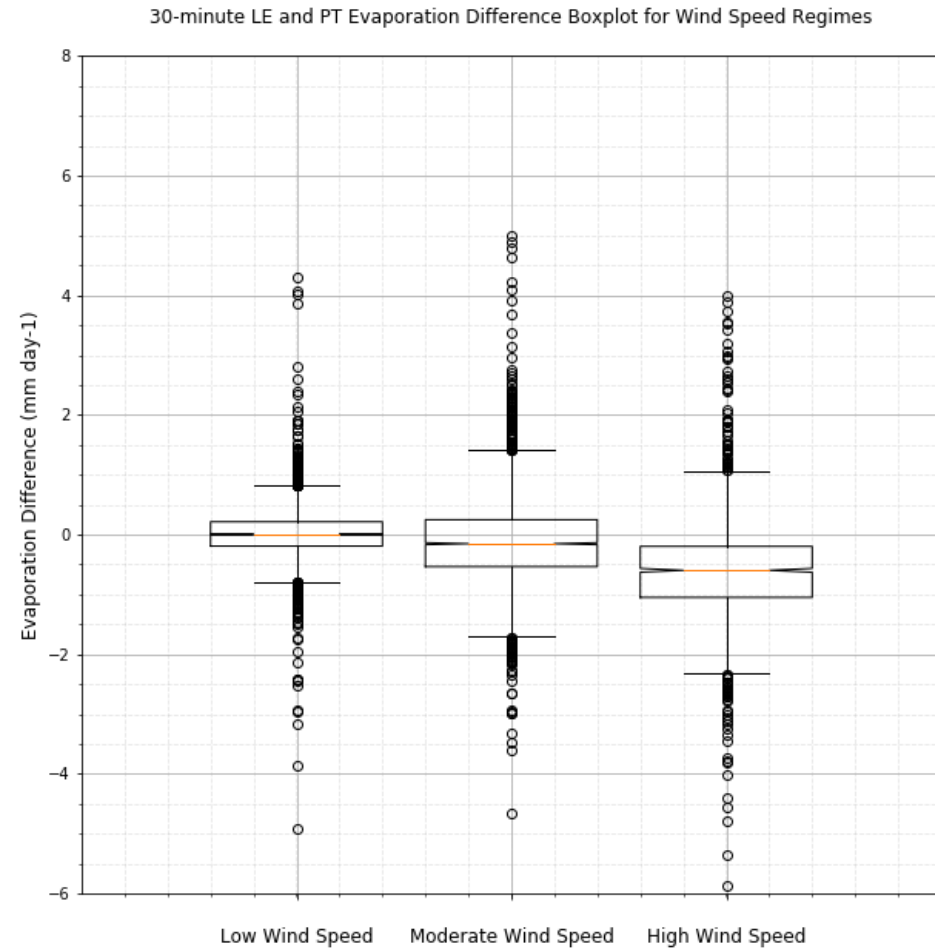


Figure 18: Low, moderate, and high wind speed regime boxplot with evaporation difference between modeled PT and measured evaporation (mm day^{-1}) as the dependent variable. Median values indicated by the orange line in the 95th confidence interval-indicating notches. Outer 25th percentiles indicated by the whiskers.

3.3.1.2. Impact of wind speed on DBK-modeled evaporation estimates

Like PT-estimated evaporation, the DBK model could explain the most variance in measured evaporation in the low wind speed regime out of the three wind speed regimes (Figure 19). Although the high wind speed regime was once again able to explain more variance in

measured evaporation than the moderate wind speed regime with R^2 values of 0.96 and 0.954, respectively, moderate wind speed DBK-modeled evaporation performed slightly better relative to the high wind speed regime due to the lower slope and intercept in the moderate wind speed regime; moderate (high) wind speed regime slope and intercept were 1.02 and -0.13 (1.025 and -0.544), respectively. The larger magnitude slope and intercept, particularly the intercept, of high wind speed indicate that DBK evaporation estimates, on average, departed farther from the 1:1. It can again be concluded that DBK estimates of evaporation slightly decreased in accuracy as wind speed increased.

The difference in modeled DBK evaporation and measured evaporation for low wind speed had the smallest magnitude interquartile range, ranging from roughly -0.2 to 0.3 mm day⁻¹ with a near-zero median (Figure 20). Similar to the PT model, the interquartile ranges for modeled DBK and measured evaporation difference were similar in magnitude between moderate and high wind speeds, ranging from roughly -0.45 to 0.4 mm day⁻¹ and -0.8 to -0.05 mm day⁻¹, respectively. Moderate and high wind speed regimes had medians of roughly -0.05 and -0.4 mm day⁻¹, respectively. No notch overlap occurred between the three wind speed regimes, meaning modeled DBK and measured evaporation differences were statistically different to the 95th percentile confidence interval for all three wind speed regimes.

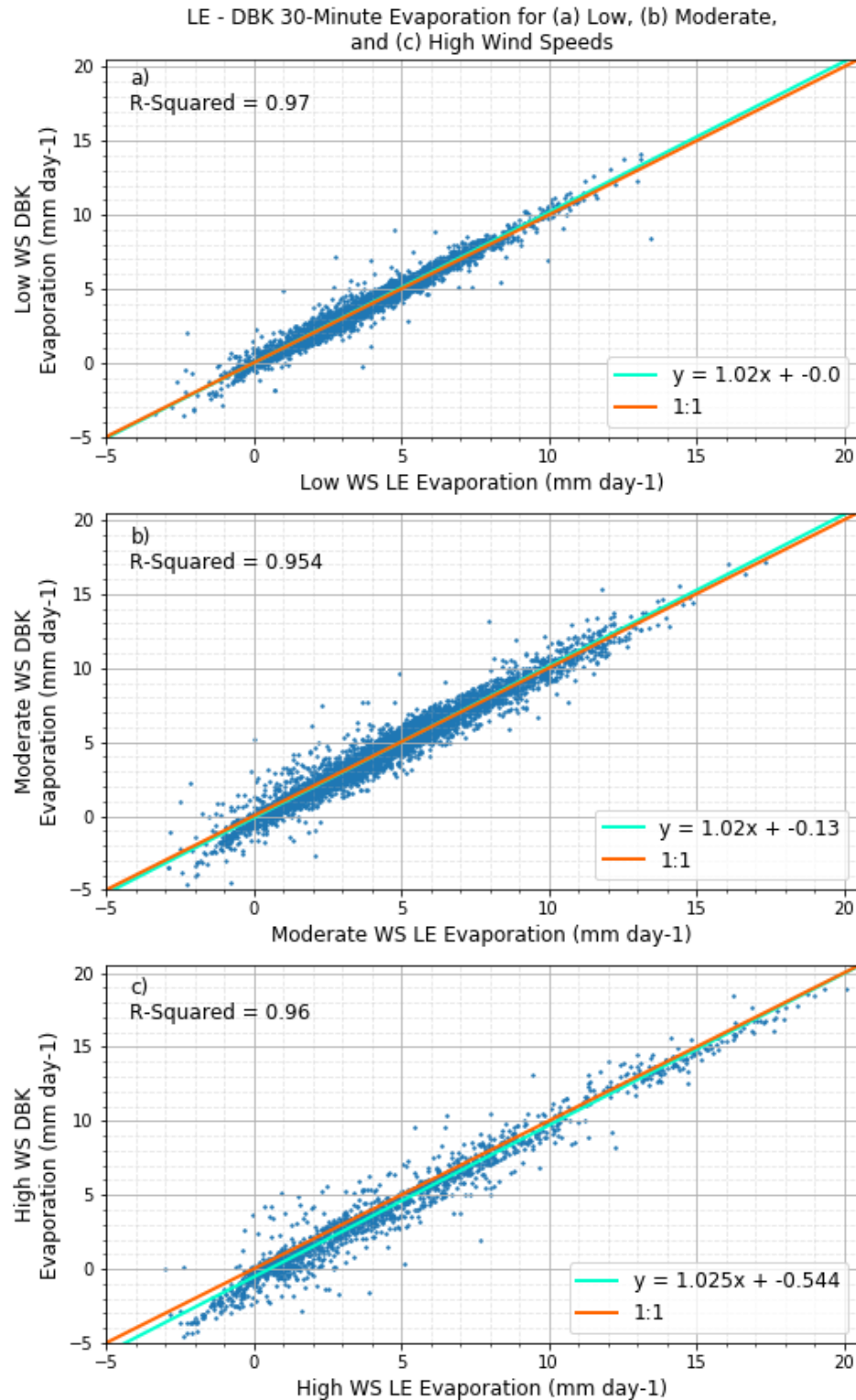


Figure 19: Linear regression of 30-minute modeled DBK evaporation (mm day^{-1}) versus measured evaporation (mm day^{-1}) for low (a), moderate (b), and high (c) wind speed regimes for 2008.

30-minute LE and DBK Evaporation Difference Boxplot for Wind Speed Regimes

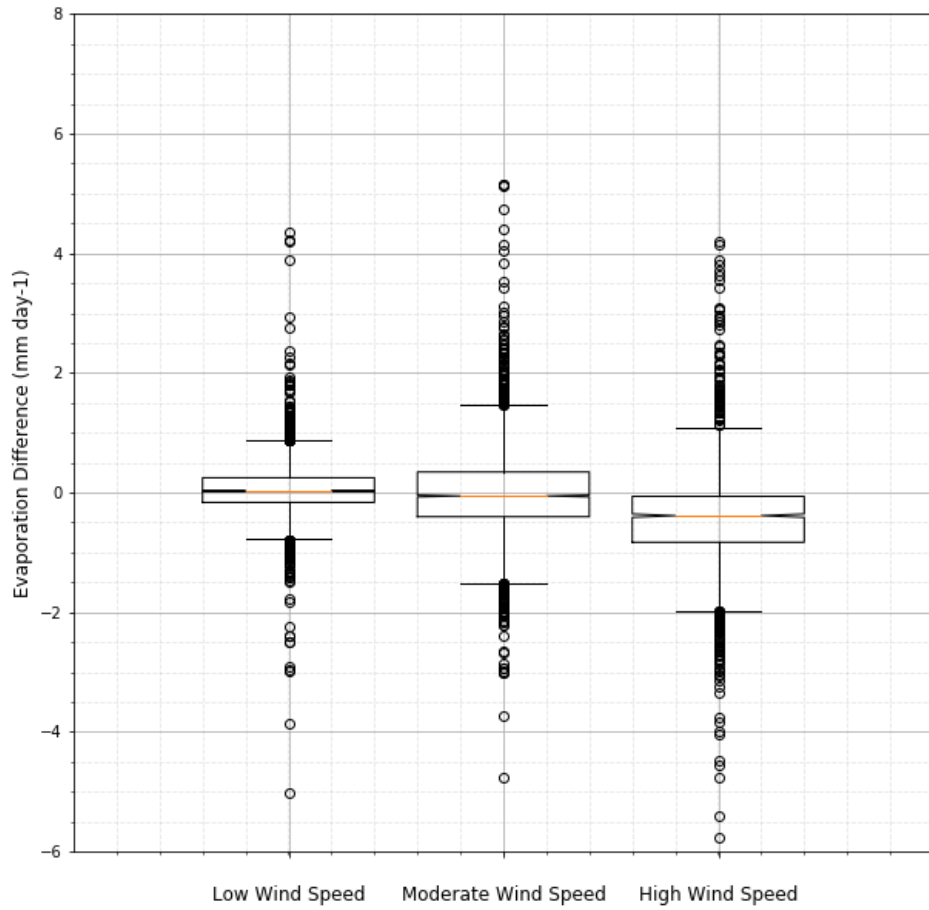


Figure 20: Low, moderate, and high wind speed regime boxplot with evaporation difference between modeled DBK and measured evaporation (mm day^{-1}) as the dependent variable. Median values indicated by the orange line in the 95th confidence interval-indicating notches. Outer 25th percentiles indicated by the whiskers.

3.3.1.3. Impact of wind speed on BREB-modeled evaporation estimates

Modeled BREB evaporation showed a slight decrease in ability to explain the variance in measured evaporation as wind speed increased; low, moderate, and high wind speed R^2 values were 1.0, 0.999, and 0.995, respectively (Figure 21). A slight increase (decrease) in slope

(intercept) was observed as wind speed increased, with low, moderate, and high wind speed values of 0.95, 0.96, and 0.97 (0.02, 0.01, and 0.0), respectively. It was therefore concluded that modeled BREB evaporation very slightly decreased in accuracy as wind speed increased. Most BREB-estimated evaporation deviations from the 1:1 line were when measured evaporation was between 0 and 3 mm day⁻¹. The likely reasoning for the performance of the PT, DBK, and BREB models having slightly decreased evaporation estimation performance as wind speed increased could be due to the lack of inclusion of a wind speed term or term with a direct wind speed dependence in the models.

Interquartile ranges for the difference in BREB modeled evaporation and measured evaporation were once again smallest for the low wind speed regime, ranging from roughly 0 to -0.2 mm day⁻¹ (Figure 22a). Interquartile ranges for moderate and high wind speed regimes were once again relatively similar in magnitude, ranging from roughly -0.05 to -0.22 mm day⁻¹ and 0.03 to -0.2 mm day⁻¹, respectively, which can be more easily seen with a zoomed-in version of Figure 22a (Figure 22b). Medians for low, moderate, and high wind speed were roughly -0.09, -0.13, and -0.09 mm day⁻¹, respectively. As indicated by the lack of overlapping notches, moderate wind speed regime was statistically different than the low and high wind speed regimes on a 95th percentile confidence level. However, the notches do overlap for the low and high wind speed regimes, meaning the evaporation difference between the two regimes were not statistically significant to a 95th percentile of confidence.

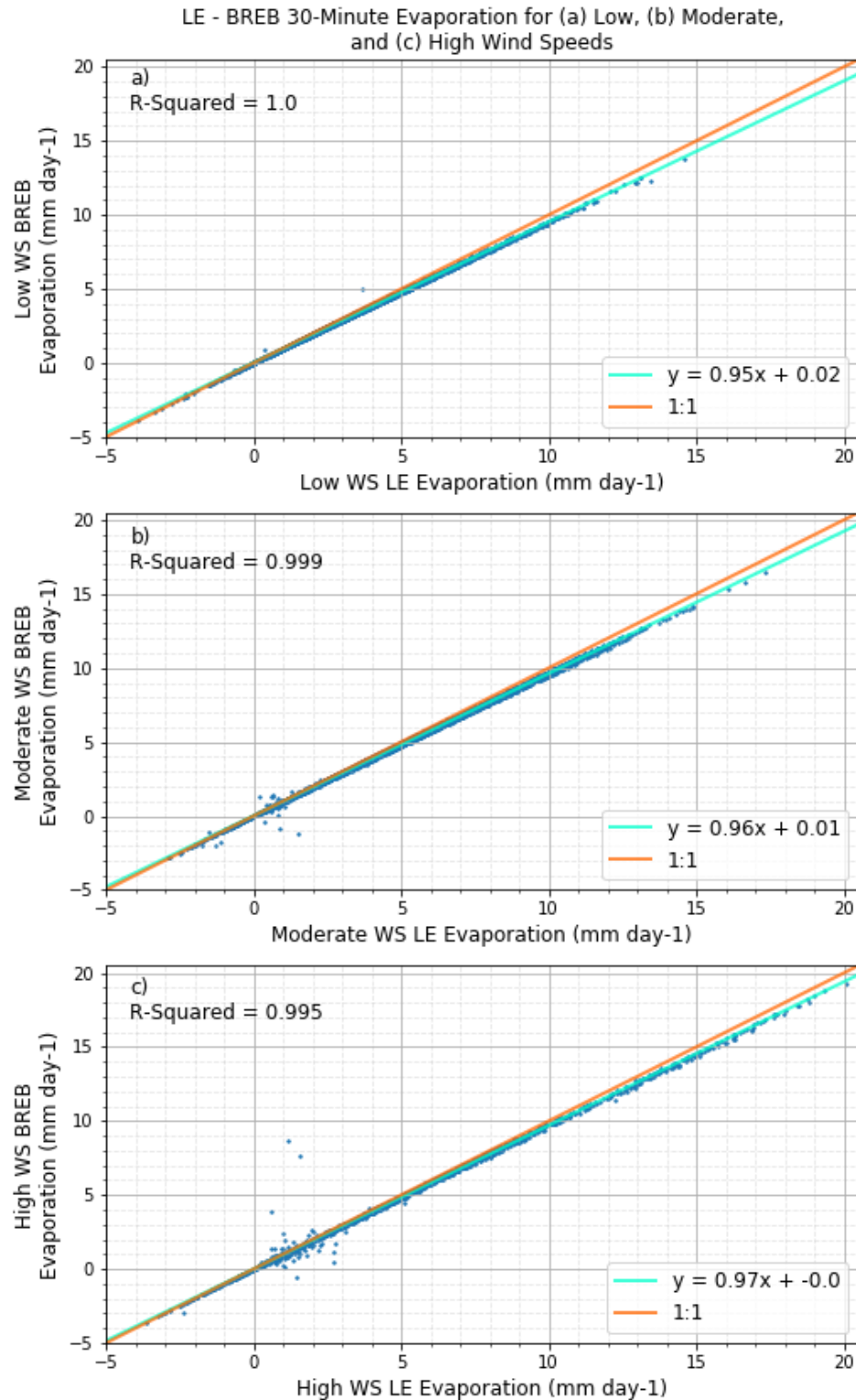


Figure 21: Linear regression of 30-minute modeled BREB evaporation (mm day^{-1}) versus measured evaporation (mm day^{-1}) for low (a), moderate (b), and high (c) wind speed regimes.

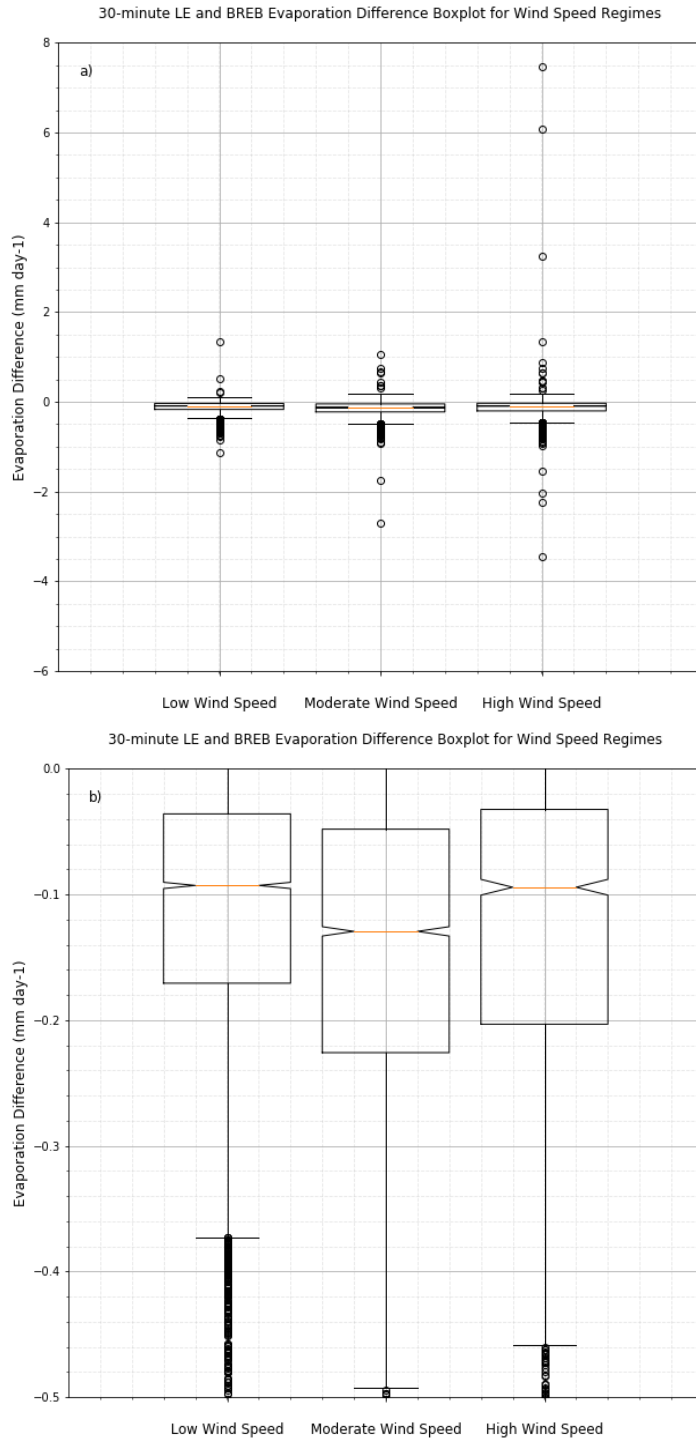


Figure 22: a) Low, moderate, and high wind speed regime boxplot with evaporation difference between modeled BREB and measured evaporation (mm day^{-1}) as the dependent variable. Median values indicated by the orange line in the 95th confidence interval-indicating notches. Outer 25th percentiles indicated by the whiskers. b) y-axis changed from -6 to 8 mm day^{-1} to -0.5 to 0 mm day^{-1} .

3.3.1.4. Impact of wind speed on PM-modeled evaporation estimates

The linear regression of modeled PM evaporation and measured LE evaporation for low, moderate, and high wind speed revealed that PM evaporation was able to explain 96.0, 94.1, and 84.2% of the variance in measured evaporation, respectively (Figure 23). The slope and intercept of PM-modeled evaporation versus measured evaporation for the low, moderate, and high wind speed regimes were 0.97, 0.91, and 0.858 mm day⁻¹ and 0.36, 0.77, and 1.787 mm day⁻¹, respectively. Consistent with the previously-analyzed models, the PM model's predictions became increasingly worse as wind speed increased, which is evident in the decreasing R² values and regression lines deviating farther from the 1:1 line as wind speed increased. Although the behavior in the PM model was similar to the behavior of the three previous models (decreasing in performance as wind speed increased), the relative decrease in performance between wind speed regimes was larger for the PM model. It should also be noted that the PM model performed worse than the previous methods, particularly with the moderate and high wind regimes, despite having a wind speed term incorporated directly into the model. This could be a result of the method in which wind speed was incorporated into the model not performing well when wind speeds were moderate or high. The method of wind speed inclusion into the PM model worked relatively well for low wind speeds, as indicated by comparable R² values between the PM model (0.96) and PT and DBK models (0.969 and 0.97).

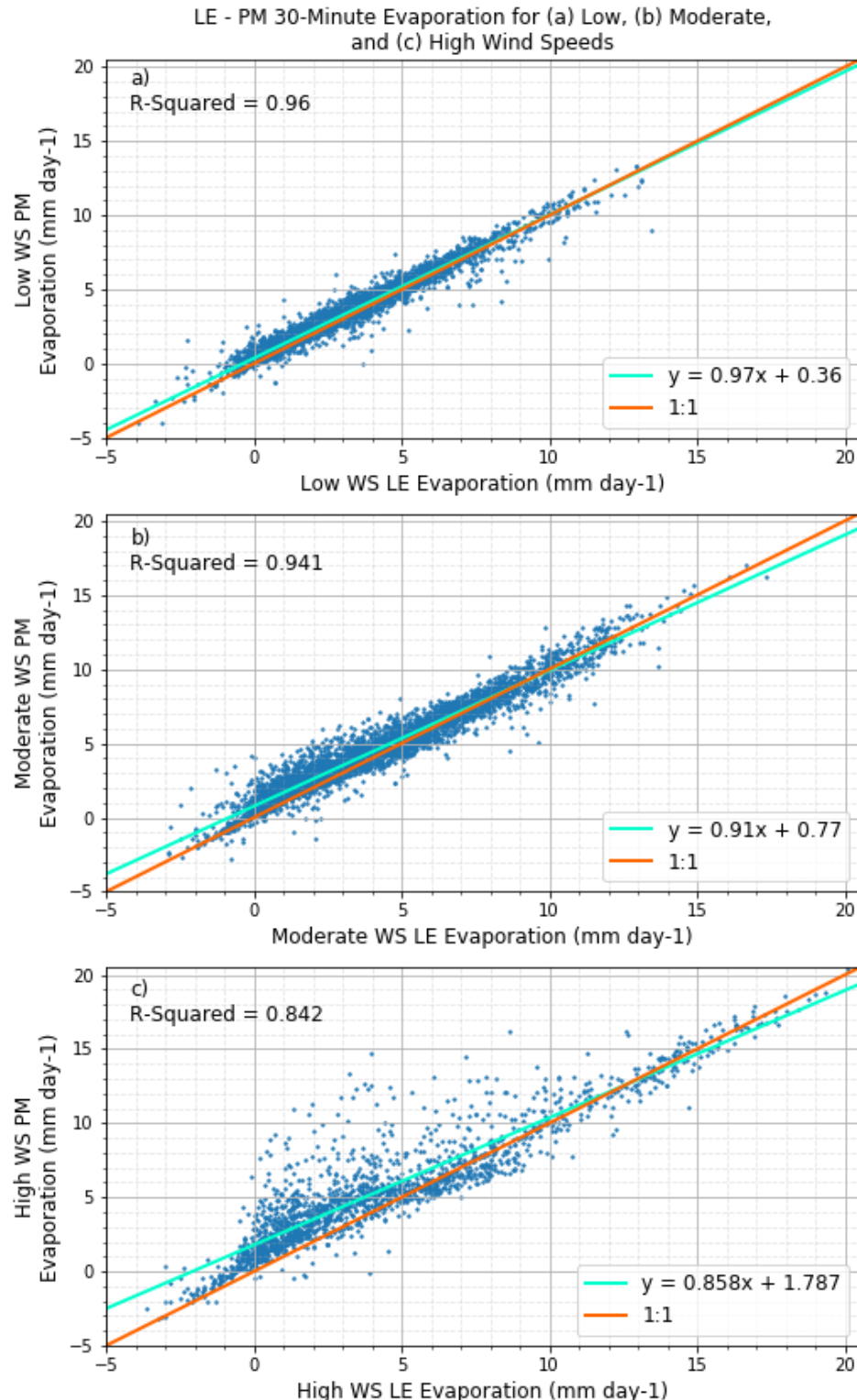


Figure 23: Linear regression of 30-minute modeled PM evaporation (mm day^{-1}) versus measured evaporation (mm day^{-1}) for low (a), moderate (b), and high (c) wind speed regimes for 2008.

The difference in PM-modeled evaporation and measured evaporation for low, moderate, and high wind speeds had interquartile ranges from roughly 0.05 to 0.5, 0.05 to 0.75, and 0.1 to 2.8 mm day⁻¹, respectively (Figure 24a). Low, moderate, and high wind speed regime medians were roughly 0.25, 0.38, and 0.94 mm day⁻¹, respectively, which can be more easily seen in a zoomed-in Figure 24a (Figure 24b). Evaporation difference between modeled PM evaporation and measured evaporation between the low, moderate, and high wind speed regimes were statistically significantly different to the 95th confidence percentile.

3.3.1.5. Impact of wind speed on BS-modeled evaporation estimates

Similar to the previous models, the BS model decreased in ability to explain the variance in measured LE evaporation as wind speed increased from the low wind speed regime to the high wind speed regime, with R² values of 0.908, 0.844, and 0.798, respectively (Figure 25). The modeled BS evaporation versus measured evaporation regression lines became increasingly farther from the 1:1 line as wind speed increased, as indicated by the slopes and intercepts being 1.07, 1.09, and 1.105 and -0.44, -1.06, and -2.862 for low, moderate, and high wind speed regimes, respectively. The BS model performed relatively poorly when compared to the PM model for all wind speed regimes. However, the decrease in performance as wind speed increased for the BS model was more linear than the observed decrease in PM model performance between wind speed regimes.

Difference in BS-modeled and measured evaporation interquartile ranges increased in magnitude as wind speed increased (Figure 26). Modeled DB and measured evaporation difference interquartile ranges were roughly from 0.2 to -0.8, 0.3 to -1.7, and -1 to -4.6 mm day⁻¹, with medians of roughly -0.2, -0.7, and -2.0 mm day⁻¹ for low, moderate, and high wind speed regimes, respectively. The evaporative difference in modeled BS and measured evaporation was statistically significant at the 95th confidence level.

3.3.1.6. Impact of wind speed on DB-modeled evaporation estimates

As concluded in previous sections, the performance of how well DB-modeled evaporation explained the variance of measured evaporation was the worst of all tested models (Figure 27). This finding is true for all low, moderate, and high wind speed regimes, with the DB model being able to explain 40.7, 14.8, and 6.8% of the variance in measured evaporation. Although DB-modeled evaporation did not follow the 1:1 well for any wind speed regime, the high wind speed regime regression line was nearest to being perpendicular to the 1:1 line relative to the low and moderate wind speed regimes. The DB model exhibited the largest decrease in ability to explain measured evaporation variance between low and high wind speed regimes, decreasing from a low wind speed regime R² of 0.407 to a high wind speed regime R² of 0.068.

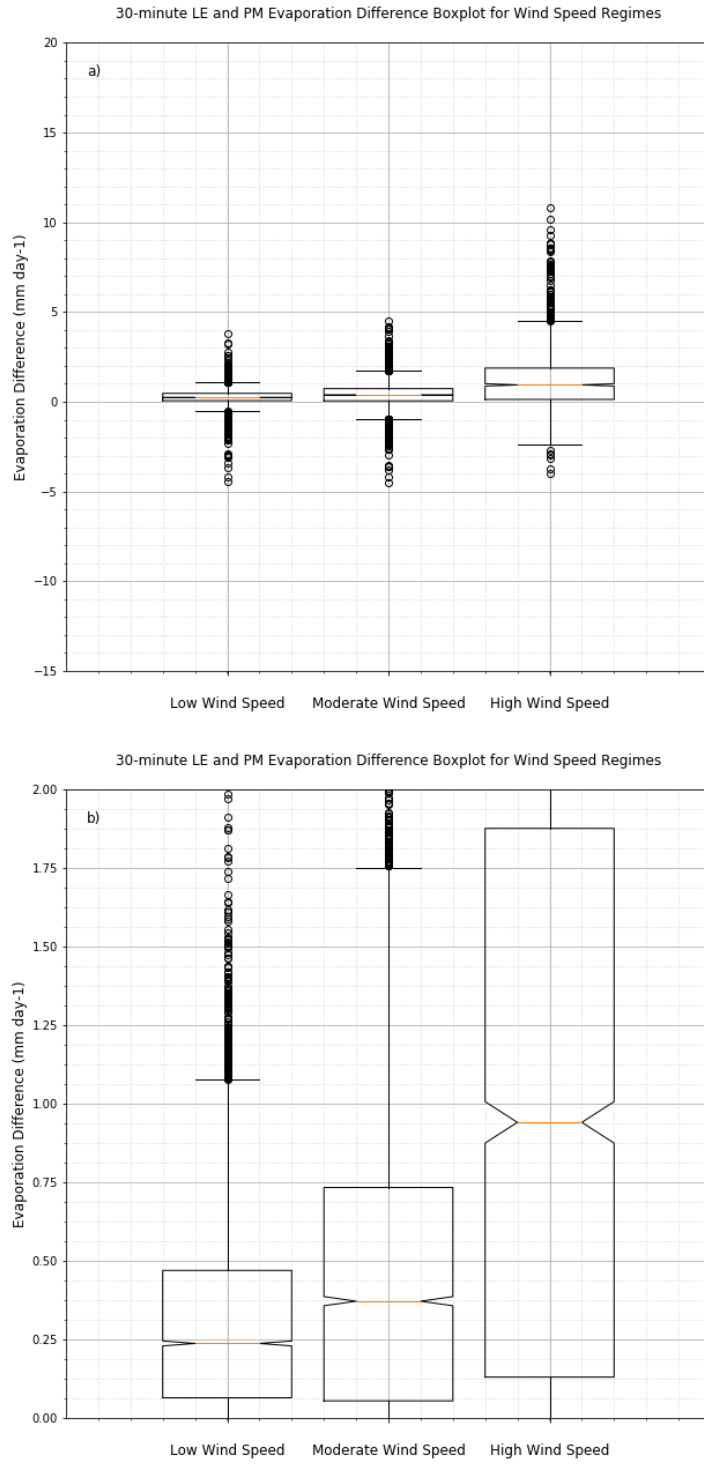


Figure 24: a) Low, moderate, and high wind speed regime boxplot with evaporation difference between modeled PM and measured evaporation (mm day^{-1}) as the dependent variable. Median values indicated by the orange line in the 95th confidence interval-indicating notches. Outer 25th percentiles indicated by whiskers. b) y-axis changed from -15 to 20 mm day^{-1} to 0 to 2 mm day^{-1} .

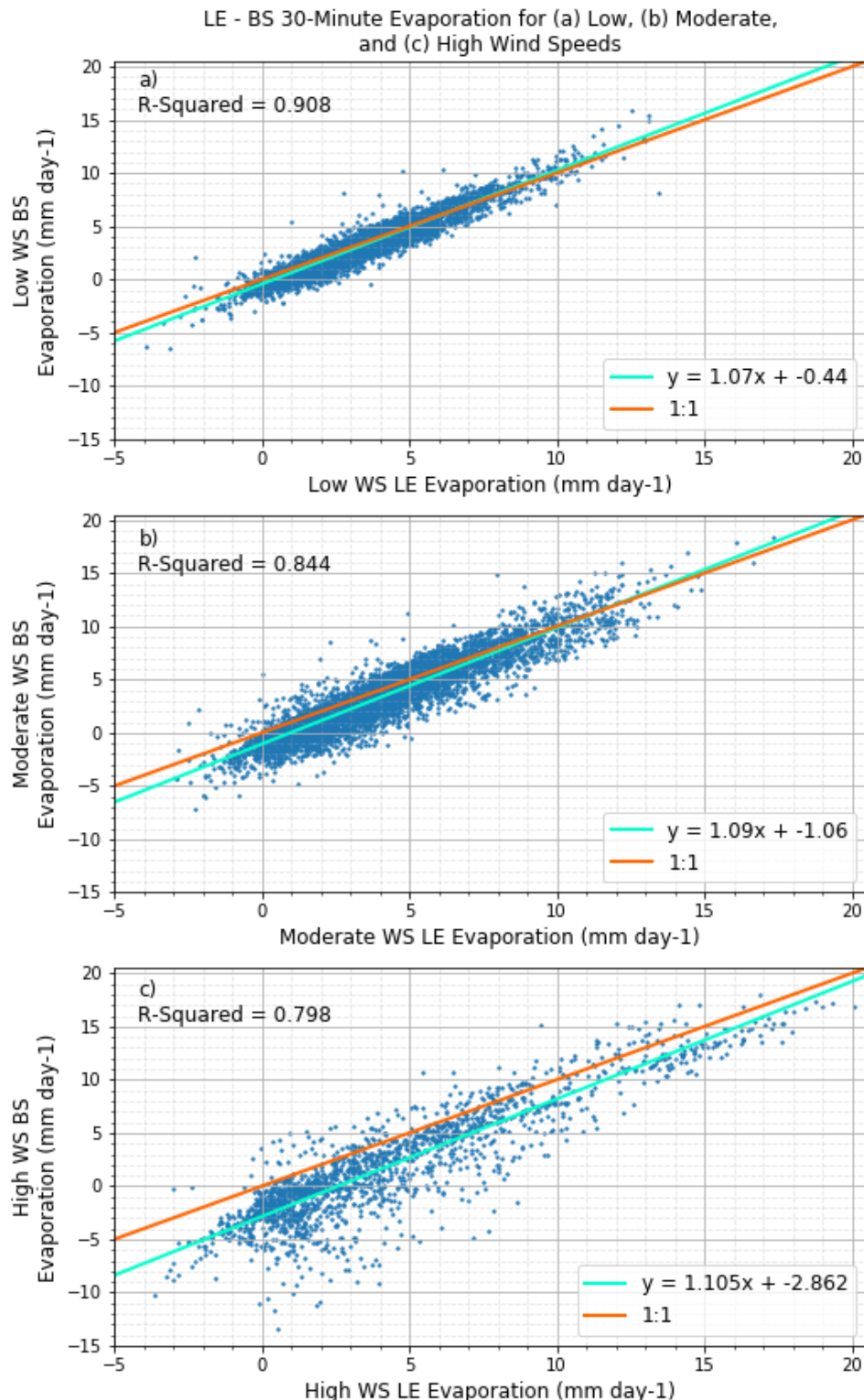


Figure 25: Linear regression of 30-minute modeled BS evaporation (mm day^{-1}) versus measured evaporation (mm day^{-1}) for low (a), moderate (b), and high (c) wind speed regimes for 2008.

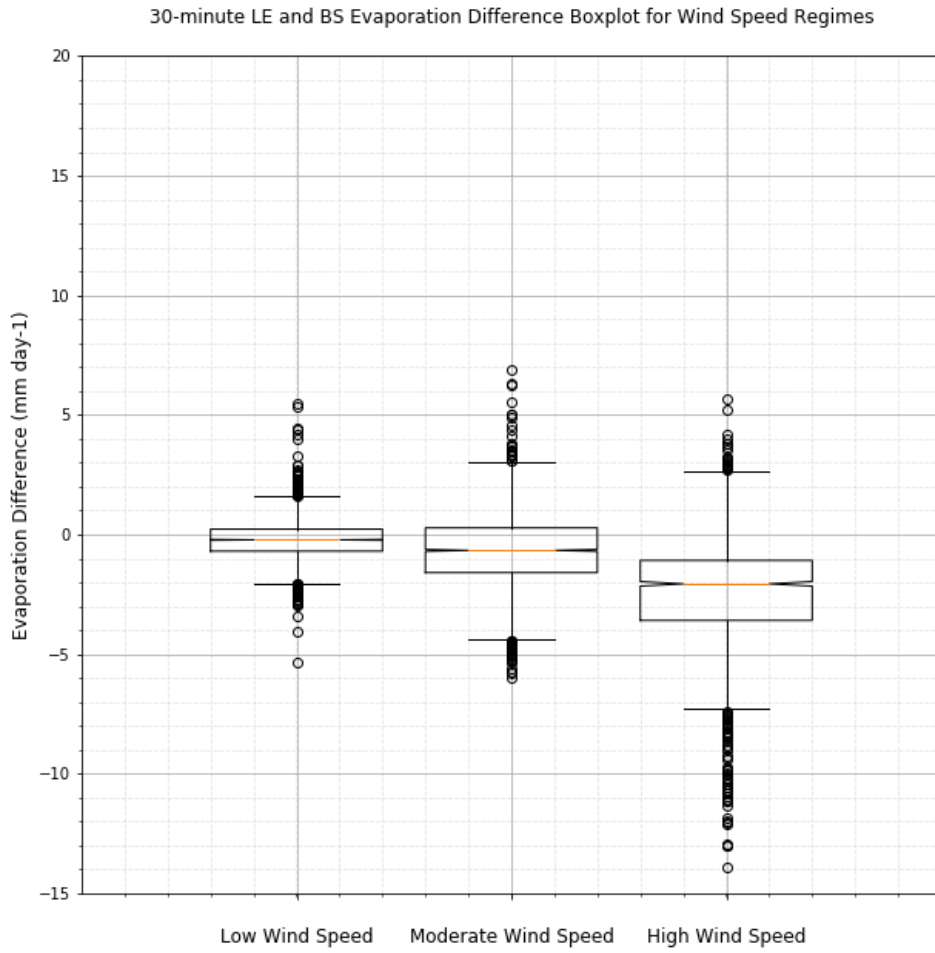


Figure 26: Low, moderate, and high wind speed regime boxplot with evaporation difference between modeled BS and measured evaporation (mm day^{-1}) as the dependent variable. Median values indicated by the orange line in the 95th confidence interval-indicating notches. Outer 25th percentiles indicated by the whiskers.

Low, moderate, and high wind speed interquartile ranges spanned the largest ranges of models, ranging from roughly -0.5 to 1.5, -1.5 to 2.5, and -0.2 to 7 mm day^{-1} , respectively (Figure 28a). Medians for DB-modeled and measured evaporation in low, moderate, and high wind speed regimes were roughly 0.5, 0.5, and 3.5 mm day^{-1} , which can be more easily seen in Figure 28b. Difference in high wind speed modeled DB and measured evaporation was statistically different

at the 95th confidence interval from the low and moderate wind speed regimes. However, the evaporation difference in modeled DB and measured evaporation were not statistically significantly different between the low and moderate wind speed regimes.

3.3.1.7. Summary of wind speed impact on modeled evaporation estimates

Throughout all methods for modeling evaporation, a negative feedback response was observed between wind speed and model performance; as wind speed increased, model performance decreased. An increasing trend in interquartile range magnitude was also observed as wind speed increased. Modeled and measured evaporation differences between low, moderate, and high wind speed regimes were typically statistically significantly different at the 95th percentile confidence interval; the two exceptions to this were between low and high wind speed regimes for BREB-modeled evaporation and low and moderate wind speed regimes for DB-modeled evaporation. The cause of the negative feedback trend between wind speed and model performance was likely due to the lack of inclusion of a wind speed-dependent term or the method in which wind speed was included into the models not being suitable for relatively moderate and high wind speeds. However, the method of inclusion of wind speed into the latter three models worked relatively well for low wind speeds.

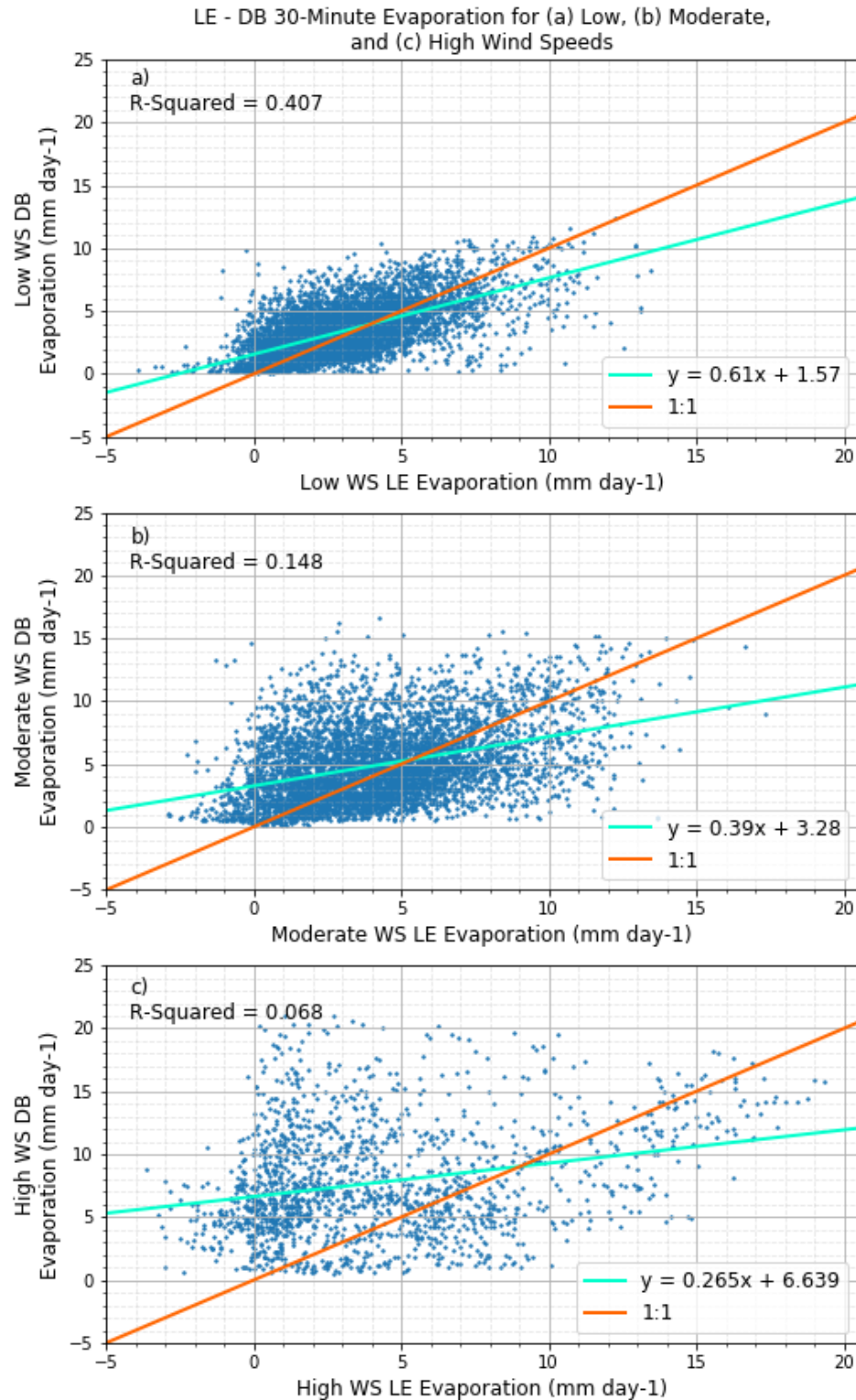


Figure 27: Linear regression of 30-minute modeled DB evaporation (mm day^{-1}) versus measured evaporation (mm day^{-1}) for low (a), moderate (b), and high (c) wind speed regimes for 2008.

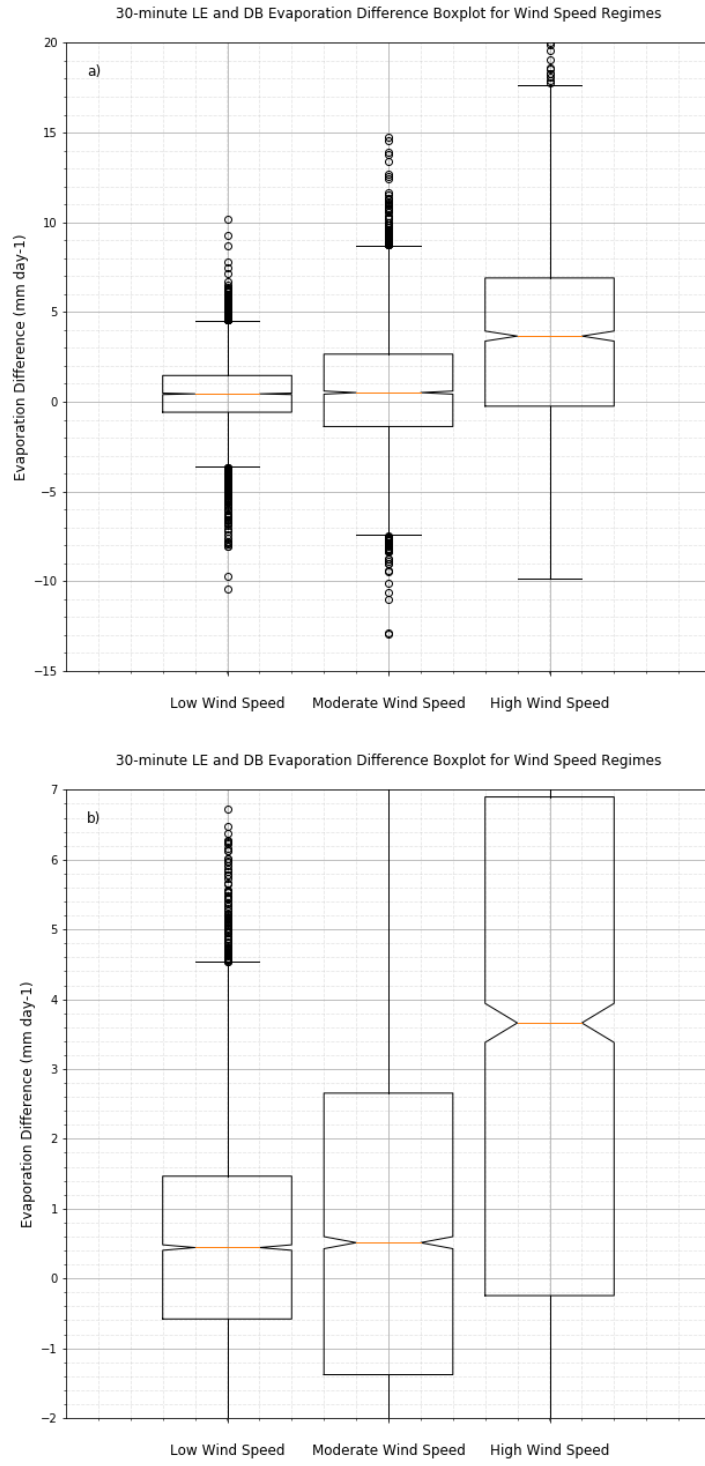


Figure 28: a) Low, moderate, and high wind speed regime boxplot with evaporation difference between modeled DB and measured evaporation (mm day^{-1}) as the dependent variable. Median values indicated by the orange line in the 95th confidence interval-indicating notches. Outer 25th percentiles indicated by whiskers. b) y-axis changed from -15 to 20 mm day^{-1} to -2 to 7 mm day^{-1} .

3.3.2. Impact of stability on modeled evaporation estimates

Stable (unstable) atmospheric conditions have been shown in previous studies to suppress (promote) evaporation (Granger and Hedstrom, 2011; Liu et al., 2009; Rouse et al., 2005; Yusup and Liu, 2016; Zhang and Liu, 2014). Over-water stability for this site, and in general, was driven by the temperature difference between the water surface and overlying air. For example, when the water was cooler (warmer) than the overlying air, the atmospheric conditions were stable (unstable). This was the cause of over-water diurnal variation in stability, meaning over-water atmospheric stability was typically stable during the late afternoon and unstable at night. Note this diurnal atmospheric stability cycle is opposite of the typical terrestrial diurnal stability cycle, which experiences a stable nocturnal atmosphere and unstable atmosphere during the day.

The Obukhov length (z/L ; unitless) was calculated and used as the stability parameter for this study, with positive (negative) z/L being indicative of stable (unstable) atmospheric conditions. Points when z/L calculations exceeded a magnitude of greater than 10 or less than -10 were assumed to be errors or points that were not truly representative of the atmospheric conditions for that 30-minute period and were subsequently excluded from this study (Yusup and Liu, 2016). Similar to the previous section, this portion of the study was done only for a 30-minute timescale.

For the location of the site used in this study, a correlation between wind direction and atmospheric stability was observed (Figure 29). The highest percentage of stable atmospheric

conditions occurred when wind directions were coming from the south. This observation was to be expected as southerly winds tend to advect warm, moist air to the area, causing the air directly over the reservoir to be warmer than the underlying water.

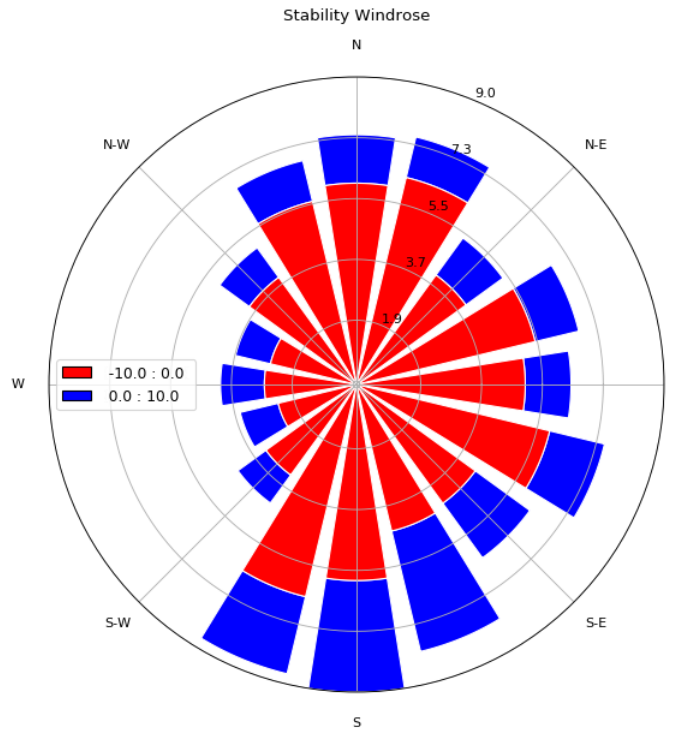


Figure 29: Wind direction windrose with stable (z/L greater than zero) and unstable (z/L less than zero) stability regime percentage increments in blue and red, respectively.

3.3.2.1. Impact of stability on PT-modeled evaporation estimates

Linear regressions of modeled evaporation versus measured evaporation for all evaporative models were analyzed for both the stable and unstable stability regimes. Modeled PT evaporation

could explain more of the variance in measured evaporation for the unstable regime relative to the stable regime, with respective R^2 values of 0.962 and 0.949 (Figure 30). PT estimates of evaporation generally overestimated evaporation when measured evaporation was less than 5 mm day^{-1} when the atmosphere was unstable. Unstable stability performance of the PT model was relatively consistent when measured evaporation values were greater than 5 mm day^{-1} , roughly equally underestimating and overestimating evaporation. A stable atmosphere consistently promoted an underestimation of modeled PT evaporation throughout all magnitudes of measured evaporation. Additionally, the regression line during stable conditions was farther from the 1:1 line relative to unstable conditions, although a consistent bias was observed when the atmosphere was unstable.

Boxplots were made for all modeled evaporation methods with boxes for the stable and unstable stability regimes with the evaporation difference between modeled and measured evaporation plotted as the dependent variable. The difference in modeled PT and measured evaporation resulted in interquartile ranges ranging from roughly -0.25 to -0.8 mm day^{-1} and -0.25 to 0.25 mm day^{-1} for stable and unstable atmospheric conditions, respectively (Figure 31). Stable (unstable) atmospheric conditions yielded a median value of roughly -0.5 (0) mm day^{-1} for modeled and measured evaporation difference. No notch overlap was observed in the difference between modeled PT and measured evaporation for stable and unstable conditions, indicating the difference between values for the stability regimes were significantly different to a 95th interval of confidence.

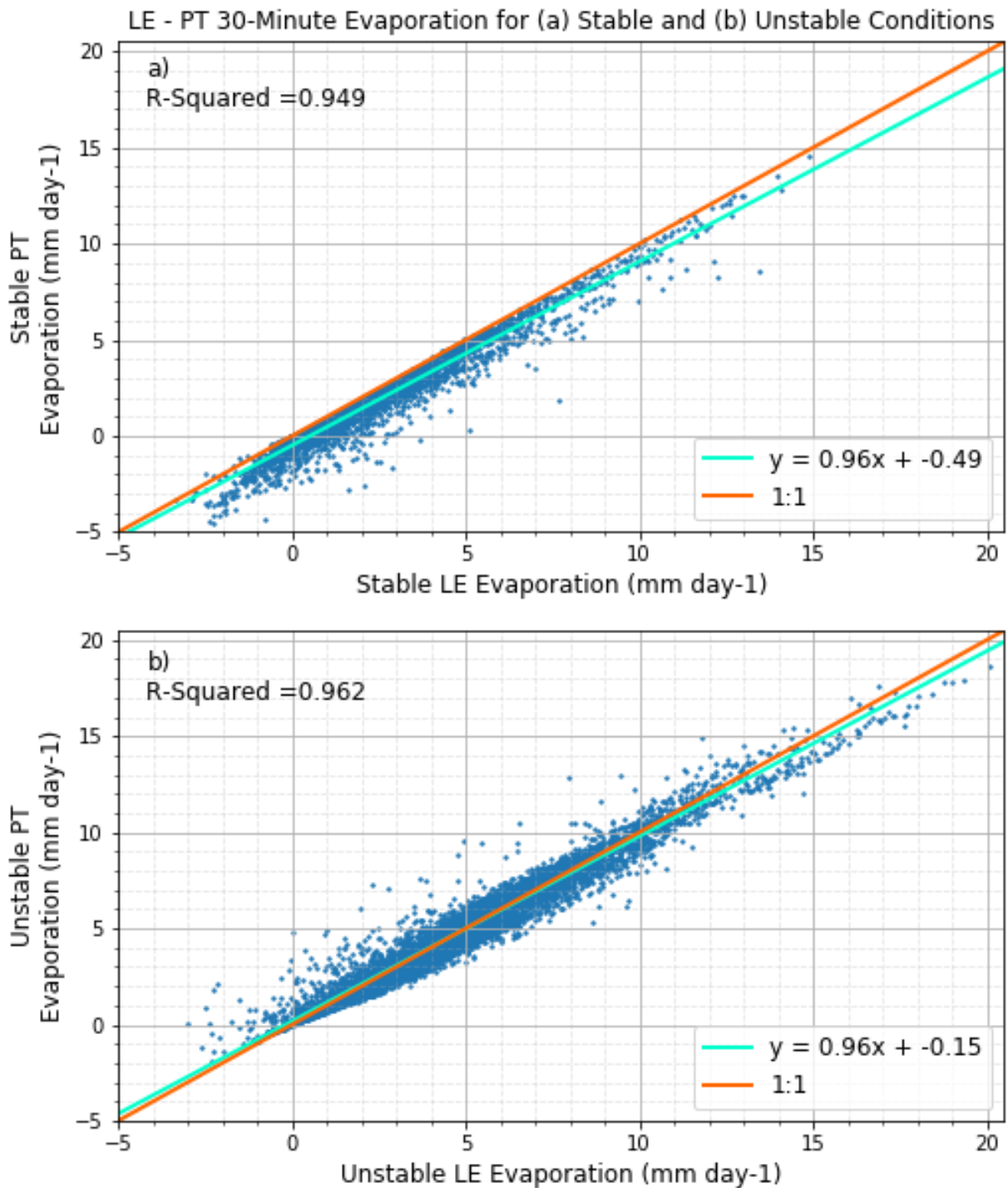


Figure 30: Linear regression of 30-minute modeled PT evaporation (mm day^{-1}) versus measured evaporation (mm day^{-1}) for stable (a) and unstable (b) stability regimes for 2008.

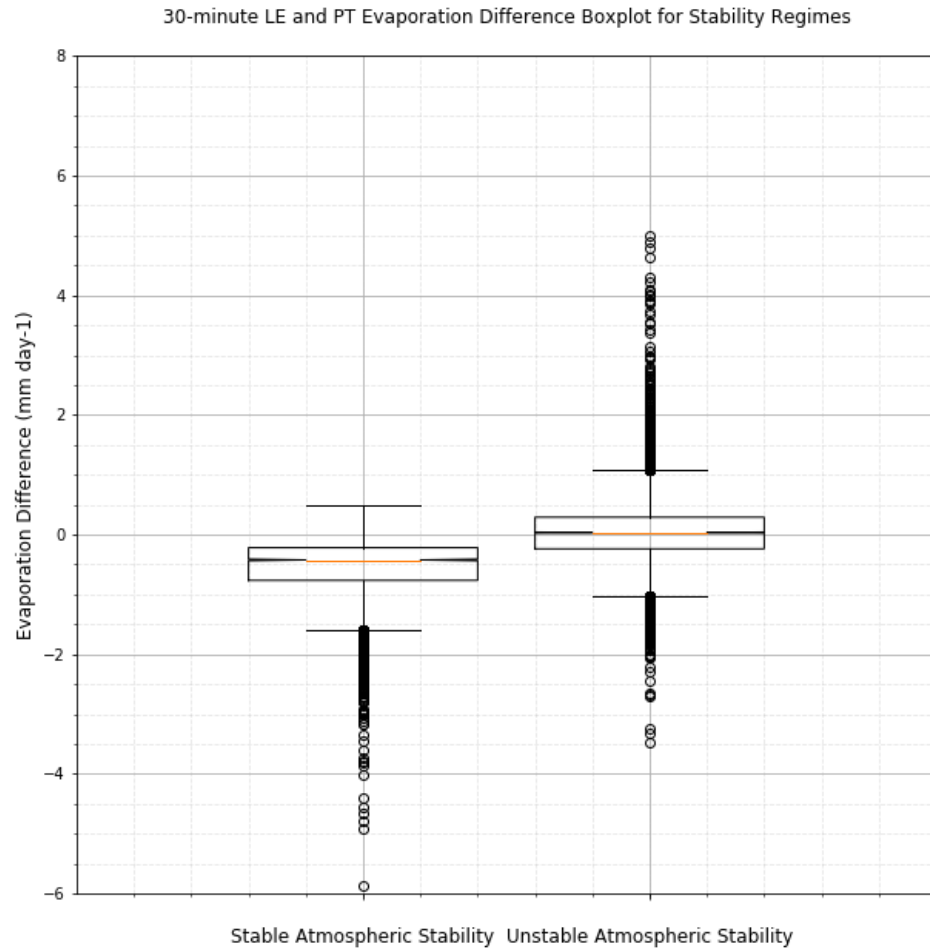


Figure 31: Stable and unstable stability regime boxplot with evaporation difference between modeled PT and measured evaporation (mm day^{-1}) as the dependent variable. Median values indicated by the orange line in the 95th confidence interval-indicating notches. Outer 25th percentiles indicated by the whiskers.

3.3.2.2. Impact of stability on DBK-modeled evaporation estimates

The DBK model once again performed similarly to the PT model when comparing the linear regression of the DBK-modeled evaporation and measured evaporation. The DBK model could explain 95.0 and 96.9% of the variance in measured evaporation for stable and unstable

conditions, respectively, which, although slight, was an improvement in performance to the PT model for both stability regimes (Figure 32). A similar trend to that seen with the PT model was observed in unstable DBK-modeled evaporation, in which the largest (lowest) overestimations in evaporation occurred when measured evaporation was less (greater) than 5 mm day^{-1} . Modeled DBK evaporation consistently underestimated evaporation when atmospheric stability was positive.

The similarity in performance between the PT and DBK model could once again be seen in the difference in the modeled DBK and measured evaporation boxplot (Figure 33). Interquartile ranges (medians) for a stable atmosphere and unstable atmosphere ranged roughly from -0.3 to -0.8 (were $-0.45 \text{ mm day}^{-1}$) and -0.1 to 0.4 (0.1) mm day^{-1} , respectively, for the difference between modeled DBK and measured evaporation. The difference in evaporation estimated using the DBK method and measured evaporation were statistically significantly different between the stable and unstable stability regimes to the 95th confidence interval.

3.3.2.3. Impact of stability on BREB-modeled evaporation estimates

Consistent with the previous models, BREB-modeled evaporation performed better during unstable atmospheric conditions compared to stable atmospheric conditions. This conclusion was indicated by the difference in the BREB model's ability to explain variance in measured evaporation, with 99.1% of explained variance for stable conditions and 99.9% explained variance

for unstable atmospheric conditions (Figure 34). Most of the slightly poor BREB evaporation estimates occurred when modeled evaporation was between 0 and 5 mm day⁻¹ for stable conditions and was negative for unstable conditions. Poorly-modeled BREB estimates both underestimated and overestimated for unstable conditions, while poor BREB-modeled estimates were generally confined to underestimates for stable conditions. Excluding the poorly-estimated points, BREB evaporation estimates were consistently underestimated for both stability regimes. Deviation from the 1:1 line was very slightly greater during stable conditions when compared to unstable conditions.

Stable and unstable stability regime interquartile ranges for the difference between modeled BREB evaporation and measured evaporation ranged from roughly -0.01 to -0.17 mm day⁻¹ and -0.05 to -0.2 mm day⁻¹, respectively, with medians of roughly -0.07 and -0.11 mm day⁻¹, respectively (Figure 35a). No notch overlap occurred between the stability groups, meaning the difference in modeled BREB evaporation and measured evaporation was statistically different between the stability regimes; this can be more easily seen in a more zoomed-in Figure 35a (Figure 35b).

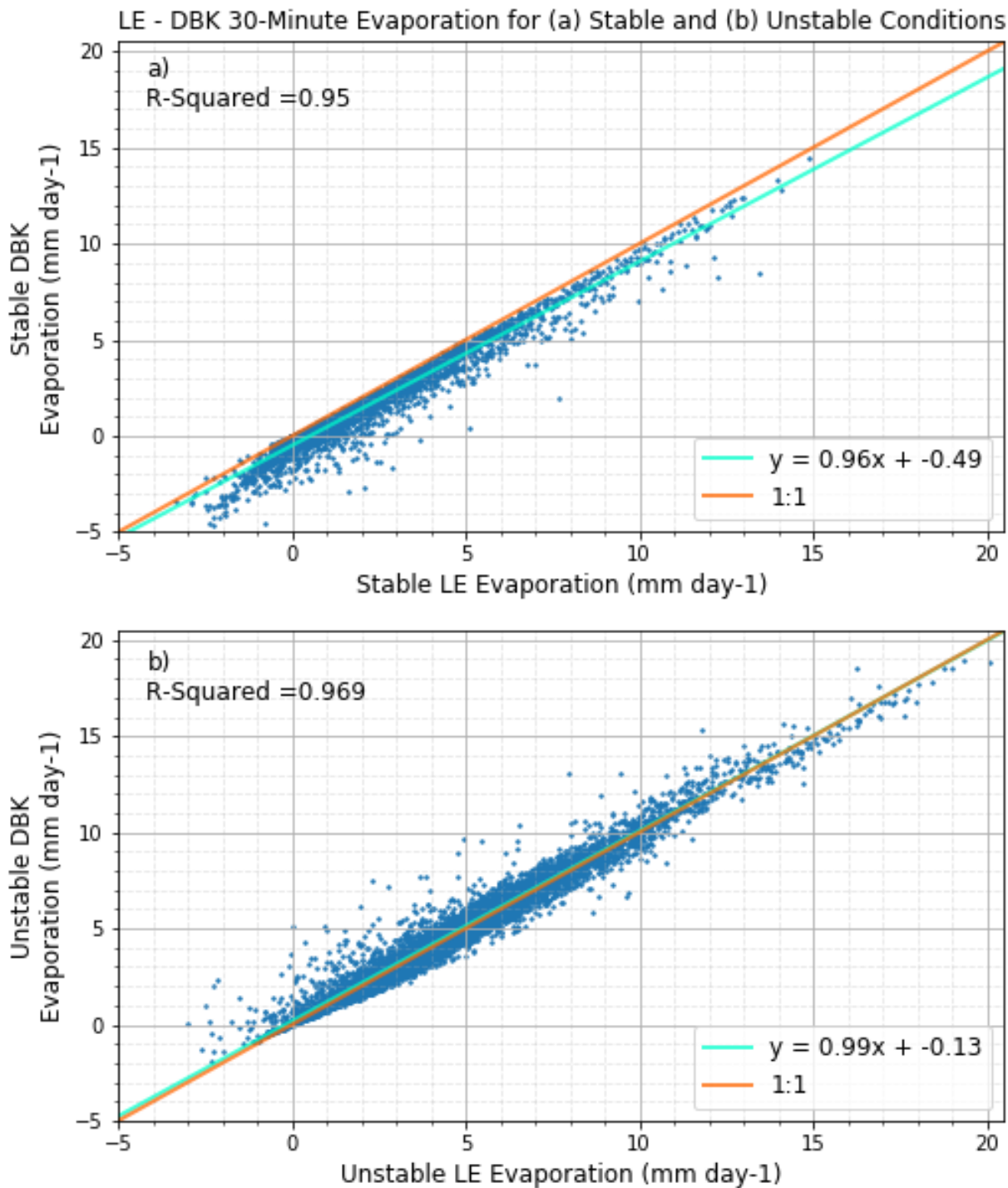


Figure 32: Linear regression of 30-minute modeled DBK evaporation (mm day^{-1}) versus measured evaporation (mm day^{-1}) for stable (a) and unstable (b) stability regimes for 2008.

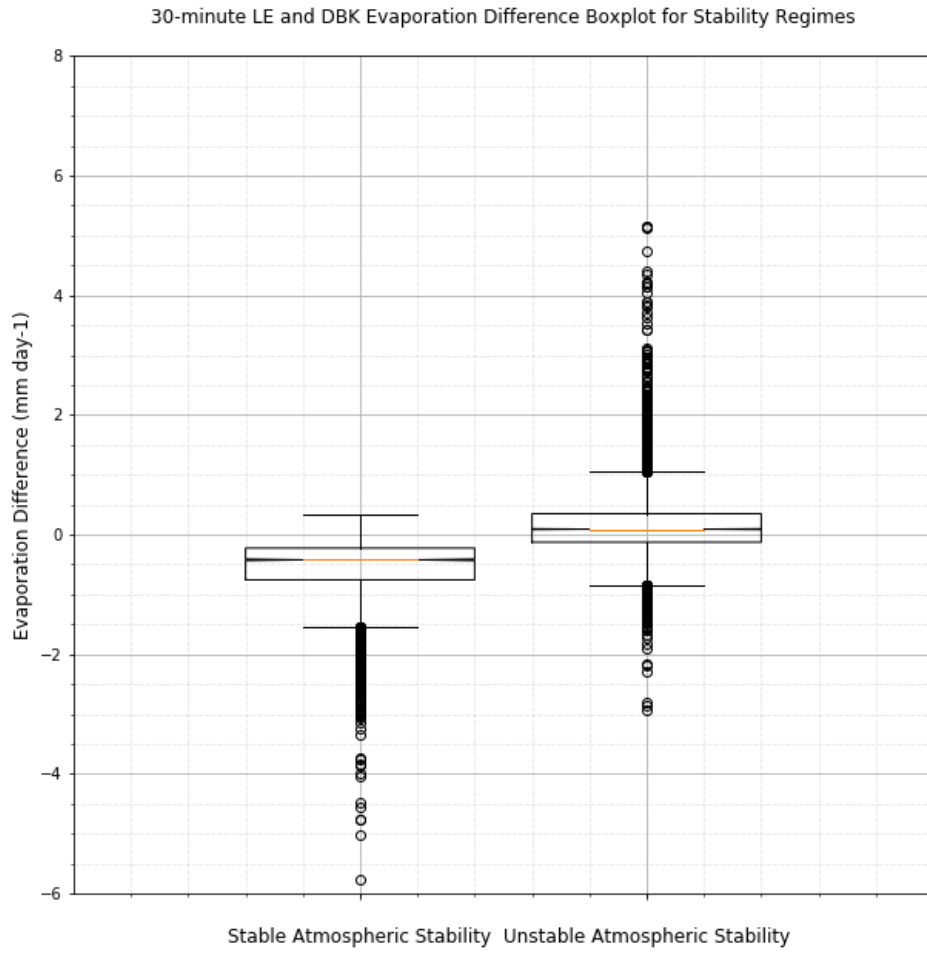


Figure 33: Stable and unstable stability regime boxplot with evaporation difference between modeled DBK and measured evaporation (mm day^{-1}) as the dependent variable. Median values indicated by the orange line in the 95th confidence interval-indicating notches. Outer 25th percentiles indicated by the whiskers.

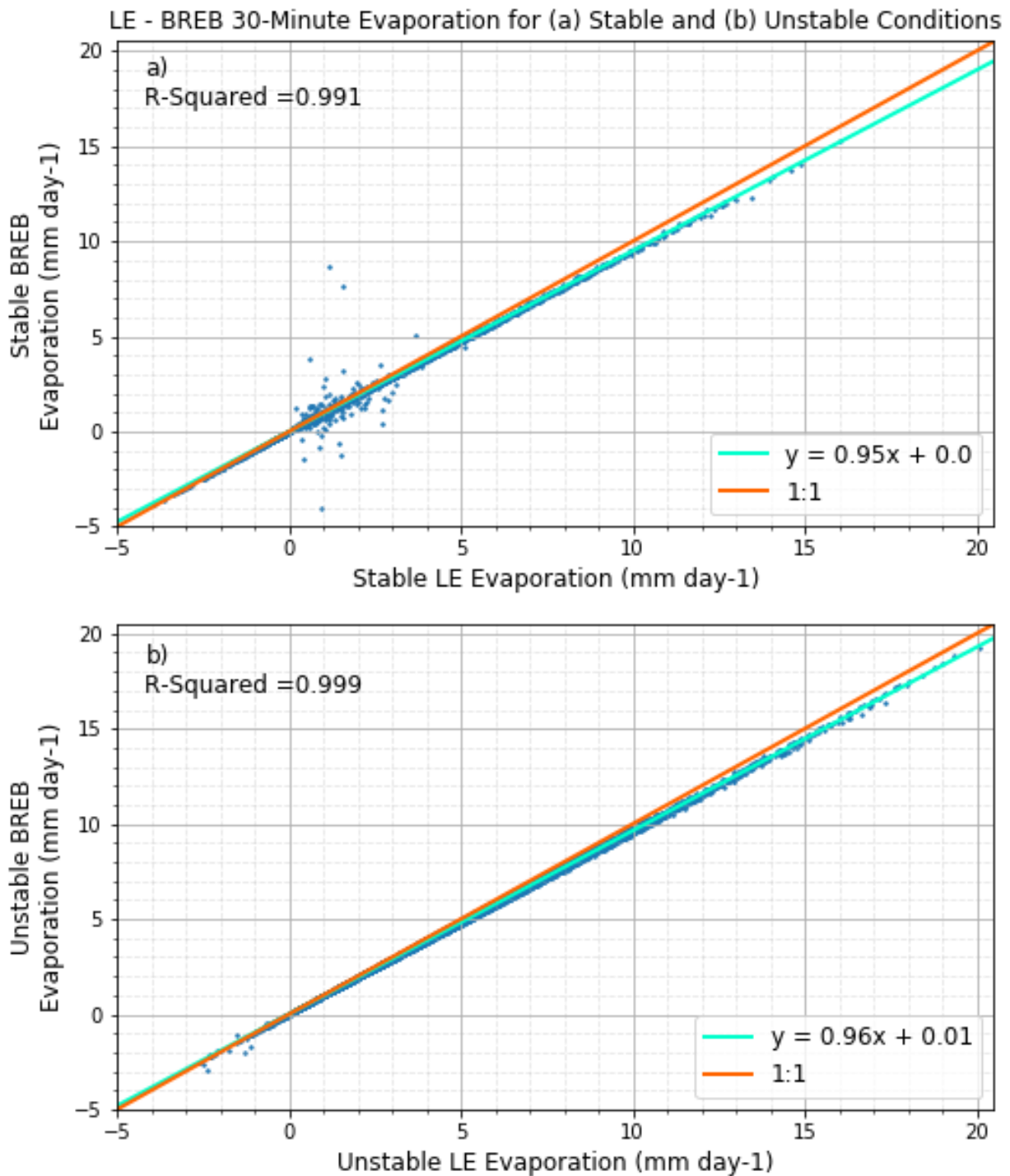


Figure 34: Linear regression of 30-minute modeled BREB evaporation (mm day^{-1}) versus measured evaporation (mm day^{-1}) for stable (a) and unstable (b) stability regimes for 2008.

3.3.2.4. Impact of stability on PM-modeled evaporation estimates

PM-modeled evaporation could explain less variance in measured evaporation when atmospheric was stable, R^2 of 0.822, relative to when the atmosphere was unstable, R^2 of 0.947 (Figure 36). The discrepancy between explainable variance in measured evaporation in the stability regimes was larger for the PM model relative to the previous models. Stable (unstable) evaporation predicted by the PM model showed the largest deviations from measured evaporation when measured evaporation ranged from 0 to 5 (5 to 10) mm day^{-1} . The PM model overestimated measured evaporation relatively consistently when the atmosphere was stable. Of the two stability regimes, the linear regression between modeled PM and measured evaporation deviated from the 1:1 line more when the atmosphere was stable.

The interquartile range magnitude for difference in PM-modeled and measured evaporation was smaller for an unstable atmosphere relative to a stable atmosphere, with values ranging from roughly 0.25 and 1.1 mm day^{-1} and 0 and 0.5 mm day^{-1} , respectively (Figure 37). Medians for stable and unstable stability regimes were roughly 0.5 and 0.2 mm day^{-1} , respectively, for the difference in modeled PM and measured evaporation. Stable and unstable stability groups for difference in modeled PM and measured evaporation were statistically significantly different, as indicated by the lack of notch overlap between the two stability regimes.

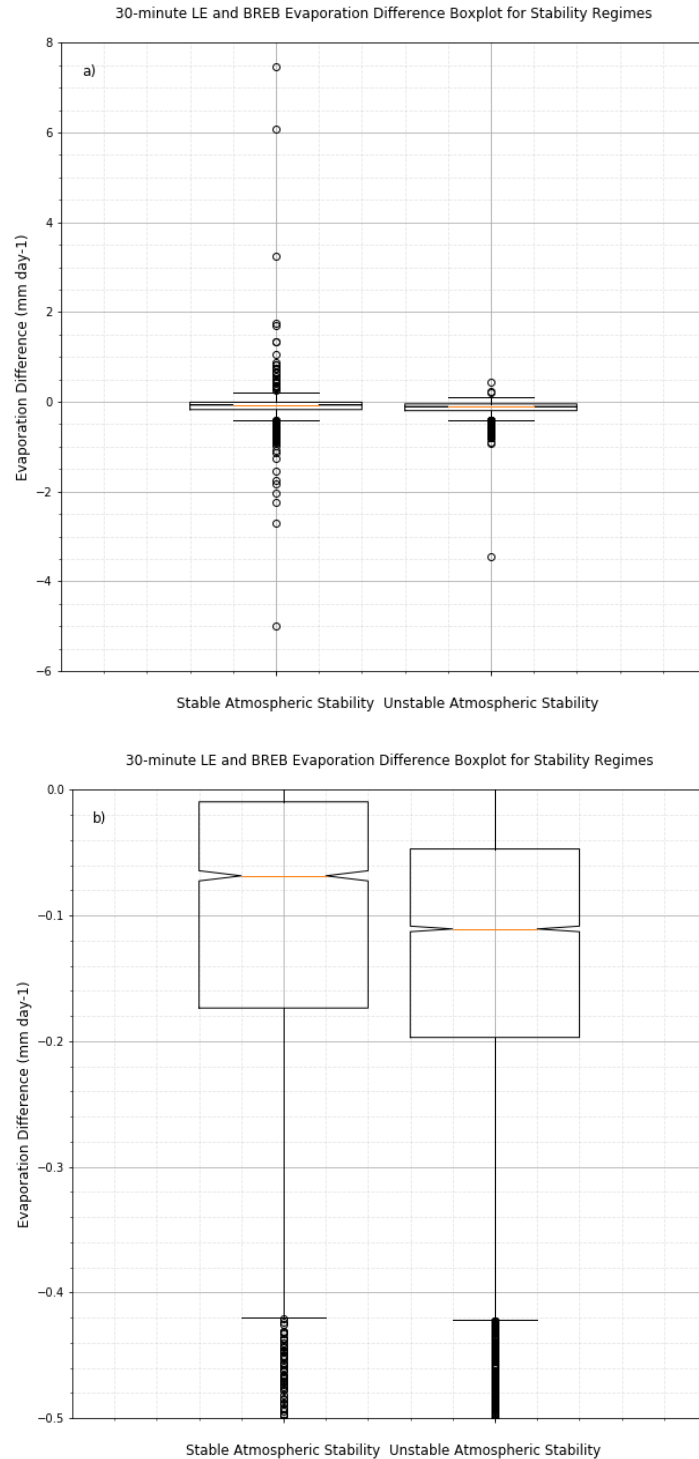


Figure 35: a) Stable and unstable stability regime boxplot with evaporation difference between modeled BREB and measured evaporation (mm day^{-1}) as the dependent variable. Median values indicated by the orange line in the 95th confidence interval-indicating notches. Outer 25th percentiles indicated by whiskers. b) y-axis changed from -6 to 8 mm day^{-1} to -0.5 to 0 mm day^{-1} .

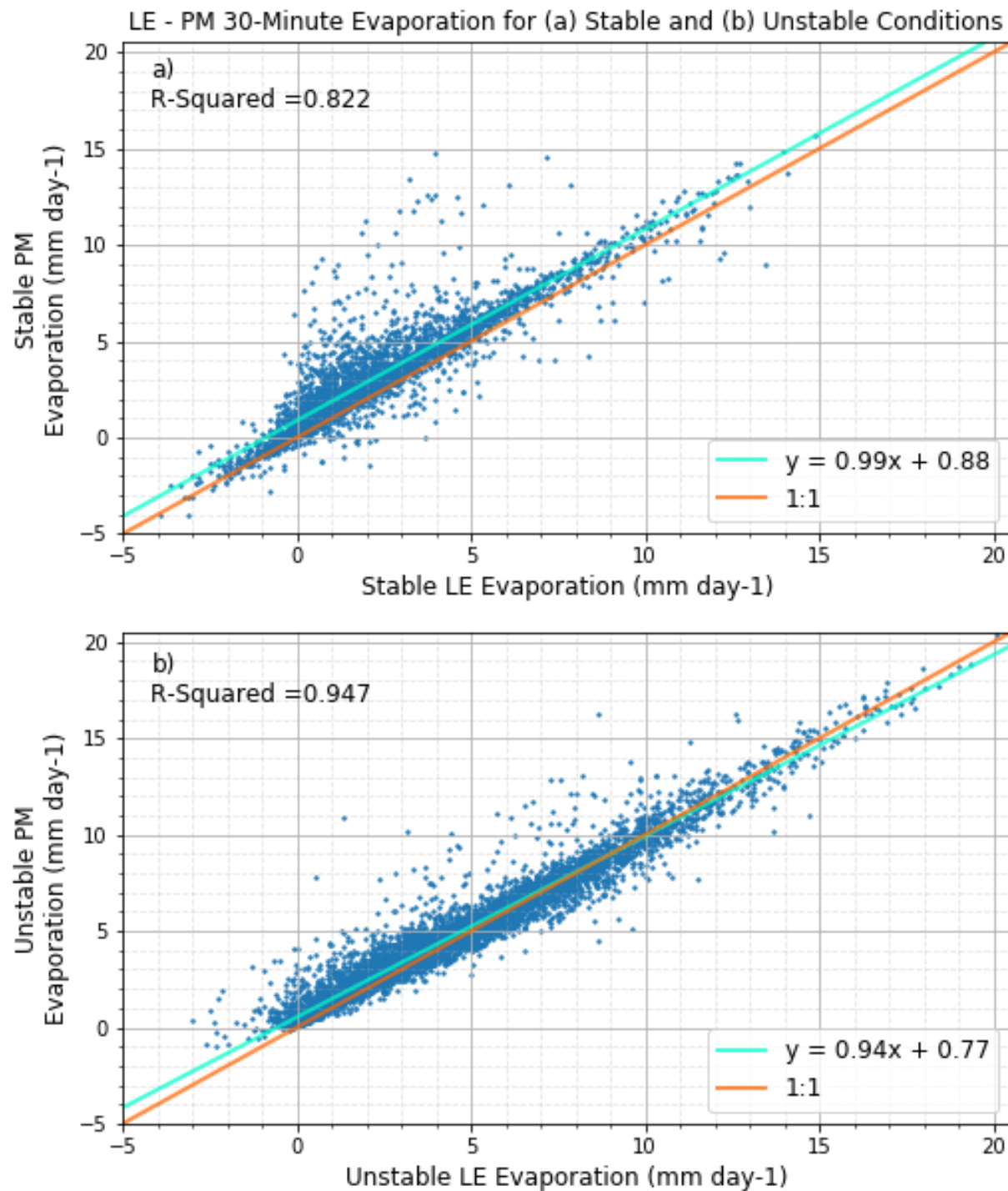


Figure 36: Linear regression of 30-minute modeled PM evaporation (mm day^{-1}) versus measured evaporation (mm day^{-1}) for stable (a) and unstable (b) stability regimes for 2008.

3.3.2.5. Impact of stability on BS-modeled evaporation estimates

The linear regression of modeled BS evaporation versus measured evaporation could explain less of the variance in measured evaporation when stability was positive relative to when it was unstable; modeled BS evaporation was able to explain 66.6% of measured evaporation variance when the atmosphere was stable and 86.5% when the atmosphere was unstable (Figure 38). Modeled BS evaporation was consistently underestimated when the atmosphere was stable, with the most extreme underestimations occurring when measured evaporation was less than roughly 8 mm day^{-1} . Overestimation and underestimation of evaporation was relatively even when the atmosphere was unstable, with a slight bias toward underestimating evaporation. The regression line for modeled BS evaporation versus measured evaporation largely deviated from the 1:1 line when the atmosphere was stable.

The magnitude of the interquartile range between stable and unstable regimes for the difference in modeled BS and measured evaporation was larger for stable than unstable, with values of roughly 1.7, ranging from roughly -2.7 to -0.9 mm day^{-1} , and 1.2 mm day^{-1} , ranging from roughly -0.9 and 0.3 mm day^{-1} , respectively (Figure 39). Notches of the differences in modeled BS evaporation and measured evaporation did not overlap between stability regimes, meaning that the data groups were different to the 95th confidence interval.

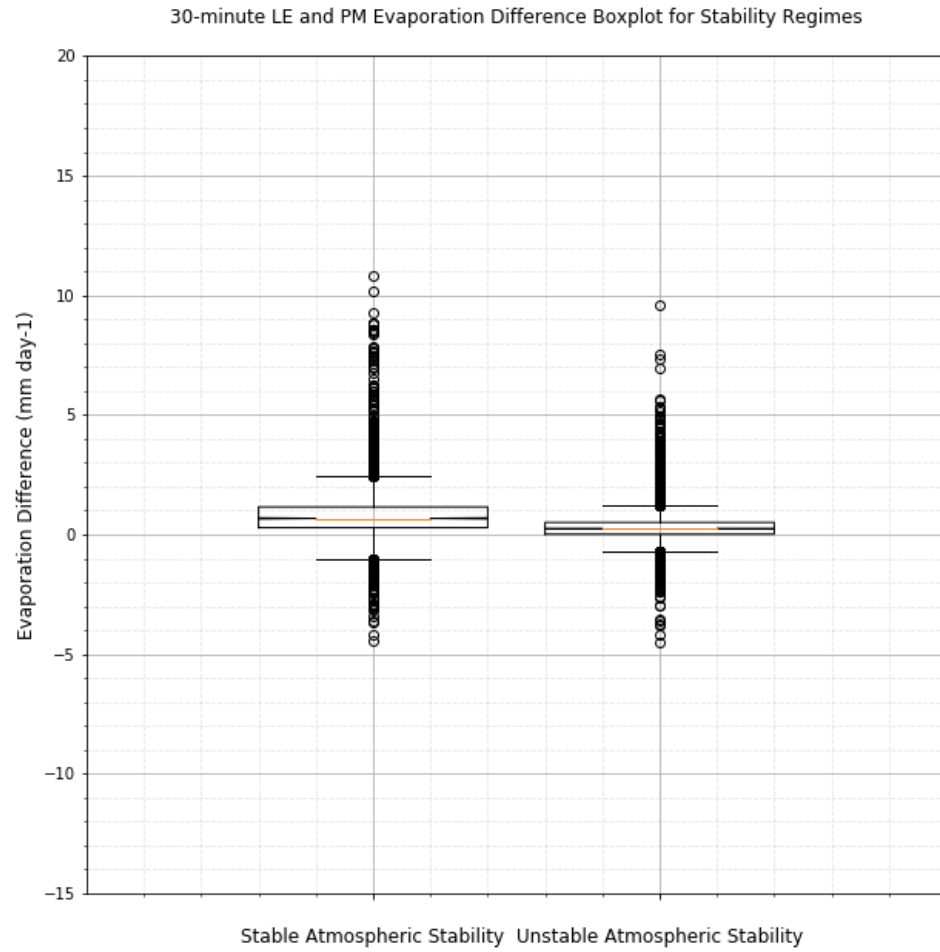


Figure 37: Stable and unstable stability regime boxplot with evaporation difference between modeled PM and measured evaporation (mm day^{-1}) as the dependent variable. Median values indicated by the orange line in the 95th confidence interval-indicating notches. Outer 25th percentiles indicated by the whiskers.

3.3.2.6. Impact of stability on DB-modeled evaporation estimates

DB-modeled evaporation could predict the least amount of variance in measured evaporation of all modeled methods for both stability regimes, with only being to explain 25.2 and

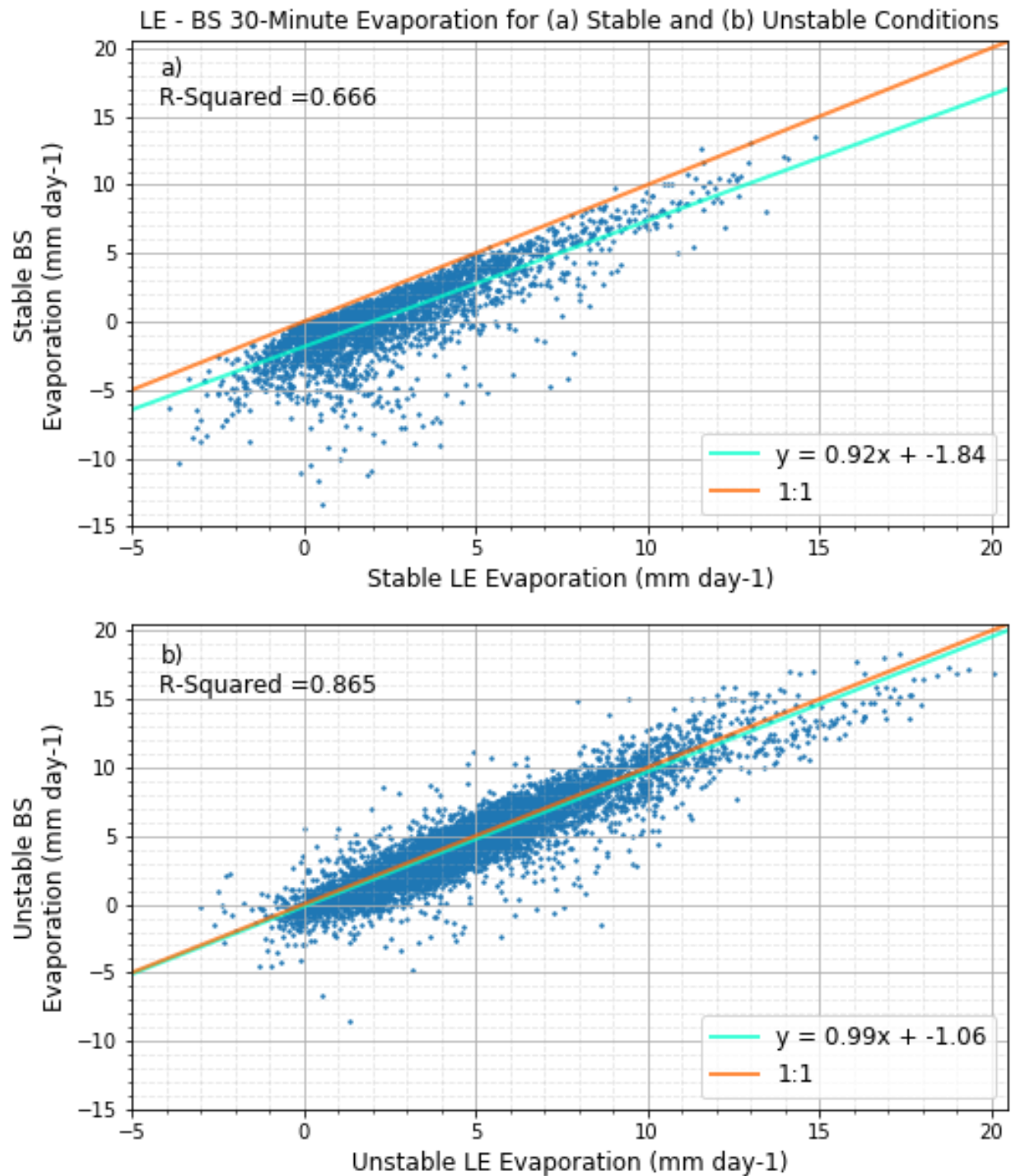


Figure 38: Linear regression of 30-minute modeled BS evaporation (mm day^{-1}) versus measured evaporation (mm day^{-1}) for stable (a) and unstable (b) stability regimes for 2008.

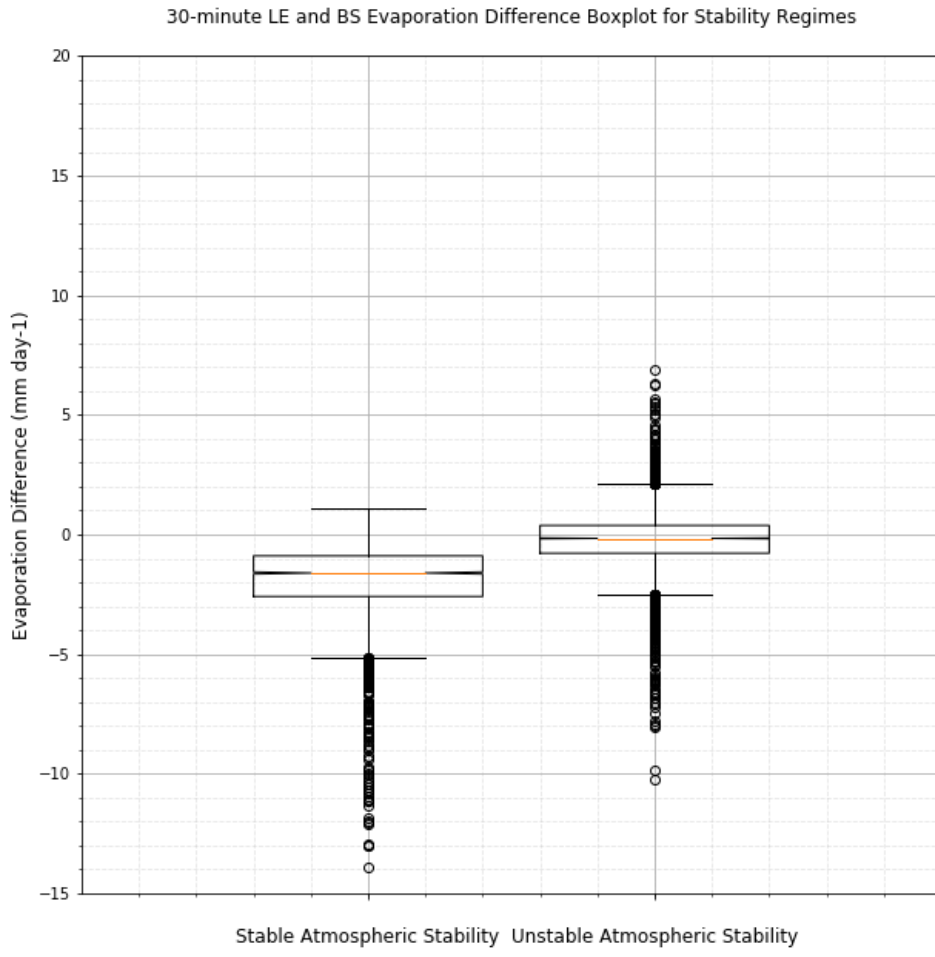


Figure 39: Stable and unstable stability regime boxplot with evaporation difference between modeled BS and measured evaporation (mm day^{-1}) as the dependent variable. Median values indicated by the orange line in the 95th confidence interval-indicating notches. Outer 25th percentiles indicated by the whiskers.

37.8% of the variance for the stable and unstable stability regimes, respectively (Figure 40).

Modeled DB evaporation deviated largely for both stability regimes, but did so in different manners between stable and unstable atmospheric stability. For example, DB-modeled evaporation during unstable conditions generally overestimated (underestimated) evaporation when measured

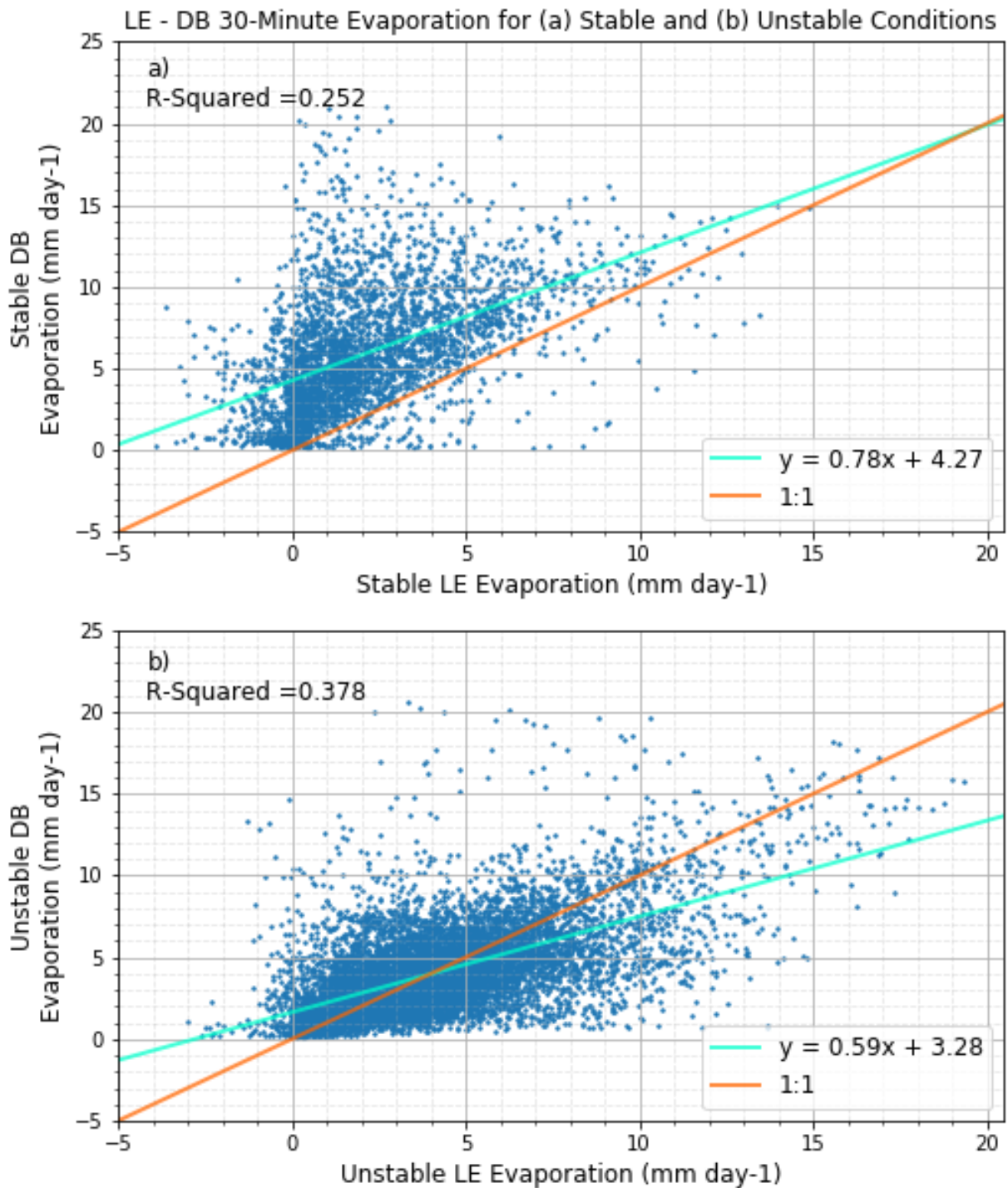


Figure 40: Linear regression of 30-minute modeled DB evaporation (mm day^{-1}) versus measured evaporation (mm day^{-1}) for stable (a) and unstable (b) stability regimes for 2008.

evaporation was less (greater) than 4 mm day⁻¹, while the DB model consistently overestimated evaporation throughout all values of measured evaporation for stable conditions.

Interquartile ranges for DB-modeled and measured evaporation differences were largest for both stable and unstable stability regimes, ranging from roughly 1.7 to 5.4 and -1.2 to 1.1 mm day⁻¹, of all models (Figure 41). Medians were located at 3.1 and 0 mm day⁻¹ for the stable and unstable stability regimes, respectively. It can also be concluded that the differences in modeled DB and measured evaporation for stable and unstable atmospheres were statistically different to the 95th level of confidence.

3.3.1.7. Summary of wind speed impact on modeled evaporation estimates

Throughout all modeled evaporation methods, modeled evaporation could explain the variance in measured evaporation better under unstable relative to stable atmospheric conditions. A discernible difference in performance was observed in all modeled evaporation methods, although less-so for PT and DBK, and measured evaporation between measured evaporation values of 0 and 5 mm day⁻¹, particularly for the stable stability regime. All modeled methods for estimating evaporation deviated from the 1:1 line by a larger amount when the atmosphere was stable relative to when it was unstable, once again indicating that modeled evaporation performance was worse when the atmosphere was stable. Interquartile ranges were either similar

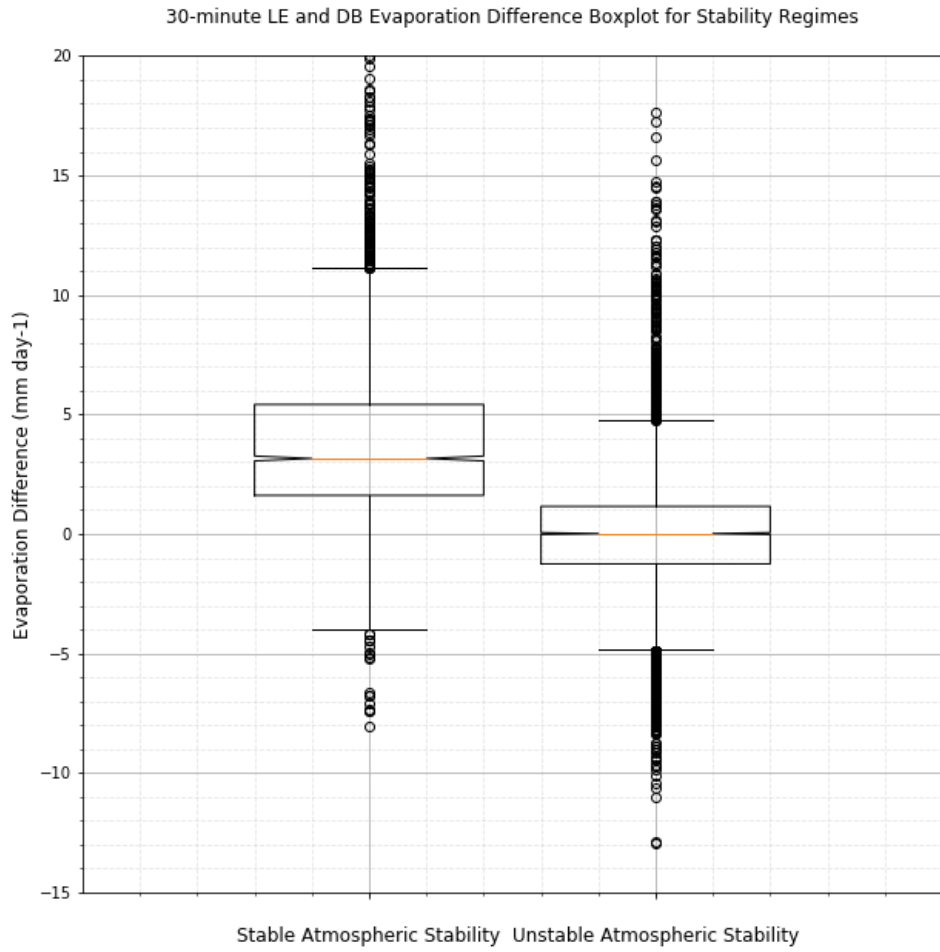


Figure 41: Stable and unstable stability regime boxplot with evaporation difference between modeled DB and measured evaporation (mm day^{-1}) as the dependent variable. Median values indicated by the orange line in the 95th confidence interval-indicating notches. Outer 25th percentiles indicated by the whiskers.

or larger in magnitude for the stable stability regime compared to the unstable regime. Additionally, all differences in modeled and measured evaporation were statistically significantly different between the two stability regimes to the 95th confidence interval. The generally greater ability to explain more variance in measured evaporation for unstable stability conditions could

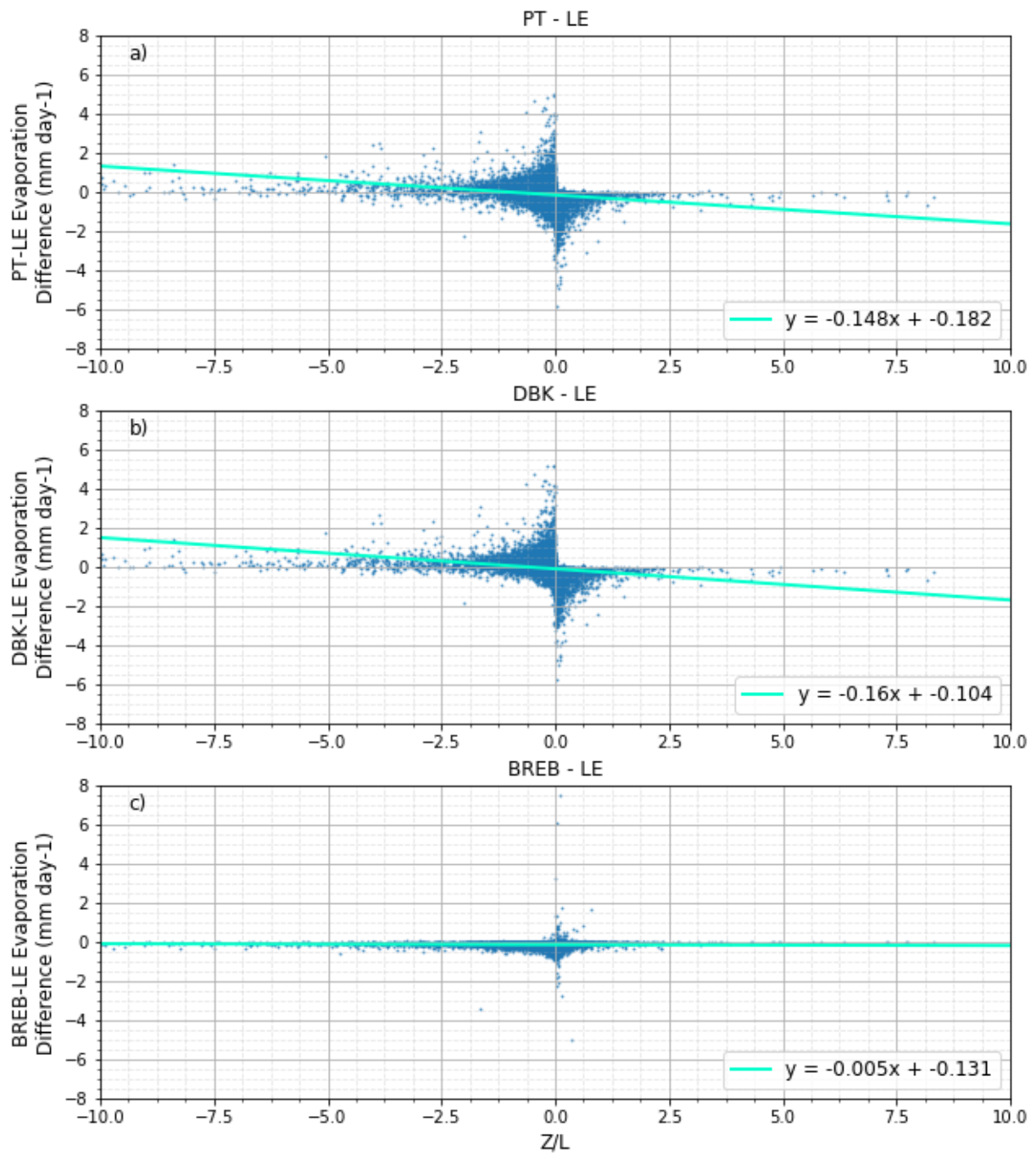
likely be attributed to the relatively equal under/overestimation of evaporation throughout all measured evaporation values. Although models could explain less variance in measured evaporation when the atmosphere was stable, stable evaporation was generally more predictable with consistent biases.

3.4. Physical causes of poor evaporation estimates during near-neutral stability

To determine the cause(s) of poor model performance in estimating evaporation, linear regressions were made for the difference in modeled and measured evaporation versus different physical measurements made at the study location. The tested independent variables included Δe , temperature gradient (ΔT), z/L , wind direction, and wind speed, with the only easily-discernible pattern being observed in the linear regression of modeled and measured evaporation difference versus atmospheric stability. In the modeled and measured evaporation difference and atmospheric stability regressions, it is evident that most occurrences of poor evaporation estimation are centered around near-neutral stability for all evaporative models (Figure 42); near-neutral stability being when z/L is between -0.05 and 0.05, as defined in *Yusup and Liu (2016)*.

Interestingly, the PT, DBK, and BS (DB and PM) models consistently underestimated (overestimated) evaporation during stable conditions. This trend could be due to the models not accurately estimating the general suppression of evaporation during stable conditions. Little to no

Modeled - LE Evaporation Difference vs. Stability



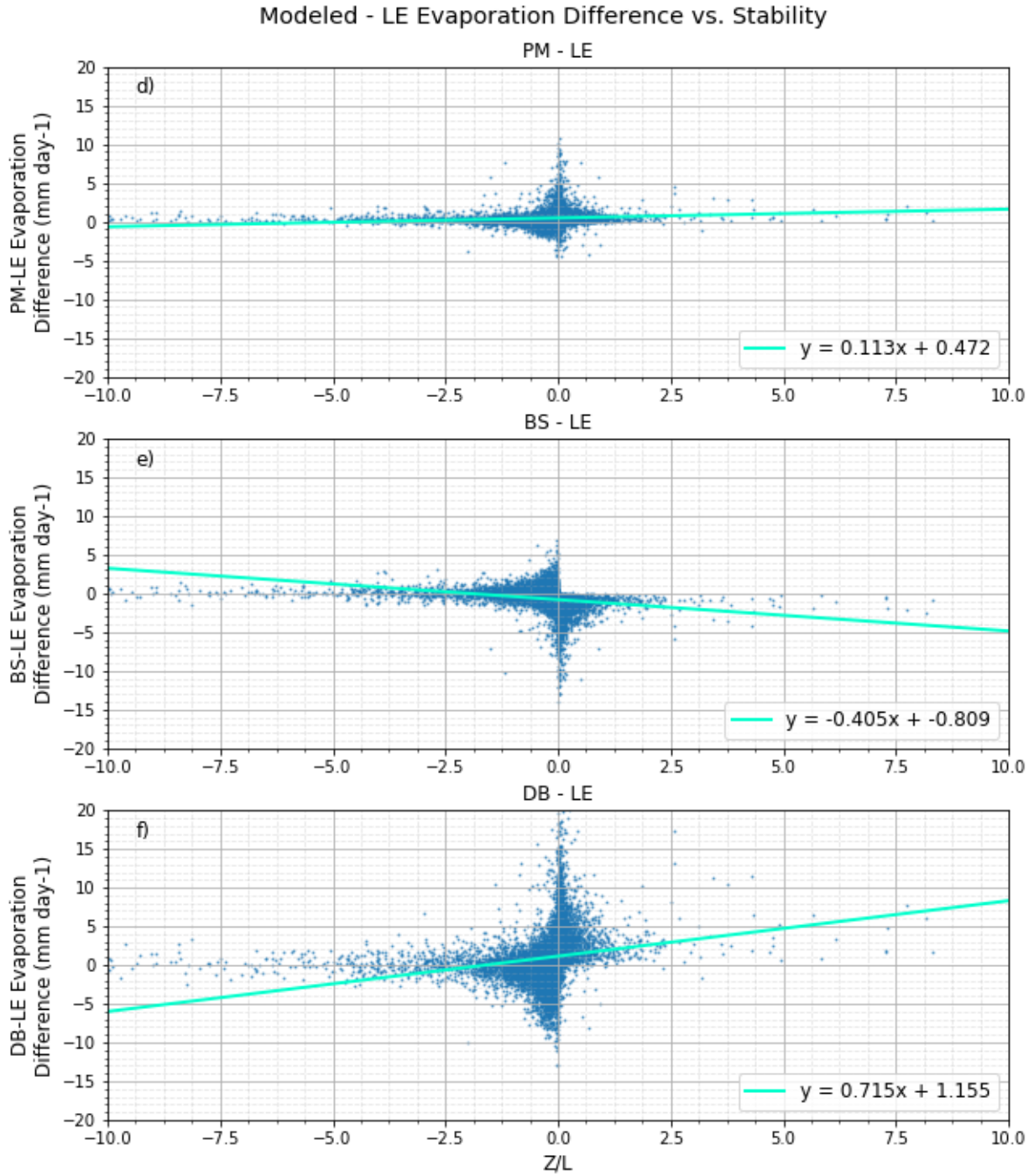


Figure 42: Difference in modeled evaporation and measured evaporation (mm day^{-1}) plotted against stability for PT (a), DBK (b), BREB (c), PM (d), BS (e), and DB (f) models.

discernible trend in stability-dependent underestimation or overestimation of evaporation was observed with the BREB model. The difference in ability to predict evaporation when the atmosphere was stable between the PT, DBK, PM, BS, and DB models and the BREB model could be a result of the method in which a stability-influencing variable, temperature, was implemented into the models. The only form of inclusion of a stability, stability-dependent, or stability-influencing term for the PT, DBK, PM, BS, and DB models was through the s (slope of the saturation vapor pressure-temperature curve at mean air temperature) term (Equation 6), which utilized 2-meter air temperature. The s term, and subsequently the PT, DBK, PM, BS, and DB models, was not able to accurately capture the stable stability-induced suppression of evaporation. On the other hand, the BREB model directly incorporated a stability-influencing term, T_s (water surface temperature), into the model. Although it is possible the T_s term was not incorporated into the BREB model to capture the impact of stability on evaporation throughout all ranges of stability, this term might have done just that.

Since many 30-minute stability points fell within the stability range that was considered near-neutral, near-neutral points with magnitudes of evaporation under/overestimation exceeding ± 3 standard deviations were isolated for comparison with other physical parameters to see if any correlations existed. In other words, points with z/L values between -0.05 and 0.05 and evaporation differences greater than ± 3 evaporation difference standard deviations were isolated. The physical parameters the isolated points were tested against included Δe , ΔT , H, LE, BR, wind direction, and wind speed. Of all tested physical parameters, the only term that had a correlation with the isolated points was wind speed (Figure 43). The correlation between the isolated points and wind speed

revealed that most isolated points occurred when wind speeds fell into the moderate and, even more-so, high wind speed regimes, as indicated by the relative percentage of low, moderate, and high wind speed regime occurrence for the isolated points relative to all points. For example, all-point (isolated-point) low, moderate, and high wind speed regimes contained roughly 48-49% (2-10%), 38-39% (30-50%), and 12.5% (40-65%) of the total points, respectively, for all models (Table 3). It can therefore be concluded that all models performed the worst when both wind speed was high and stability was near-neutral. Poorest model performance during times of high wind speed and near-neutral stability was likely due to the methods in which stability and wind speed, if at all, were incorporated into the models. Since both parameters were not captured well by the models, the poor model performance was compounded by the combination of the two physical characteristics.

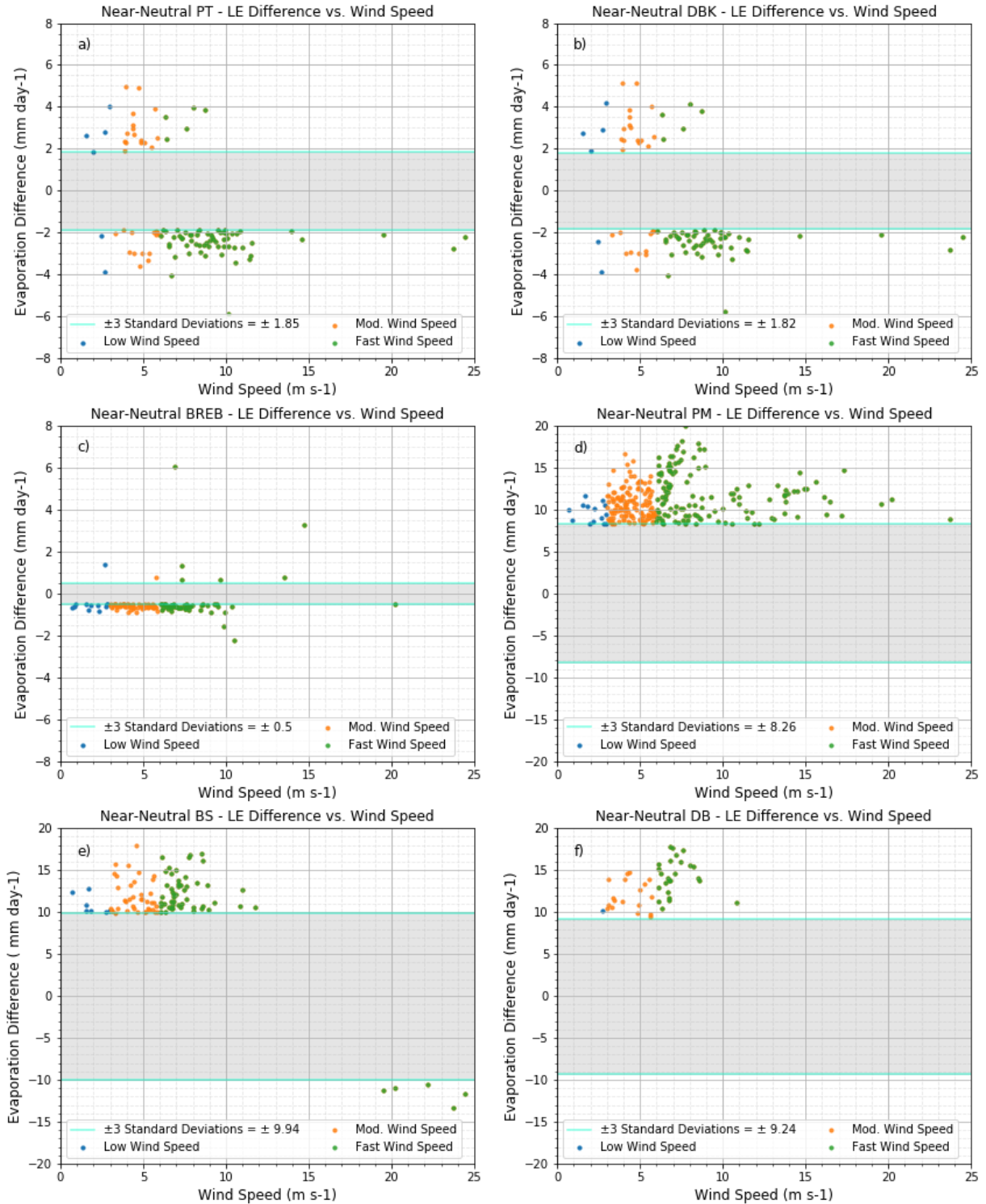


Figure 43: Regression of the measured and modeled evaporation difference (mm day^{-1}) of isolated near-neutral stability points versus wind speed (m s^{-1}) for PT (a), DBK (b), BREB (c), PM (d), BS (e), and DB (f) models.

4. Summary and Conclusion

In this study, the performance of PT, DBK, BREB, PM, BS, and DB evaporative models were validated against direct measurements of evaporation using eddy covariance and meteorological measurements from the Ross Barnett Reservoir in 2008 for monthly, daily, and 30-minute timescales. Analyses for determining the causes of poor modeled evaporation estimates were also completed in this study. The following conclusions were made:

1. When considering the ability for the models to explain the variance in measured evaporation, magnitude of evaporation difference, and consistency in bias, the six evaporative models naturally fell into three performance categories. PT, DBK, and BREB were the top three performing models of all tested models. Despite being able to explain less variance in measured evaporation, the BREB model performed better than the PT and DBK models due to its consistent bias toward underestimating evaporation. PT and DBK had similar performance on a monthly timescale. PM and BS models fell into the middle performance tier, with the PM model performing slightly better than the BS model. Like the BREB model, the better performance of the PM model was due to the model's consistent bias of estimating, in this case overestimating, evaporation throughout the year, despite the BS model being able to explain more variance in measured evaporation. Of the six models, the DB model performed the worst by a considerable amount, with an inconsistent bias throughout the year, largest magnitude of under/overestimation of evaporation, and ability to only explain 5.4% of the variance in measured evaporation.

2. Daily analysis revealed that the models fell into the same three performance tiers as the monthly timescale, with the PT, DBK, and BREB (PM and BS) models falling into the highest (middle) performance tier and the DB model falling into the lowest performance tier. Of the models in the highest tier of performance, the BREB model performed the best due to its relatively consistent bias throughout the year, ability to closely follow the 1:1 line, and ability to explain the most variance in measured evaporation. The DBK model performed slightly better than the PT model on a daily timescale due to its ability to explain slightly more of the variance in measured evaporation. PM-modeled evaporation again performed better than BS-modeled evaporation estimates in terms of explainable measured evaporation variance and more closely following the 1:1 line. Consistent with monthly timescale findings, DB-modeled evaporation estimates were the worst of all methods.

3. Model performance for a 30-minute timescale did not fall into performance tiers as naturally as monthly and daily timescales. Consistent with the monthly and daily timescales, the BREB model performed the best of all models, as indicated by the model's consistent bias for underestimating evaporation and its ability to accurately explain measured evaporation variance. PT and DBK models both performed equally well and second best relative to the other models, based on their ability to explain a high amount of the variance in measured evaporation. Of the two models, the DBK model performed very slightly better than the PT model. PM-modeled evaporation predicted evaporation better than the BS model due to the greater ability to explain measured evaporation variance and a generally lower magnitude of modeled and measured evaporation difference. Of all models, the DB model could estimate evaporation least accurately on a 30-minute timescale.

4. The change in relative model performance as the analyzed timescale degraded from a monthly to daily timescale revealed that the BREB model improved in performance with a greater ability to explain measured evaporation variance. Quality of performance between the PT and DBK models was greater for the DBK model as timescale decreased from monthly to daily. Additionally, the PM model could explain more variance in measured evaporation relative to the BS model for a daily timescale, which was the opposite conclusion for a monthly timescale; although, model performance for the PM model was greater for both timescales. As the timescale decreased from monthly to daily, an increase (decrease) was observed in ability for the BREB, PM, and DB (PT, DBK, and BS) models to explain measured evaporation variance. As the timescale decreased from a daily to a 30-minute timescale, a decrease in ability for modeled evaporation to explain measured evaporation variance was observed for all models, excluding the DB model.

Relative performance of the models was consistent throughout all tested timescales and could be ranked as follows: BREB, DBK/PT, PM, BS, and DB. It should be noted that performance of the PT and DBK models was very similar throughout all timescales, with the DBK model slightly, if at all, performing better than the PT model. Although the PM model performed better than the BS model for all tested timescales, the difference in performance between the two models was greatest for the 30-minute timescale. The likely reason for the PM, BS, and DB models consistently performing worse than the PT, DBK, and BREB models was due to the fact that wind speed was incorporated into the models. DB-modeled evaporation was consistently and

considerably less accurate than the other five models. This was likely due to the lack of inclusion of the $R_n - Q_x$, or in this case $H + LE$, in the model.

5. When the low, moderate, and high wind speed regimes were compared to performance of the evaporative models, a clear negative feedback response was observed between wind speed magnitude and model performance; model performance consistently decreased in response to an increase in wind speed. Wind speed regime interquartile ranges generally increased in magnitude as wind speed increased. With the exceptions being between low and high wind speed regimes for BREB-modeled evaporation and the low and moderate wind speed regimes for DB-modeled evaporation, modeled and measured evaporation differences between low, moderate, and high wind speed regimes were statistically significantly different at the 95th percentile confidence interval. The negative feedback trend between wind speed and evaporative model performance was likely due to the lack of inclusion or method of inclusion of a wind speed or wind speed-dependent term for all models. The method in which wind speed was included in the PM, BS, and DB models did work relatively well when wind speeds fell into the low wind speed regime.

6. Unstable atmospheric stability consistently resulted in higher ability for models to explain measured evaporation variance for all models relative to stable atmospheric conditions. All evaporative models deviated from the 1:1 line more for a stable atmosphere relative to an unstable atmosphere. Relative to an unstable atmosphere, stable atmospheric stability had either similar or larger-in-magnitude modeled and measured evaporation difference interquartile ranges, with statistically significant differences to the 95th confidence interval, for all models. The relatively

equal under/overestimation of evaporation throughout all magnitudes of measured evaporation could have been the cause of the models being able to explain more measured evaporation variance during unstable conditions. Although less measured evaporation variance could be explained during stable atmospheric conditions, consistent biases in evaporation estimation made modeled evaporation under stable conditions more predictable than that under unstable conditions.

7. Isolated points, near-neutral stability points with evaporation under/overestimation exceeding ± 3 standard deviations, displayed a discernible correlation with wind speed. The correlation between the isolated points and wind speed revealed that the isolated points primarily occurred when wind speeds were high, as indicated by the relative occurrence of low, moderate, and high wind speed points between all points and the isolated points. It was therefore concluded that all models performed poorest when atmospheric stability was near-neutral and wind speeds were high. This finding is likely due to the compounding of errors associated with the model's ability to accurately capture these two physical characteristics.

References

- Abtew, W., 2001: Evaporation estimation for Lake Okeechobee in South Florida. *J. Irrig. Drain. Eng.*, 127(3), 140–147.
- Allen, R. G., Walter, I. A., Elliot, R. L., Howell, T.A., Itenfisu, D., Jensen, M. E., and Snyder, R., 2005: The ASCE standardized reference evapotranspiration equation. ASCE and American Society of Civil Engineers.
- Baldocchi D., 1994: A comparative study of mass and energy exchange over a closed C3 (wheat) and an open C4 (corn) canopy: I. The partitioning of available energy into latent and sensible heat exchange. *Agric. For Meteorol.*, 67:191–220.
- Bates, G. T., F. Giorgi, and S. W. Hostetler, 1993: Toward the simulation of the effects of the Great Lakes on regional climate. *Mon. Wea. Rev.*, 121, 1373–1387.
- Bates, G.T., S.W. Hostetler, and F. Giorgi, 1995: Two-year simulation of the Great Lakes region with a coupled modeling system. *Mon. Wea. Rev.*, 123, 1505–1522.
- Baumgartner, A., Reichel, E., 1975: The World Water Balance. R. Oldenbourg-Verlag, Munchen, Wien, 1–179.
- Blanken, P. D., and Coauthors, 2000: Eddy covariance measurements of evaporation from Great Slave Lake, Northwest Territories, Canada. *Water Resour. Res.*, 36, 1069–1077.
- Blanken, P.D., Rouse, W.R., Schertzer, W.M., 2003: Enhancement of evaporation from a large northern lake by the entrainment of warm, dry air. *J. Hydrometeor.*, 4, 680–693.
- Bonan, G. B., 1995: Sensitivity of a GCM simulation to inclusion of inland water surfaces. *J. Clim.*, 8, 2691–2704.

Bouin, M.-N., G. Caniaux, O. Traullé, D. Legain, and P. Le Moigne, 2012: Long-term heat exchanges over a Mediterranean lagoon. *J. Geophys. Res.*, 117, D23104.

Bowen, I.S., 1926: The ratio of heat losses by conduction and by evaporation from any water surface. *Phys. Rev.*, 779–787.

Brutsaert, W., 1982: Evaporation Into the Atmosphere: Theory, History and Applications. *D. Reidel Publishing Company*, Dordrecht.

Brutsaert, W., Stricker, H., 1979: An Advection-Aridity Approach to Estimate Actual Regional Evapotranspiration. *Water Resour. Res.*, 15 (2), 443–450.

Brutsaert, W., and G.-T. Yeh, 1970: Implications of a type of empirical evaporation formula for lakes and pans. *Water Resour. Res.*, 6 (4), 1202–1208.

Cheng, W., 1978: A Study of Evaporation From Lake Albert, Using Meteorological and Hydrological Observations. Flinders Univ., Bedford Park, South Australia, 193.

Cole, J. J., and Coauthors, 2007: Plumbing the global carbon cycle: Integrating inland waters into the terrestrial carbon budget. *Ecosystem*, 10, 171–184.

Dalton, M.S., Aulenbach, B.T., Torak, L.J., 2004: Ground-water and surface-water flow and estimated water budget for Lake Seminole, northwestern Georgia and northwestern Florida. *Sci. Inves. Rep.*, 2004-5073.

Davies J. A., Allen C. D., 1973: Equilibrium, potential and actual evaporation from cropped surfaces in southern Ontario. *J. Appl. Meteorol.*, 12:649–657.

deBruin, H.A.R., 1978: A simple model for shallow lake evaporation. *J. App. Meteorol.*, 17 (8), 1132–1134.

deBruin, H.A.R., Keijman, J.Q., 1979: The Priestley-Taylor evaporation model applied to a large, shallow lake in the Netherlands. *J. App. Meteorol.*, 18 (7), 898–903.

Downing, J.A. et al, 2006: The global abundance and size distribution of lakes, ponds, and impoundments. *Limnol. and Oceanog.*, 51 (5), 2388–2397.

Eaton, A. K., Rouse, W. R., Lafleur, P. M., Marsh, P., and Blanken, P. D., 2001: Surface energy balance of the western and central Canadian sub-Arctic: Variations in the energy balance among five major terrain types. *J. Climate*, 14, 3692–3703.

Eichinger, W. E., Parlange, M. B., Stricker, H., 1996: On the concept of equilibrium evaporation and the value of the Priestley–Taylor coefficient. *Water Resour. Res.*, 32:161–164

Eugster, W., Kling G., Jonas, T., McFadden, J., Wüest, A., MacIntyre, S., and Chapin III, F. S., 2003: CO₂ exchange between air and water in an Arctic Alaskan and mid-latitude Swiss lake: Importance of convective mixing. *J. Geophys. Res.*, 108, 4362.

Gibblett, M. A., 1921: Some problems connected with evaporation from large expanses of water. *Proc. R. Soc. London A.*, 99 (701), 472–490.

Gibson, J. J., 2002: Short-term evaporation and water budget comparisons in shallow Arctic lakes using non-steady isotope mass balance. *J. Hydrol.*, 264 (1-4), 242–261.

Granger, R. J., and Hedstrom, N., 2011: Modelling hourly rates of evaporation from small lakes. *Hydrol. Earth Syst. Sci.*, 15, 267– 277.

Gunaji, N. N., 1968: Evaporation investigations at Elephant Butte Reservoir in New Mexico. *Internat. Assoc. Sci. Hydro.*, 78, 308–325.

Guo, X., Liu, H., and Yang K., 2015: On the application of the Priestley–Taylor relation on sub-daily time scales. *Bound.-Layer Meteorol.*, 156, 489–499.

Harbeck, G. E. J., Kohler, M. A., Koberg, G. E., 1958: Water-loss investigations: Lake Mead studies. *Prof. Paper USGS*, 298.

Holtslag, A. A. M. and Van Ulden, A. P., 1983: A Simple Scheme for Daytime Estimates of Surface Fluxes from Routine Weather Data. *J. Cli. Appl. Meteorol.* 22, 517–529.

Jensen, M. E., Burman, R. D., Allen, R. G., 1990: Evapotranspiration and Irrigation Water Requirements. *ASCE Manuals and Rep. on Eng. Pract.*, 70, 352.

Jonsson, A., Åberg, J., Lindroth, A., and Jansson, M., 2008: Gas transfer rate and CO₂ flux between an unproductive lake and the atmosphere in northern Sweden. *J. Geophys. Res.*, 113, G04006.

Kaufman, Y. J. and Gao, B. C., 1992: Remote sensing of water vapor in the near IR from EOS/MODIS, in IEEE Transactions on Geoscience and Remote Sensing, vol. 30, no. 5, 871-884.

Kohler, M. A., Nordenson, T. J., Fox, W. E., 1955: Evaporation from pans and lakes. *US Wea. Bur. Res. Paper*, 38, 21.

Lenters, J. D., Kratz, T. K., Bowser, C. J., 2005: Effects of climate variability on lake evaporation: results from a long-term energy budget study of Sparkling Lake, northern Wisconsin (USA). *J. Hydro.*, 308, 168–195.

Liu, H, Zhang, Y., Liu, S., Jiang, H., Sheng, L., and Williams, Q. L., 2009: Eddy covariance measurements of surface energy budget and evaporation in a cool season over southern open water in Mississippi. *J. Geophys. Res.*, 114, D04110.

Liu, H, Blanken, P. D., Weidinger, T., and Nordbo A., 2011: Variability in cold front activities modulating cool-season evaporation from a southern inland water in the USA. *Environ. Res. Lett.*, 6, 024022.

- Liu, H., Zhang, Q., and Dowler, G., 2012: Environmental controls on the surface energy budget over a large southern inland water in the United States: An analysis of one-year eddy covariance flux data. *J. Hydrometeorol.*, 13 (6), 1893–1910.
- Long, Z., Perrie, W., Gyakum, J., Caya, D., and Laprise, R., 2007: Northern lake impacts on local seasonal climate. *J. Hydrometeorol.*, 8, 881–896.
- Lowe, P.R., 1977: An approximating polynomial for the computation of saturation vapor pressure. *J. App. Meteorol.*, 16 (1), 100–103.
- Lowe, L. D., Webb, J. A., Nathan, R. J., Etchells, T., and Malano, H. M., 2009: Evaporation from water supply reservoirs: An assessment of uncertainty. *J. Hydrol.*, 376 (1–2), 261–274.
- McGowan, H. A., Sturman, A. P., Mackellar, M. C., Weibe, A. H., and Neil, D. T., 2010: Measurements of the surface energy balance over a coral reef flat, Heron Island, southern Great Barrier Reef, Australia. *J. Geophys. Res.*, 115, D19124.
- McJannet, D.L., Cook, F. J., McGloin, R. P., McGowan, H. A., and Burn, L. S., 2011: Estimation of evaporation and sensible heat flux from open water using a large-aperture scintillometer. *Water Resour. Res.*, 47, W05545,
- McJannet, D. L., Cook, F. J., and Burn, S., 2013: Comparison of techniques for estimating evaporation from an irrigation water storage. *Water Resour. Res.*, 49, 1415–1428.
- Meijninger, W. M. L., Green, A. E., Hartogensis, O. K., Kohsieck, W., Hoedjes, J. C. B., Zuurbier, R. M., and De Bruin, H. A. R., 2002: Determination of area-averaged water vapour fluxes with large aperture and radio wave scintillometers over a heterogeneous surface—Flevoland Field Experiment. *Bound. Lay. Meteorol.*, 105 (1), 63–83.
- Morton, F.I., 1983: Operational estimates of lake evaporation. *J. Hydrol.*, 66, 77–100.

Nordbo, A., Launiainen, S., Mammarella, I., Leppäranta, M., Huotari, J., Ojala, A., and Vesala, T., 2011: Long-term energy flux measurements and energy balance over a small boreal lake using eddy covariance technique. *J. Geophys. Res.*, 116, D02119.

Rasmussen, A. H., Hondzo, M., Stefan, H. G., 1995: A test of several evaporation equations for water temperature simulations in lakes. *Water Res. Bullet.*, 31 (6), 1023–1028.

Rosenberry, D. O., Stannard, D. I., Winter, T. C., Martinez, M. L., 2004: Comparison of 13 equations for determining evapotranspiration from a prairie wetland, Cottonwood Lake area, North Dakota, USA. *Wetlands. J. Hydrol.*, 24 (3), 483–497.

Rosenberry, D. O., Winter, T. C., Buso, D. C., and Likens, G. E., 2007: Comparison of 15 evaporation methods applied to a small mountain lake in the northeastern USA, *J. Hydrol.*, 340, 149–166.

Rouse W. R., Oswald, C. J., Binyamin, J., Spence, C., Schertzer, W. M., Blanken, P. D., Bussières, N., and Duguay, C. R., 2005: The role of northern lakes in a regional energy balance. *J. Hydrometeorol.*, 6, 291–305.

Sadek, M. F., Shahin, M. M., and Stigter, C. J., 1997: Evaporation from the reservoir of the High Aswan Dam, Egypt: A new comparison of relevant methods with limited data. *Theor. Appl. Climatol.*, 56 (1-2), 57–66.

Sartori, E., 2000: A critical review on equations employed for the calculation of the evaporation rate from free water surfaces. *Sol. Energy*, 68 (1), 77–89.

Shepherd, K. J., 1971: Evaporation losses from Lake Alexandrina and Albert during the 1967-8 drought. *Eng. and Water Supply Dep.*, 7377/71. P.D. 89, 15.

Shuttleworth, J. W., 1992: Evaporation, in *Handbook of Hydrology*, edited by D.R. Maidment, 4.1–4.53.

Singh, V.P., and Xu, C.-Y., 1997: Evaluation and generalization of 13 mass-transfer equations for determining free water evaporation. *Hydrol. Process.*, 11, 311–323.

Stewart, R. B., and W. R. Rouse, 1976: A simple method for determining the evaporation from shallow lakes and ponds, *Water Resour. Res.*, 12 (4), 623-628.

Stewart, R. B., Rouse, W. R., 1977: Substantiation of the Priestley and Taylor parameter $\alpha = 1.26$ for potential evaporation in high latitudes. *J. Appl. Meteorol.*, 16:649–650.

Sturrock, A. M., Winter, T. C., Rosenberry, D. O., 1992: Energy budget evaporation from Williams Lake: a closed lake in north central Minnesota. *Water Resourc. Res.*, 28 (6), 1605– 1617.

Sumner, D. M., Jacobs, J. M., 2005: Utility of Penman-Monteith, Priestley-Taylor, reference evapotranspiration, and pan evaporation methods to estimate pasture evapotranspiration. *J. Hydro.*, 308, 81–104.

Tanny, J., Cohen, S., Assouline, S., Lange, F., Grava, A., Berger, D., Teltch, B., and Parlange, M. B., 2008: Evaporation from a small water reservoir: Direct measurements and estimates. *J. Hydrol.*, 351 (1–2), 218–229.

Verburg, P. and Antenucci, J. P., 2010: Persistent unstable atmospheric boundary layer enhances sensible and latent heat loss in a tropical great lake: Lake Tanganyika. *J. Geophys. Res.*, 115, D11109.

Vercauteren, N., Bou-Zeid, E., Huwald, H., Parlange, M. B., and Brutsaert, W. 2009: Estimation of wet surface evaporation from sensible heat flux measurements. *Water Resour. Res.*, 45, W06424.

Weisman, R. N., and Brutsaert, W. 1974: Evaporation and cooling of a lake under unstable atmospheric conditions, *Water Resour. Res.*, 9, 1242-1257.

Winter, T. C., Rosenberry, D. O., Sturrock, A. M., 1995: Evaluation of 11 equations for determining evaporation for a small lake in the north central United States. *Water Resour. Res.*, 31 (4), 983–993.

Xu, C.-Y. and Singh, V. P., 2001: Evaluation and generalization of temperature-based methods for calculating evaporation. *Hydrol. Process.*, 15, 305–319.

Yusup, Y. and Liu, H., 2016: Effects of atmospheric surface layer stability on turbulent fluxes of heat and water vapor across the water-atmosphere interface, *J. Hydrometeorol.*, 17, 2835–2851.

Zhang, Q. and Liu, H., 2013: Interannual variability in the surface energy budget and evaporation over a large southern inland water in the United States. *J. Geophys. Res. Atmos.*, 118, 4290–4302.

Zhang, Q. and Liu, H., 2014: Seasonal changes in physical processes controlling evaporation over inland water. *J. Geophys. Res. Atmos.*, 119, 9779–9792.

Zotarelli, L., Dukes, M. D., Romero, C. C., Migliaccio, K. W., Morgan, K. T., 2015: Step by Step Calculation of the Penman-Monteith Evapotranspiration (FAO-56 Method). University of Florida, AE459, 10.